EMBRY-RIDDLE
Aeronautical University™
SCHOLARLY COMMONS

10-2001

Design and Construction of a 1/3-Scale, 1986 Cessna 172P Flight-Test Aircraft

Michael J. Hinton
Embry-Riddle Aeronautical University - Daytona Beach

Follow this and additional works at: https://commons.erau.edu/db-theses

Part of the Aerospace Engineering Commons

**Design and Construction of a 1/3-Scale,
1986 Cessna 172P Flight-Test Aircraft**

by

Michael J. Hinton

A Graduate Thesis Project Submitted to the
Department of Aerospace Engineering
in Partial Fulfillment of the Requirements for the degree of
Master of Science in Aerospace Engineering

Embry-Riddle Aeronautical University

Daytona Beach, Florida

OCTOBER 2001

UMI Number: EP31890

INFORMATION TO USERS

The quality of this reproduction is dependent upon the quality of the copy submitted. Broken or indistinct print, colored or poor quality illustrations and photographs, print bleed-through, substandard margins, and improper alignment can adversely affect reproduction.
In the unlikely event that the author did not send a complete manuscript and there are missing pages, these will be noted. Also, if unauthorized copyright material had to be removed, a note will indicate the deletion.
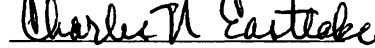
UMI®

Design and Construction of a 1/3-Scale,
1986 Cessna 172P, Flight-Test Aircraft

by

Michael J Hinton

This thesis was prepared under the direction of the candidate's thesis committee
chair, Professor Charles Eastlake, Department of Aerospace Engineering,
and has been approved by the members of his thesis committee. It was
submitted to the Department of Aerospace Engineering and was accepted
in partial fulfillment of the requirements for the degree of
Master of Science in Aerospace Engineering.

THESIS COMMITTEE:

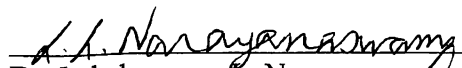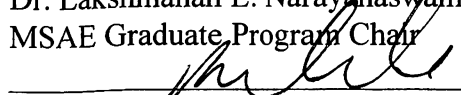Professor Charles Eastlake
Chair

Dr. James Ladesic
Member

Dr. Albert Helfrick
Member

Dr. Lakshmanan L. Narayanaswami   Oct 12, 2001
MSAE Graduate Program Chair

Dr. Reda R. Mankbadi
Department Chair, Aerospace Engineering

ACKNOWLEDGEMENTS

ABSTRACT

Author: Michael J. Hinton
Title: Design and Construction of a 1/3-scale, 1986 Cessna 172P,
             Flight-Test Aircraft
Institution: Embry-Riddle Aeronautical University
Degree: Master of Science in Aerospace Engineering
Year: 1998

The incredible cost of prototype flight testing can be a very limiting factor in the optimization of new designs as they proceed from the drawing board to the flight line. The use of low-cost scaled models to predict full-scale prototype performance is the focus of this project. It will be shown that by strictly following geometric and dynamic scaling criteria, the scaled aircraft's flight performance can be predictably related to the full-scale aircraft's performance. Many companies have performed scaled flight-testing of Remotely Piloted Vehicles (RPV's) and there is much speculation as to the results of these tests, but non-proprietary information about low-cost, scaled flight-testing is rare. The focus of the project at hand, therefore, is to compare the in-flight performance characteristics of a 1/3-scale flying "prototype" to the in-flight performance characteristics of a well-known full-scale flying "prototype," a 1986 Cessna 172P. Much flight testing has been done by ERAU's department of Aerospace Engineering on the 1986 172P so that using this aircraft as the model for determining the validity of the scaling hypotheses is obvious. The author, with the aid of students from capstone design classes at ERAU, "designed" and constructed a 1/3-scale replica 172 as the flying test-bed from which a series of future scaled prototype projects will draw vital conceptual and procedural ideas. The model 172 will be flown by remote control and will have an array of on-board sensors to collect information about key flight characteristics. Along with the on-board data acquisition system and real-time display ground base, the sub-scale aircraft also has a real-time video/audio link to the ground to allow the pilot to fly maneuvers using the same flight cues as they would if in the real aircraft.

TABLE OF CONTENTS

LIST OF TABLES

LIST OF FIGURES

REFERENCES

1. Aircraft Design: A Conceptual Approach, *Raymer, Daniel P.*, AIAA Publications, Washington, D.C., 1992.

2. Airplane Performance Stability and Control, *Courland D. Perkins and Robert E. Hage*, John Wiley and Sons, New York, 1949.

3. Fundamentals of Flight, *Richard S. Shevell*, Prentice Hall, Englewood Cliffs, New Jersey, 1989.

4. Experimental Aerodynamics and Wind Tunnels, *Eastlake, Charles N.*, Embry-Riddle Aeronautical University Publications, Daytona Beach, Fl. 1998.

5. Dynamic Modeling, *Stan Hall*, Sport Aviation Magazine, July 1987.

6. Theory of Wing Sections, *I. Abott and A. Von Doenhoff*, Dover Publishing, New York.

7. Design of Wood Aircraft Structures, ANC-18, United States Government Printing Office, Washington D.C., 1944.

8. Airframe Structural Design, *Michael Chun-Yung Niu*, Conmilit Press Ltd., 1988.

Chapter 1: Introduction

The process of bringing a new design from concept to production consists of many necessary stages, processes, and sub-processes. In order to reduce the overall amount of time that it takes for a new design to complete the progression through these stages, the amount of time required by at least one of the processes, which exists on the critical time path of the project, must be reduced. With any design, some amount of testing must be conducted early in the project to supply the designers with the information required to make accurate and correct decisions. The advantages of supplying this information as early and accurately as possible go far beyond time savings alone.

1.1: Overview of the Problem

A new aircraft often spends many years progressing through the stages of conceptual and preliminary design. After a prototype aircraft is built, the aircraft begins the process of flight testing. Depending upon the size of the project and complexity of the aircraft, this stage can take years to complete. The costs of a full-scale prototype flight test program can be large. Problems which arise during flight testing can result in an extension of the flight test plan and a further increase in the project cost. To avoid having unforeseen problems during flight testing, the designers must be able to accurately predict all characteristics of the aircraft before production of a flyable prototype is begun.

To supply the design teams with the information that they need to be successful, many test methods are used to determine the final characteristics of the design. Tests can

be conducted to examine the aircraft's characteristics pertaining to performance, stability and control, structural stress and fatigue, systems operation and interaction, and ergonomics and human factors. At least three types of tests can be used to determine the performance, stability, and controllability/maneuverability of the aircraft; wind tunnel tests, flight tests, and scale model tests. Traditionally, the first of these types of tests (wind tunnel testing) is used to predict the characteristics of the aircraft while the second type (flight testing) is used to validate the design. The third type has not yet been widely accepted as an accurate and dependable predictor or evaluator of a design.

Wind tunnel testing has been utilized since the days of the first aircraft. According to Eastlake[1], wind tunnel testing can be a quick and relatively inexpensive way of evaluating the performance of a new design. Wind tunnel tests, however, can be very extensive, and, considering the cost of time in a major tunnel facility, can still be very expensive. Wind tunnel testing has the distinct advantage, however, of allowing the collection of data in a controlled environment. In addition, since wind tunnel testing is done on the ground, the danger of a crash is eliminated.

Since flight testing of a design cannot occur until a flyable prototype has been built, then many of the problems that arise are found much too late in the program to be swiftly and adequately dealt with without drastically altering the schedule. Flight testing of a full-scale prototype can be very expensive, costing both time and money. A fully instrumented aircraft is a very complex piece of laboratory equipment, which can tie up a significant portion of a company's human, monetary, and physical resources. A

catastrophic event for the prototype can be devastating for the project, the company, and the people involved.

The other alternative method, while not entirely new, is growing in usefulness and accuracy. That is, flight testing of remotely-piloted, sub-scale vehicles. Flight testing of RPV's is not a new concept. For many years, companies have used scaled versions of prototype aircraft to prove basic performance characteristics and, even sometimes, just to see if their design is airworthy. Only within the most recent design generation has the miniaturization of electronics allowed these companies to collect large amounts of data from an almost unlimited range of parameters. Because of this, flight-testing of scaled versions of prototype aircraft can be considered a viable alternative method for producing the data originally obtainable only from full-scale flight testing. Since construction of a sub-scale flight-test vehicle can occur faster and earlier than that of a full-scale prototype, this testing method lends itself well to being inserted into the schedule between wind tunnel tests and flight tests, allowing the designers another chance to evaluate their design. Since the sub-scale flight tests could be conducted earlier in the program, some potential problems could be averted much sooner than during full-scale flight testing, when the impact on the schedule would be much greater.

Table 1.1 shows a summary of some of the advantages and disadvantages to using wind tunnel testing, full-scale flight testing, and sub-scale flight testing. Although each testing method has distinct advantages, sub-scale flight testing provides the tester with an intermediate test method with advantages from both other types.

1.3

Table 1.1: Performance Evaluation Methods

Type of Testing	Time Span Required	Project Cost ($)	Safety	Instrumentation Type	Data Accuracy
* Flight Test	Years	10^7-10^8	Dangerous	Packaging Difficult, Telemetry Required	Best Available
* Wind Tunnel Test	Months	10^6	Safe	Stationary, Fairly Easy	Good
RPV Scaled Flight Test	Months to Years	10^4-10^5	Safe	Packaging Difficult, Telemetry Required	Good to Best**

*- Taken from reference 4
**- Dependent upon the ability to produce precision maneuvers remotely

The primary goal of ERAU's efforts in projects involving sub-scale model design and testing, is to show that the use of moderately large, sub-scale models can be used to gather data to evaluate a new design. It is assumed, though, that the model will be constructed and flown in a very precise manner. It is intended to show, through this and other continuing projects, that a sub-scale model that is constructed and flown in a controlled, precise manner can be an accurate evaluation tool.

1.2: Previous Research

As part of the Advanced General Aviation Transport Experiments (AGATE) projects over the last few years, aerospace engineering students at ERAU have designed a next generation general aviation trainer/moderate performance aircraft. In 1996, the author served as the lead engineer on the team responsible for the final configuration of the design. That year, the design took first place in the annual AGATE design

competition. It was then decided that the continuation effort be placed into building and flying a 1/3-scale prototype model. The students quickly realized that to validate the sub-scale flight-testing of an unproven design, sub-scale flight-testing of a proven design would have to be conducted to verify the accuracy of scaling laws to be used in the project.

The Aerospace Engineering Department at Embry-Riddle has been conducting flight tests using a 1986 Cessna 172P as part of an elective lab course. From years of successful testing, ERAU has acquired a sizable knowledge of the basic performance and flight characteristics of the C172P. It is because of this large database of performance data on the C172P that the make and model of aircraft on which to start sub-scale flight testing was obvious.

1.3: Current Research

The students and staff at Embry-Riddle Aeronautical University have undertaken a large and multi-faceted project. The project is centered on the verification of the predicted characteristics of a design that has been evolving throughout the preliminary and detail design classes since 1994. The completion of this thesis project forms a significant stepping-stone for the remainder of the project.

Chapter 2: Background Theory

This chapter will describe the techniques used in scaling the aircraft. Section 2.1 gives an overview of the scaling technique followed by validation of the technique through the laws of physics in section 2.2. Following the discussion of the scaling laws, section 2.3 shows a method for predicting the full-scale performance of an aircraft from 1/3-scale flight testing. Chapter 3 discusses the performance of the 1/3-scale C172P.

2.1: Dynamic Modeling Scaling Technique

A distinction exists between geometrically scaled models and dynamically similar models. A geometrically scaled model's dimensions are proportional to those of the full-scale aircraft's by the reciprocal of the scale factor, λ. The value of λ used in this project is 3. A model is dynamically similar if its dynamic characteristics are in scale with the full-scale article. A dynamically similar aircraft will respond to inertial loads, as well as aerodynamic loads, in a manner that is in scale with the full-scale aircraft. Geometrically scaled models are not necessarily dynamically similar to the full-scale aircraft. A model whose size, propulsive power, weight, and weight distribution are in scale with the full-scale aircraft's can be both geometrically and dynamically similar. It is the intention of this project to construct a geometrically and dynamically similar model of the 1986 Cessna 172P. This model will validate the scaling techniques and provide insight into the use of scaled models for preliminary flight testing experimentation. To accomplish this, comparisons of data from 1/3-scale and full-scale C172P flight test experiments will be made.

A geometrically and dynamically scaled model intended for use as design validation such as the 1/3-scale C172P, must be considered a piece of laboratory equipment. A model that does not strictly adhere to the scaling laws will not provide useful engineering data and, therefore, serves only a recreational purpose. Careful consideration to structural sizing and component placement is vital to the construction of a truly useful sub-scale model. Precise building techniques must also be employed in order to achieve the most accurate representation of the full-scale aircraft.

Table 2.1 presents the scaling factors used in this project to define the characteristics of the 1/3-scale C172P. The ratio of the full-scale aircraft's linear dimensions to the scaled model's linear dimensions defines the scale factor, λ. Section 2.2 details the derivation of the scale factors presented in table 2.1. Table 2.2 details the scaled values of some of the key characteristics of the model. See section 3.2 for more details about the geometry of the full-scale and 1/3-scale aircraft.

In addition to geometric and dynamic scaling, a model can possibly exhibit scaled stress characteristics. A model whose structural members encounter stress levels that are in scale with those found in similar structural members on the full-scale article is a stress-scaled model. The final row of table 2.1 shows the factor relating stress on the model to stress on the full-scale aircraft. Section 2.2 describes the assumptions required when dealing with stress scaling. Section 2.2 also details the verification of the stress scaling factor shown here.

Table 2.1: Scaling Factors

Parameter	Full-scale quantity times:	Multiplier for this project ($\lambda=3$)
Length	λ^{-1}	0.3333
Mass	λ^{-3}	0.0370
Time	$\lambda^{-0.5}$	0.5774
Area	λ^{-2}	0.1111
Volume	λ^{-3}	0.0370
Force	λ^{-3}	0.0370
Weight	λ^{-3}	0.0370
Moment	λ^{-4}	0.0123
Mass Moment of Inertia	λ^{-5}	0.0041
Area Moment of Inertia	λ^{-4}	0.0123
Linear Velocity	$\lambda^{-0.5}$	0.5774
Linear Acceleration	1	1.0000
Angles	1	1.0000
Angular Velocity	$\lambda^{0.5}$	1.7321
Angular Acceleration	λ	3.0000
Work and Energy	λ^{-4}	0.0123
Power	$\lambda^{-3.5}$	0.0214
Wing Loading	λ^{-1}	0.3333
Power Loading	$\lambda^{0.5}$	1.7321
Stress	λ^{-1}	0.3333

Table 2.2: Characteristics of the 1/3-scale C172P

Parameter	Full-scale 1986 Cessna 172P	1/3-scale 1986 Cessna 172P
Lengths:		
Wingspan	36.0 ft	12.0 ft
Fuselage Length	26.9 ft	9.0 ft
Overall Height	8.8 ft	2.9 ft
Tail Width	11.3 ft	3.8 ft
Wing Planform Area	174.0 ft^2	19.3 ft^2
Weights:		
Maximum Ramp	2407 lb	90 lb
Maximum Takeoff or Landing	2400 lb	89 lb
Standard Empty	1433 lb	53 lb
Maximum Useful Load	974 lb	36 lb
Power:		
Horsepower Rating	160.0 Hp	3.4 Hp
Speeds:		
Never Exceed Speed	158 kts	91 kts
Maximum (at sea level)	123 kts	71 kts
Cruise (75% power at 8,000 ft)	120 kts	69 kts
Stall (flaps retracted)	51 kts	29 kts
Stall (flaps extended)	46 kts	26 kts
Fuel Volume:		
Standard Configuration	43 gal	1.59 gal

Table 2.2 (cont'd): Characteristics of the 1/3-scale C172P

Parameter	Full-scale 1986 Cessna 172P	1/3-scale 1986 Cessna 172P
Other:		
Wing Loading	13.8 lb/ft^2	4.6 lb/ft^2
Power Loading	15.0 lb/Hp	25.9 lb/Hp
Mean Aerodynamic Chord	4.9 ft	1.63 ft
Never Exceed Speed, V_{NE}	152 kts	87.9 kts
Propeller Diameter	75 in	25 in
Engine/Propeller Speed	2700 RPM	4677 RPM
Pitch Mass Moment of Inertia	1346 sl-ft^2	5.54 sl-ft^2

2.2: Validation of Scaling Laws (Theoretical)

The use of dimensional analysis allows for the validation of the scaling laws used throughout this project. The accepted dimensions of a given parameter that defines a characteristic of either the full or 1/3-scale aircraft are determined by the relationship that quantifies the parameter. For example, resolving the pressure distribution acting on either aircraft at some point in time, determines the drag of the aircraft. Pressure exerts its effect in pounds per square foot. The pressure distribution, multiplied by the area of the aircraft on which it acts, results in drag, measured in pounds. Therefore, a force such as drag derives its units from the parameters used to quantify it, in this case pressure and area.

The basic unit of linear measurement is that of length, or L. Area units are, therefore, length times length or length squared (L^2). Likewise, volume units are length cubed, or L^3. The units of some of the more complex parameters include the basic units mass (M) and time (T) as well. The units of all of the parameters scaled throughout the analysis shown here are a combination of the basic units of length (L), mass (M), time

(T). These three parameters, therefore, will lay the groundwork for the basis of the validation of the scaling laws. The scaling factor for each of these three basic units must be found to properly define the scaling factors of the more complex parameters. Following the development of scale factors for these three basic units, validation of the scale factors of the parameters shown in section 2.1 is given.

Length

By definition, a geometrically scaled model's dimensions (i.e. wingspan, fuselage length, etc.) are proportional to the dimensions of the full-scale aircraft by the scale factor, λ. A 1/3-scale model's linear dimensions are equal to $1/\lambda$ or 1/3 that of the full-scale dimensions. Let the subscript $_{FS}$ denote a parameter that describes a characteristic of the full-scale aircraft. Similarly, the subscript $_{1/3}$ denotes parameters characteristic of the 1/3-scale aircraft. L_{FS} describes a linear dimension of the full-scale aircraft and $L_{1/3}$ describes the linear dimension of the 1/3-scale aircraft that is similar. The 1/3-scale aircraft's linear dimension, $L_{1/3}$, therefore, is related to the full-scale's by equation 2.1.

$$L_{1/3} = \frac{1}{\lambda} L_{FS} \qquad \text{(EQ 2.1)}$$

Mass

To see how the mass of the aircraft scales, consider a single homogeneous item somewhere within both aircraft. If we assume that this item is made entirely from the same material on the 1/3-scale aircraft as it was on the full-scale aircraft, then the density of the material would remain constant. Any item we choose to consider here would have

a finite volume L_{FS}^3 on the full-scale aircraft and $L_{1/3}^3$ on the 1/3-scale aircraft. It was shown above that the volume of the item on the 1/3-scale aircraft is 1/27 of the volume of the item on the full-scale aircraft. Since the density is constant, 1/27 of the molecules exist in the 1/3-scale item making the mass of that item also 1/27 of full-scale. Equation 2.2 shows the mass scaling relationship.

$$M_{1/3} = \frac{1}{\lambda^3} M_{FS} \qquad\qquad \text{(EQ 2.2)}$$

Time

The concept of scaling time as shown here serves one major purpose -- adjusting time history data for comparison with full-scale. The need for scaled time arises from the following two governing criteria. Consider two aircraft, one full-scale and one 1/3-scale, flying identical maneuvers in earth's atmosphere. As shown above, the 1/3-scale aircraft's dimensions must all be 1/3 of the full-scale aircraft's. This is the first criterion.

In addition, the weight of both aircraft is determined by the magnitude of the earth's gravitational acceleration (32.2 ft/s^2). This fundamental linear acceleration must be constant for both aircraft. In similar fashion to gravity, all linear accelerations must be equal in magnitude for both aircraft. This is the second criterion. The need for time scaling arises in the consideration of the dimensional analysis.

The units of the gravitational acceleration of the earth, g, can be simplified to length per time squared, or L/T^2. Linear accelerations experienced by the 1/3-scale

2.6

aircraft can be related to those on the full-scale aircraft by the following: $(L/T^2)_{1/3} =$

$(L/T^2)_{FS}$. However, the length unit in this equation will scale by $1/\lambda$ as shown earlier

causing a necessary correction to time to retain equality. Equation 2.3, therefore,

introduces the concept of time scaling. From this equation, the time scale relationship

shown in equation 2.4 is derived.

$$\left(\frac{L}{T^2}\right)_{1/3} = \left(\frac{\frac{1}{\lambda} \cdot L}{\left(\left(\frac{1}{\sqrt{\lambda}} \cdot T\right)\right)^2}\right)_{FS} \qquad \text{(EQ 2.3)}$$

$$T_{1/3} = \frac{1}{\sqrt{\lambda}} T_{FS} \qquad \text{(EQ 2.4)}$$

The thought of flying precision maneuvers while watching a clock that is running

$\sqrt{\lambda}$ (1.732 for $\lambda=3$) times faster than normal can be quite unrealistic. Instead, the

maneuvers can be flown in full-scale time and the data can be post-processed to correct

for scaled time.

Equations 2.1, 2.2, and 2.4 show the scaling relationships of the basic units of

length, mass, and time. Scale factors for the remaining parameters discussed in section

2.1 are determined by combining the relationships presented in these three equations.

2.7

Area and Volume

Multiplication of a length by a length defines the area of an object. The area of the 1/3-scale model would be denoted by length squared or $(L_{1/3})^2$. This is related to a similar area on the full-scale aircraft by the following relationship: $(L_{1/3})^2 = (1/\lambda\ L_{FS})^2 = 1/\lambda^2\ L_{FS}^2 = 1/9\ L_{FS}^2$. Likewise, volume of the 1/3-scale aircraft is length cubed or $(L_{1/3})^3 = (1/\lambda\ L_{FS})^3 = 1/\lambda^3\ L_{FS}^3 = 1/27\ L_{FS}^3$.

Weight and Force

Newton's second law of motion states that the force required to move an object of constant or fixed mass is proportional to the mass of the object time the time derivative of the velocity of the object (its acceleration). The weight of an object is calculated by multiplying its mass times the acceleration of gravity, g, in the same manner that the force applied to an object is found by multiplying its mass times the acceleration of the object. The units of force, therefore, can be written as $(ML)/T^2$. Using the relationships previously discussed, a force (i.e. weight), acting on the 1/3-scale aircraft scales as shown in equation 2.5.

$$F_{1/3} = \left(\frac{M \cdot L}{T^2}\right)_{1/3} = \left(\frac{\frac{1}{\lambda^3}M \cdot \frac{1}{\lambda}L}{\left(\frac{1}{\sqrt{\lambda}}T\right)^2}\right)_{FS} = \frac{1}{\lambda^3}\left(\frac{M \cdot L}{T^2}\right)_{FS} = \frac{1}{\lambda^3}F_{FS} \qquad \text{(EQ 2.5)}$$

Moment

A moment results when a force is applied at some distance from a given point. The basic units of moment are given, therefore, by equation 2.6. Equation 2.7 shows the resulting scale factor for moment.

$$Moment = \frac{M \cdot L}{T^2} \cdot L \qquad\qquad (EQ\ 2.6)$$

$$Moment_{1/3} = \frac{\frac{1}{\lambda^3} M_{FS} \cdot \frac{1}{\lambda} L_{FS}}{\left(\frac{1}{\sqrt{\lambda}}\right)^2 T_{FS}^2} \cdot \frac{1}{\lambda} L_{FS} = \frac{1}{\lambda^4} Moment_{FS} \quad (EQ\ 2.7)$$

Mass and Area Moments of Inertia

Mass moment of inertia quantifies an object's resistance to changes in angular velocity. As a moment is applied to a rigid body, the magnitude of the mass moment of inertia determines the angular acceleration of the body; the greater the mass moment of inertia, the slower the angular acceleration. Equation 2.8 defines mass moment of inertia whose basic units are mass times length squared (ML^2). Equation 2.9 presents the scaling factor for mass moment of inertia.

$$I_m = \int_V r^2 \rho dV = \int_V r^2 dm \qquad\qquad (EQ\ 2.8)$$

$$\left(I_m\right)_{1/3} = \frac{1}{\lambda^3} M_{FS} \cdot \left(\frac{1}{\lambda}\right)^2 L_{FS}^2 = \frac{1}{\lambda^5}\left(I_m\right)_{FS} \qquad\qquad (EQ\ 2.9)$$

2.9

Area moment of inertia is used throughout the structural substantiation analysis performed on the 1/3-scale C172P. Applying a scale factor to the area moment of inertia of a structural member found on both the 1/3-scale and full-scale aircraft is validated only if the geometry of the object is properly scaled. In most cases, calculation of the area moment of inertia is conducted using the geometrical characteristics of the cross-section of a structural member rather than by the use of a scale factor. The scale factor presented here is given primarily for reference as it is used later in the validation of the stress scaling factor. Equation 2.10 is used to find the area moment of inertia of a plane area whose basic units are length raised to the forth power (L^4). The scale factor for area moment of inertia is presented in equation 2.11.

$$I_A = \int_A x^2 dA \quad \text{or} \quad I_A = \int_A y^2 dA \quad \text{or} \quad I_A = \int_A xy dA \qquad \text{(EQ 2.10)}$$

$$(I_A)_{1/3} = \left(\frac{1}{\lambda}\right)^4 L_{FS}{}^4 = \frac{1}{\lambda^4}(I_A)_{FS} \qquad \text{(EQ 2.11)}$$

Linear Velocity

The steady state velocity of a body is defined as the ratio of the linear distance traversed per unit time. The basic units of linear velocity are, therefore, length over time (L/T). Equation 2.12 shows the derivation of the scaling factor used for linear velocity.

$$V_{1/3} = \frac{\frac{1}{\lambda} L_{FS}}{\frac{1}{\sqrt{\lambda}} T_{FS}} = \frac{1}{\sqrt{\lambda}} V_{FS} \qquad \text{(EQ 2.12)}$$

2.10

Scaled velocity, like scaled time, is used to correct the resulting flight test data in preparation for comparisons. Asking a pilot to fly a maneuver at a scaled velocity is inherently contradictory. Therefore, flight test data is flown at full-scale and corrected during post-processing.

Linear Acceleration

Linear acceleration is defined as the time derivative of the linear velocity of an object. The basic units of linear acceleration are, therefore, length over time squared (L/T^2). The scaling factor used for linear acceleration is derived in equation 2.13. A second verification of this was presented earlier in the derivation of the scale factor for time. Since gravitational acceleration (a linear acceleration quantity) remains constant, irrespective of scale factor, then the scale factor for linear acceleration must be 1. Equation 2.13 verifies this assumption.

$$a_{1/3} = \frac{\frac{1}{\lambda} L_{FS}}{\left(\frac{1}{\sqrt{\lambda}}\right)^2 T_{FS}^{\ 2}} = a_{FS} \qquad \text{(EQ 2.13)}$$

Angles

The scale factor used to scale angles can be found by considering the pair of triangles presented in figure 2.1. Although the linear dimensions of the scaled triangle are proportional to the full-scale triangle by the inverse of the scale factor, the angles between each of the sides of the triangles remain unchanged (termed similar triangles).

2.11
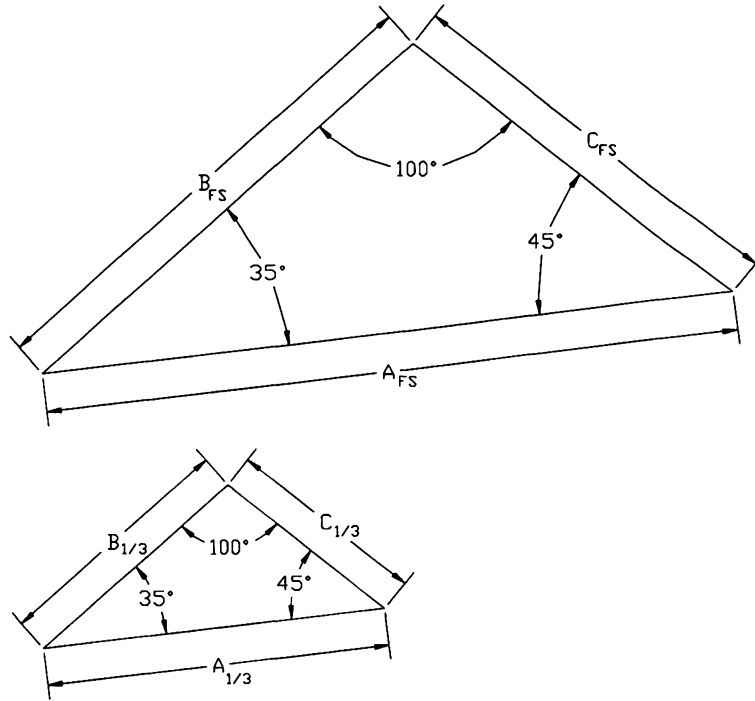
Figure 2.1: Scaling Angles

Angular Velocity

The steady state rate at which a body rotates defines the angular velocity of the

body. The basic units of angular velocity are radians (unitless) over time (1/T). Equation

2.14 shows the derivation of the scale factor for angular velocity.

$$\omega_{1/3} = \frac{1}{\frac{1}{\sqrt{\lambda}}T_{FS}} = \sqrt{\lambda} \cdot \omega_{FS} \qquad \text{(EQ 2.14)}$$

2.12

Angular Acceleration

Similarly to linear acceleration, angular acceleration is defined as the time derivative of angular velocity. The basic units of angular acceleration are radians over time squared ($1/T^2$). The mass moment of inertia of the rotating body governs the amount of moment required to induce an angular acceleration, as discussed earlier. Equation 2.15 shows the scale factor derivation for angular acceleration.

$$\alpha_{1/3} = \frac{1}{\left(\dfrac{1}{\sqrt{\lambda}}\right)^2 T_{FS}^{\;2}} = \lambda \cdot \alpha_{FS} \qquad \text{(EQ 2.15)}$$

Work and Energy

Work is defined as the dot product of a force applied to a rigid body and the distance the body moves. Equation 2.16 restates this definition using mathematical symbolism. The net work performed on a body is given as the sum of the energy changes due to body translation, body rotation, and changes in potential energy. Equation 2.17 shows these three components to net work. Both work and energy have the basic units of mass times length squared all over time squared ($(ML^2)/T^2$). Equation 2.18 shows the scale factor used for work and energy.

$$W = \int \vec{F} \cdot d\vec{s} \qquad \text{(EQ 2.16)}$$

$$W_{net} = \Delta E_{trans} + \Delta E_{rot} + \Delta E_{pot} = \frac{1}{2} m V^2 + \frac{1}{2} I_m \omega^2 + mgh \qquad \text{(EQ 2.17)}$$

2.13

$$W_{1/3} = \frac{\frac{1}{\lambda^3} M_{FS} \cdot \left(\frac{1}{\lambda}\right)^2 L_{FS}^2}{\left(\frac{1}{\sqrt{\lambda}}\right)^2 T_{FS}^2} = \frac{1}{\lambda^4} W_{FS}$$

(EQ 2.18)

Power

Work applied per unit time defines power. The basic units of power are, therefore, mass times length squared all over time squared per time $(((ML^2)/T^2)/T)$, or mass times length squared all over time cubed $((ML^2)/T^3)$. Equation 2.19 shows the resulting scale factor for power.

$$P_{1/3} = \frac{\frac{1}{\lambda^3} M_{FS} \cdot \left(\frac{1}{\lambda}\right)^2 L_{FS}^2}{\left(\frac{1}{\sqrt{\lambda}}\right)^3 T_{FS}^3} = \frac{1}{\lambda^{3.5}} P_{FS}$$

(EQ 2.19)

Wing Loading and Power Loading

In addition to the more generalized physical parameters described above, scale factors for commonly used parameters that are specific to aircraft, such as wing loading and power loading, can also be found. Wing loading is found by dividing the aircraft's weight by the wing reference area. Similarly, power loading is found by dividing the aircraft's weight by the engine's maximum horsepower rating. The units of wing loading are force per unit area; power loading has units of force per unit power. Equations 2.20 and 2.21 show the resulting scale factors for wing loading and power loading. These equations use the previously presented scale factors for weight, power, and area in their derivations.

2.14

$$\left(\frac{W}{S}\right)_{1/3} = \frac{\frac{1}{\lambda^3}W_{FS}}{\frac{1}{\lambda^2}S_{FS}} = \frac{1}{\lambda}\left(\frac{W}{S}\right)_{FS}$$

(EQ 2.20)

$$\left(\frac{W}{P}\right)_{1/3} = \frac{\frac{1}{\lambda^3}W_{FS}}{\frac{1}{\lambda^{3.5}}P_{FS}} = \frac{1}{\lambda^{0.5}}\left(\frac{W}{P}\right)_{FS}$$

(EQ 2.21)

Stress

Consider a model whose every dimension is properly in scale with the full-scale aircraft. This model's skin thickness, for example, is $1/\lambda$ thinner than the full-scale aircraft's skin. Similarly, the stress area in a given stringer is $1/\lambda^2$ smaller than full-scale. These factors, presented previously, define the model to be a truly geometrically scaled model. Also, assume that the materials used to construct the components of this model are identical to those used in the full-scale aircraft. In many real world cases, however, construction of a model with these characteristics is impractical due to the inability to fabricate such small parts out of the same materials used in the full-scale version.

Throughout the scaling process, the material properties of the model will remain the same as those of the full-scale article. The model, therefore, must exert a different magnitude of force onto a structural member to achieve the same stress as seen in full-scale. In a case in which the forces exerted on the model result in stresses of the same magnitude as full-scale, a stress scale factor, λ_σ, of 1.0 exists. The forces on a properly scaled model are, however, proportional to those of the full-scale aircraft by the factor

$1/\lambda^3$, as shown earlier. Because of the differences in geometry and force between model and full-scale, a relationship is needed that describes the real-world stress scaling factor.

Consider a simply-supported, point-loaded cantilevered beam approximation of a structural member that exists on both the model and full-scale aircraft. Figure 2.2 shows these approximated beams and their respective annotations. In this example, the subscript *FS* denotes and attribute of the beam on the full-scale beam, while the subscript *1/3* is used for the 1/3-scale model. Each of the linear dimensions x, y, and h of the model are $1/\lambda$ times their full-scale counterpart. The vertical load, P, acting on the model is assumed to be $1/\lambda^3$ that which is acting on the full-scale beam.
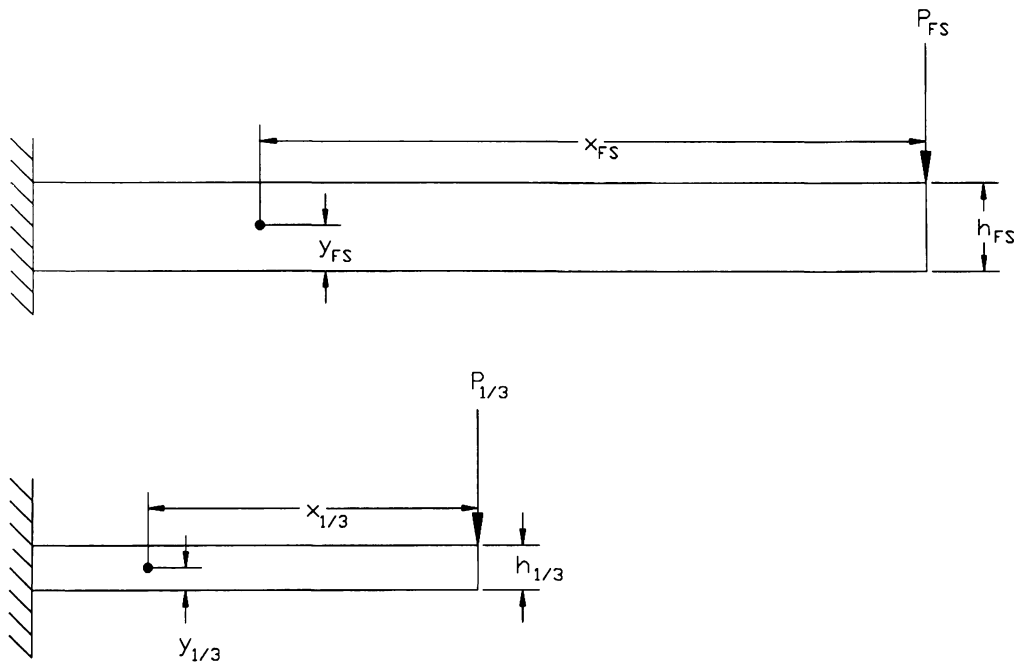
Figure 2.2: Simplified Cantilevered Beam Approximation

Equations 2.22 and 2.23 describe the bending stress at a point located x units away from the load and y units up from the bottom of the beam, for the model and full-scale beams, respectively. In these equations, M denotes the bending moment induced by the load P and I denotes the area moment of inertia of the cross-section at the point. Using the scaling factors

$$\sigma_{FS} = \frac{M_{FS} \cdot y_{FS}}{I_{FS}} \qquad \sigma_{1/3} = \frac{M_{1/3} \cdot y_{1/3}}{I_{1/3}} \qquad \text{(EQs 2.22, 2.23)}$$

presented in section 2.1, one can rewrite equations 2.22 and 2.23 as 2.24. It is concluded, therefore, that a model whose geometry is properly scaled and which is subjected to scaled loads, exhibits stress levels that are inversely proportional to the scale factor. However, often during the construction of a scaled model, it is impossible to maintain the

$$\sigma_{1/3} = \frac{\frac{1}{\lambda^4} M_{FS} \cdot \frac{1}{\lambda} y_{FS}}{\frac{1}{\lambda^4} I_{FS}} = \frac{1}{\lambda} \sigma_{FS} \qquad \text{(EQ 2.24)}$$

proper geometry scale or material properties to utilize this stress scaling characteristic. The scope of the 1/3-scale C172P project does not include stress-scaled structural members. The topic of stress scaling is presented in regards to the 1/3-scale Aquilas model.

2.3: Predicting Performance (Theoretical)

The prediction of full-scale aircraft performance from scaled model data is not the topic of this thesis project. However, because the overall project at ERAU includes flight testing for validation and prediction of an unproven full-scale design (the Aquilas), then the author felt it necessary to briefly discuss full-scale performance prediction here.

There are many reasons why full-scale performance predictions made from sub-scale model data can be inaccurate or inconsistent. The main reason for inaccuracies is Reynold's number effects. The reduced Reynold's number of the sub-scale model causes delayed boundary layer transition and premature separation when compared to full-scale boundary layer characteristics. The altered boundary layer characteristics also reduce the lift and increase the drag on the model. To minimize the effects of Reynold's number differences between the full-scale aircraft and the sub-scale model the model must be as large as possible. A scale factor of 3 was chosen for this project specifically for this reason. This scale factor allows the cruise Reynold's number of the model ($\sim$1.21x10^6) to remain within the same order of magnitude as that of the full-scale aircraft ($\sim$6.33x10^6). It is hoped that the effects of Reynold's number differences in this project will be minimized by using a scale factor of 3.

To predict the full-scale performance of an aircraft from scale model flight testing, the scaling laws from the previous sections are used in reverse. If the Reynold's number effects are minimal, relatively accurate predictions of key characteristics such as

maximum level speed can be found. However, behavioral characteristics of the full-scale

aircraft are more accurately and reliably predicted through flight testing the model.

Utilizing the scaling factors presented earlier, along with sufficiently competent data,

predictions of the characteristics found in table 2.3 can be made. It is the goal of the

continuation effort of this project to verify or discount these prediction parameters.

Table 2.3: Predicting Performance

Parameter	1/3-scale quantity times:	Multiplier for this project (λ=3)
Time	$\lambda^{0.5}$	1.7321
Maximum Speed	$\lambda^{0.5}$	1.7321
Maximum Climb Rate	$\lambda^{0.5}$	1.7321
Takeoff Distance	λ	3.0000
Pitch, Roll, and Yaw Rates	$\lambda^{-0.5}$	0.5774

Chapter 3: Design of the Aircraft and its Systems

This chapter discusses the preliminary and detail design of the 1/3-scale C172P flight test aircraft and its systems. Discussion of the design of the aircraft itself (the full-scale C172P) is unnecessary, therefore, the focus of this chapter is on the design of the 1/3-scale model with respect to its mission. Guidelines governing the design were chosen and analysis of the aircraft's performance and stability and control characteristics was performed. Discussion of the design of the aircraft systems is also given.

3.1: Guidelines

The design and construction of the 1/3-scale C172P was intended to be a project that brought together the knowledge and skills of individuals with strengths in various disciplines. To maintain a certain level of consistency throughout the project, a set of guidelines was needed. Since established design and construction guidelines do not exist for remotely piloted vehicles (RPV's), the guidelines used in this project were decided upon by the author and the project advisors. The lessons learned from the completion of the 1/3-scale C172P project are to be carried over into the construction and flight testing of a new design. In order to maintain a substantial minimum safety level throughout the design of the 1/3-scale C172P, it was decided that Part 23 of the Federal Aviation Regulations (FAR's) would be used as the primary design guidelines. The follow-up project to the 1/3-scale C172P is a general aviation revitalization effort and is subject to the regulations described in FAR Part 23.

Throughout the design, the use of FAR Part 23 has added to the safety level of the aircraft. An example of this is found in the next section, which describes the loading diagram. FAR Part 23 requires the loading diagram to be constructed using gust loads representative of real world atmospheric turbulence. For small-scale aircraft, this requires that significantly higher load factors be designed for than for full-scale aircraft, due to the reduced wing loading. Although designing to a higher load factor results in a heavier aircraft, it was felt that the weight penalty would not be a concern since the empty weight of the aircraft was certain to be far below the design scaled gross weight of 88.9 lbs.

3.2: 1/3-Scale Aircraft Geometrical Data

Much of the theoretical analysis presented in chapter 3 is based on the geometry of the aircraft. This section is used to present details about the 1/3-scale models geometrical characteristics for future use.

Figure 3.1 shows a perspective view of the 1986 Cessna 172 model P (C172P). The C172P has a single, piston-powered engine, that rotates a 75 in. diameter propeller at the front of the aircraft. The aircraft employs a high-wing and a conventional tail configuration. Fowler flaps are used on the wing to increase lift for takeoff and landing. Friese ailerons are used for reduced roll control forces and adverse yaw. The landing gear is non-retractable and have streamlined fairings to reduce drag. The full-scale airplane is a 2400 lb, 4-seat (1 pilot, 3 passengers), non-pressurized aircraft with a useable range of just over 500 statute miles.
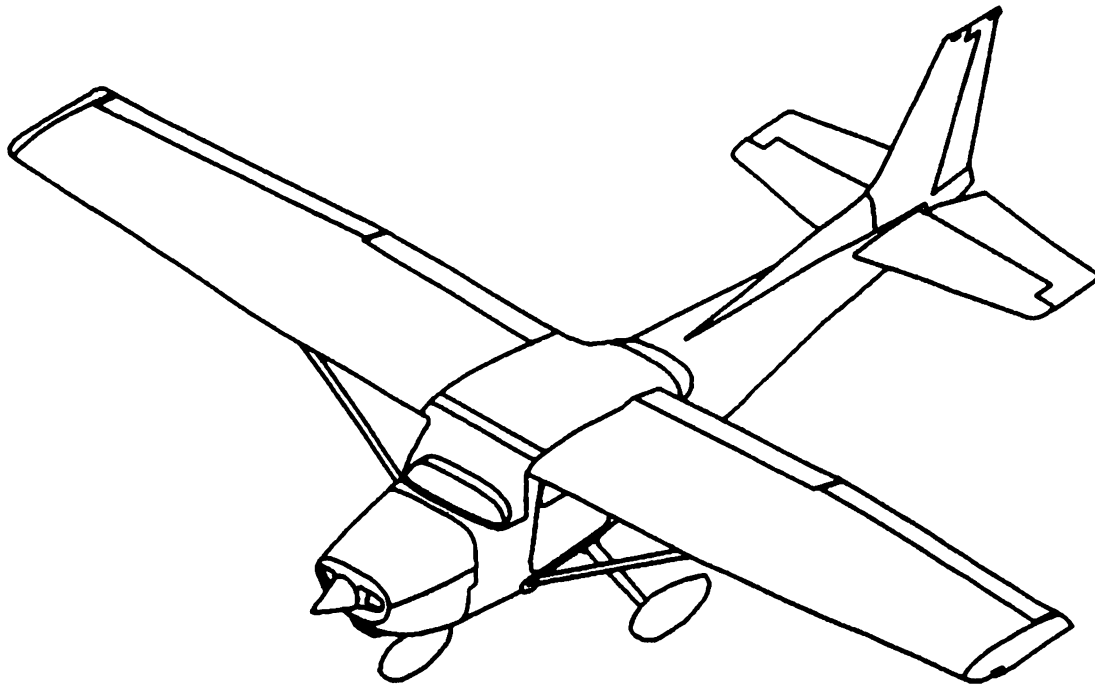
Figure 3.1: 1986 Cessna 172 Model P – Perspective View

Figure 3.2 shows top and side views of the 1/3-scale C172P. Also presented in figure 3.2 are many of the key geometrical characteristics required for detailed aerodynamic analysis. The 1/3-scale aircraft characteristics from table 2.2 are presented again here in table 3.1.

Table 3.1: 1/3-Scale C172P Characteristics

Parameter	1/3-scale 1986 Cessna 172P	Parameter	1/3-scale 1986 Cessna 172P
Lengths:		Power:	
Wingspan	12.0 ft	Horsepower Rating	3.4 Hp
Fuselage Length	9.0 ft	Speeds:	
Overall Height	2.9 ft	Never Exceed Speed	91 kts
Tail Width	3.8 ft	Maximum (at sea level)	71 kts
Wing Planform Area	19.3 ft^2	Cruise (75% power at 8,000 ft)	69 kts
Weights:		Stall (flaps retracted)	29 kts
Maximum Ramp	90 lb	Stall (flaps extended)	26 kts
Maximum Takeoff or Landing	89 lb	Fuel Volume:	
Standard Empty	53 lb	Standard Configuration	1.59 gal
Maximum Useful Load	36 lb		

3.3

HORIZONTAL STAB
MAC=14 2in =1 183ft
AREA=592 9sq in =4 117sq ft
E AREA=224 5sq in =1 559sq ft
Cr=17 65in
Ct=10 07in
└43°

─MAC1

WING
─MAC=19 6in =1 633ft
AREA=2784sq in =19 33sq ft
A AREA=320 3sq in =2 224sq ft
F AREA=344 5sq in=2 392sq ft
Cr=21 76in =1 813ft
─MAC2 Ct=14 3in =1 192ft

└02°
┌32 7°
STRAKE
AREA=59 43sq in =0 413sq ft

VERTICAL STAB
─MAC=14 57in =1 214ft
AREA=278 2sq in =1 932sq ft
R AREA=121 7sq in =0 845sq ft
Cr=18 56in
Ct=9 64in

FUSELAGE
SIDE AREA=981 9sq in=6 819sq ft
TOP AREA=957 0sq in=6 646sq ft
APPROX WETTED AREA=2908sq in =20 2sq ft

Figure 3.2: 1/3-Scale C172P Geometrical Characteristics

3.3: 1/3-Scale Aerodynamic Analysis

The aerodynamic analysis conducted, with respect to this project, was done so to estimate the characteristics of the 1/3-scale aircraft rather than to design the aircraft to meet certain criteria. Basic drag estimation is given followed by determination of the aircraft's drag polar and power required characteristics. Also presented are estimations of maximum lift, lift curve slope, and elevator and rudder hinge moments.

Drag Estimation

The proper estimation of the drag of an aircraft is critical in assessing its performance. The total aircraft drag coefficient, C_D, is a sum of the parasite drag coefficient, C_{Do}, the lift induced drag coefficient, C_{Di}, the compressible drag coefficient,

3.4

C_{Dc}, and a further summation of drag coefficient adjustments, ΔC_D's, for items like deflected spoilers or flaps, as shown in equation 3.1. An elaboration of the method used to estimate each of these contributors to the total drag coefficient follows.

$$C_D = C_{Do} + C_{Di} + C_{Dc} + \sum \Delta C_D \qquad \text{EQ (3.1)}$$

The forth term in equation 3.1 is primarily used to adjust the total drag coefficient to account for changes in the drag when items such as speed brakes or flaps are deflected. These items usually contribute significantly to drag but are not always in use. This drag adjustment is also used to quantify final additions to total drag when matching flight tested data. When determining the drag of the 1/3-scale C172P during cruise, this contribution to the total drag coefficient can be neglected.

The compressibility drag coefficient can also be neglected when calculating the drag for the 1/3-scale C172P. Since the cruise Mach number of 0.093 is much slower than the speed at which compressibility begins to affect the drag of an aircraft, then the compressibility drag coefficient is also neglected.

The lift induced drag coefficient can be written as $C_{Di} = KC_L^2$, where K is a constant determined primarily by the aspect ratio of the wing. Equation 3.2 shows the definition of C_{Di} rewritten using the definition of K. The aspect ratio, $AR=b^2/S_{ref}$, of the 1/3-scale C172P

$$C_{D_i} = \frac{C_L^{\,2}}{\pi \cdot AR \cdot e} \qquad\qquad \text{EQ (3.2)}$$

$$\text{Therefore,} \qquad C_D = C_{Do} + \frac{C_L^{\,2}}{\pi \cdot AR \cdot e} \qquad\qquad \text{EQ (3.3)}$$

wing is 7.45. The Oswald's efficiency factor, e, is calculated from equation 3.4

(reference 1) to be 0.8262. The value of K, therefore, is 0.05171. This allows equation

$$e = 1.78(1 - 0.045 \cdot AR^{0\,68}) - 0.64 \qquad \text{EQ (3.4)}$$

3.3 to be rewritten as $C_{D_i} = 0.05171 C_L^{\,2}$. During steady, straight and level cruise, the lift

must equal weight and drag must equal thrust. Using a maximum takeoff weight of 88.9

lbs and a cruise velocity of 103.8 ft/s, the cruise C_L and C_{D_i} are found to be 0.3592 and

0.006672, respectively.

The parasite drag coefficient is primarily influenced by the geometry and surface

roughness of the aircraft. The estimation of the parasite drag coefficient for the 1/3-scale

C172P was conducted using the drag build-up method described in reference 1. Equation

3.5 is used to find C_{Do}. The term C_{Dmisc} is used to account for miscellaneous

contributions to drag from items such as the landing gear and windshield. The term

$C_{DL\&P}$ represents the

3.6

$$\left(C_{Do}\right)_{subsonic} = \frac{\sum\left(C_{f_i} \cdot FF_i \cdot Q_i \cdot S_{wet_i}\right)}{S_{ref}} + C_{D_{misc}} + C_{D_{L\&P}} \qquad \text{EQ (3.5)}$$

where, FF = component form factor
   Q = component interference factor
   C_f = component skin friction coefficient
   S_{wet} = component wetted area (ft^2)

leakage and protuberance drag. It is used to provide an adjustment for air leakages in and out of the aircraft along with disturbances to the airflow caused by the protrusion of objects into the airflow. $C_{DL\&P}$ is assumed to account for an additional 7.5% of the remainder of C_{Do}.

To determine the contribution of each component to the drag of the aircraft, values for the terms within the summation of equation 3.5 are needed. The skin friction coefficient is determined by both the Reynolds number and whether the boundary layer is laminar or turbulent. For laminar boundary layers, equation 3.6 was used, while equation 3.7 was used for turbulent boundary layers. Again, since the Mach number is quite low, the second portion of the denominator of equation 3.7 can be neglected since it

$$\left(C_f\right)_{laminar} = 1.328\sqrt{R_n} \qquad \text{(EQ 3.6)}$$

$$\left(C_f\right)_{turbulent} = \frac{0.455}{\left(\log_{10} R_n\right)^{2.58}\left(1 + 0.144 \cdot M^2\right)^{0.65}} \qquad \text{(EQ 3.7)}$$

approaches one. Table 3.2 shows the values that were used to determine the skin friction coefficients for each of the aircraft components. During cruise, the 1/3-scale C172P will experience varying amounts of laminar and turbulent flow on different portions of the

3.7

Table 3.2: Skin Friction Coefficient Values

Component	Reference Length (ft)	$(R_n)_{cr}$	$(C_f)_{laminar}$	$(C_f)_{turbulent}$
Wing	1.633	1.078×10^6	0.001279	0.004409
Fuselage	7.289	4.812×10^6	0.000605	0.003386
Horizontal Stabilizer	1.183	0.781×10^6	0.001503	0.004684
Vertical Stabilizer	1.214	0.801×10^6	0.001484	0.004661
Strake	0.9976	0.659×10^6	0.001636	0.004839
Struts	0.1172	0.774×10^6	0.004773	0.007584

aircraft. To better estimate the skin friction coefficient for each component, a weighted average was used to account for laminar flow on some portions of each component, and turbulent flow on others. Table 3.3 shows the breakdown of how the laminar and turbulent flow was divided up over each component.

Table 3.3: Skin Friction Coefficient Breakdown

Component	S_{wet} (ft^2)	% Laminar	% Turbulent	C_{f_i}	FF_i	Q_i	$\dfrac{\left(C_{f_i} FF_i Q_i S_{wet_i}\right)}{S_{ref}}$
Wing	37.65	20	80	0.003783	1.102	1.000	0.008119
Fuselage	21.51	0	100	0.003386	1.235	1.000	0.004653
Horizontal Stabilizer	8.22	10	90	0.004366	1.036	1.050	0.002019
Vertical Stabilizer	3.76	10	90	0.004343	0.989	1.045	0.000873
Strake	0.84	0	100	0.004839	0.629	1.045	0.000138
Struts	0.43	5	95	0.007443	1.969	1.050	0.000342
						TOTAL	0.01614

Table 3.3 also shows the values of the form factors and interference factors which were used in this analysis. The form factor was calculated by using equation 3.8 for the wing, tail surfaces, and strake. Equation 3.9 was used to determine the form factor for the fuselage. The summation presented as the first term of equation 3.5 is found to equal 0.01614 as shown in the last column of table 3.3.

$$FF = \left[1 + \frac{0.6}{\left(x/c\right)_m}\left(\frac{t}{c}\right) + 100\left(\frac{t}{c}\right)^4\right] \cdot \left[1.34 \cdot M^{0.18}(\cos\Lambda_m)^{0.28}\right] \quad \text{EQ (3.8)}$$

$$FF = \left(1 + \frac{60}{f^3} + \frac{f}{400}\right), \text{ where } f = \frac{l}{d} = \frac{l}{\sqrt{\left(4/\pi\right)A_{max}}} \quad \text{EQ (3.9)}$$

The value of C_{Dmisc} was found by summing values of drag coefficients for the landing gear struts and fairings along with that of the abrupt geometry change due to the windshield. To determine the drag coefficients for these components, equation 3.10 was used. The term D/q is calculated from the skin friction coefficient and the equivalent frontal area of each component.

$$C_D = \frac{D/q}{S_{ref}}, \quad \text{where} \quad D/q = C_f \cdot A_x \quad \text{EQ (3.10)}$$

Using the wing reference area, the D/q values were converted to C_D values. Table 3.4 summarizes the values used in determining C_{Dmisc}. The final value of C_{Dmisc} is found to be 0.004779.

Table 3.4: C_{Dmisc} Build-Up

Component Name	C_f	A_x (ft^2)	C_D
Main Gear Tires and Fairings	0.13	0.1292 x 2	0.001738
Nose Gear Tire and Fairing	0.13	0.0972	0.000654
Main Gear Strut	0.05	0.0486 x 2	0.000251
Nose Gear Strut	0.30	0.0143	0.000222
Windshield	0.07	0.5286	0.001914
		TOTAL	0.004779

Finally, the three terms of equation 3.5 can be summed to determine the final value of C_{Do}. After the first two terms of equation 3.5 are summed, they are then multiplied by 1.075 to account for the 7.5% increase in C_{Do} due to leakage and protuberance drag.

$$C_{D_o} = 1.075 \cdot \left(\frac{\sum \left(C_{f_i} \cdot FF_i \cdot Q_i \cdot S_{wet_i} \right)}{S_{ref}} + C_{D_{misc}} \right) = 1.075 \cdot (0.01614 + 0.004779) = 0.02249$$

The total drag coefficient for the aircraft in cruise configuration was found by summing the values of C_{Do} and C_{Di} presented above in equation 3.3. In the cruise configuration the total drag coefficient is found to be 0.02916.

$$C_D = C_{D_o} + C_{D_i} = 0.02249 + 0.006672 = 0.02916$$

The Drag Polar

The drag polar is used to present the drag coefficient as a function of the lift coefficient. The values for the parasite drag coefficient and the lift induced drag coefficient were determined in the previous section. Equation 3.11 presents the equation for the drag polar for the 1/3-scale C172P. This equation is then used to generate the plot of C_D vs. C_L (the drag polar) found in figure 3.3. This drag polar represents the drag of the aircraft in the cruise configuration.

$$C_D = 0.02249 + 0.05171 \cdot C_L^{\ 2} \qquad\qquad \text{EQ (3.11)}$$

To account for a drag increase due to flap deflection, a $(\Delta C_D)_{FLAPS}$ is added to equation 3.11. The value of $(\Delta C_D)_{FLAPS}$ is also a function of the lift coefficient and will cause the drag polar curve to be shifted upwards when flaps are deflected. At this time, predictions of the effects of flap deflection on lift and drag have not been accomplished.
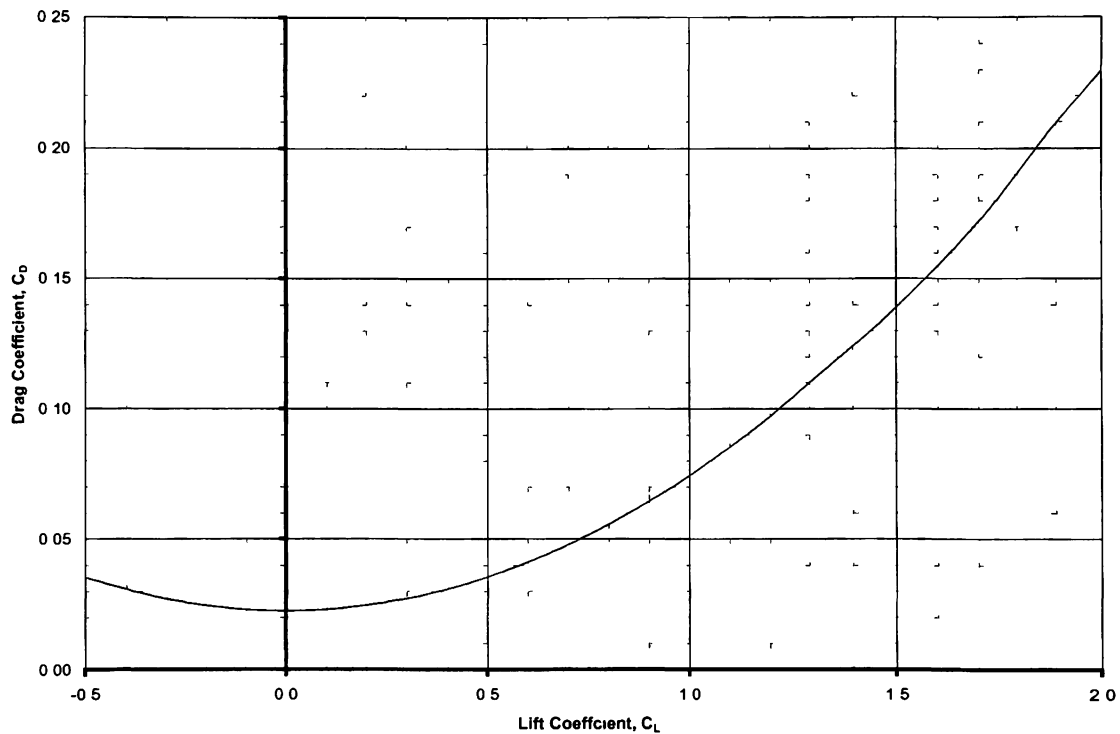
Figure 3.3: 1/3-Scale C172P Drag Polar - Cruise

Power Required and Power Available for Cruise

The amount of power required for maintaining straight and level flight is one of the key factors considered in determining the size of the engine for an aircraft. For the 1/3-scale C172P project, however, the engine size was chosen because of constraints placed upon the project by future goals.

3.11

The engine used in the 1/3-scale C172P must also be used to power the Aquilas model. Because the Aquilas model is larger and heavier, the power it requires is significantly larger than that of the 1/3-scale C172P. The engine chosen as the powerplant for both aircraft is the Quadra Aerrow Q-100XL (see figure B.3 in appendix B). This engine has a single-cylinder with a displacement of 98 cubic centimeters (6.0 cubic inches). The maximum rated power output is 9.9 Hp. The recommended propeller size is 25 inches in diameter with an 11 inch pitch. The thrust available from this propeller/engine combination is estimated at approximately 50 lbs static.

While the performance characteristics of the chosen engine/propeller combination seem far excessive for this project, this excessive margin is reduced when considering the Aquilas. Due to the unfamiliar nature of this project, a powerplant with excessive performance potential was determined to be necessary in order to provide an adequate safety margin.

To determine the amount of power required for cruise flight, the aircraft drag force is converted to power required. The drag coefficient is converted to drag force in pounds by using the definition of drag coefficient: $D = C_D \cdot Q \cdot S_{ref}$. Since the 1/3-scale C172P is intended to be flown at altitudes below 1,000 ft, the cruise altitude is assumed to be equal to sea level in all calculations. Using sea level standard conditions at a speed of 103.8 ft/s, the drag force on the 1/3-scale C172P during cruise was found to be 7.22 lb.

Straight and level flight requires that the lift equal the weight and the thrust equal the drag. Multiplying the thrust or drag by velocity allows a conversion from force to power. Drag times velocity gives the power required to maintain straight and level flight. Figure 3.4 shows the power required and power available for the 1/3-scale C172P at sea level during cruise.
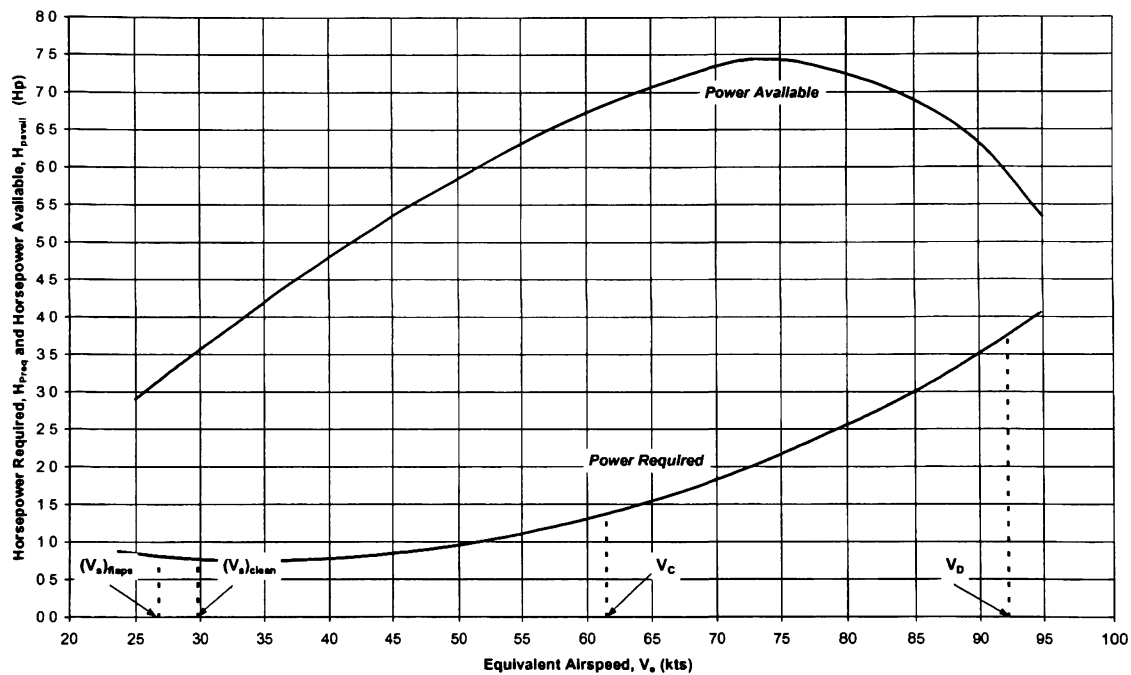
Figure 3.4: 1/3-Scale C172P Cruise Horsepower Required vs. Velocity

The power available curve shown is an approximation of the amount of horsepower available, at the prop, for translation into thrust. This curve is typical of the relationship of power available to forward velocity for a fixed-pitch, two-bladed propeller. The peak of the curve has been intentionally shifted to a speed higher than cruise to assure enough power available at the highest speeds. This relationship varies with propeller characteristics and will need to be refined once engine/propeller testing is accomplished.

3.13

This power available curve also represents a propeller efficiency of 75%. Although 75% efficiency is considered rather low, it is conservative. Regardless, a propeller with at least this minimum level of performance will provide sufficient excess power throughout the entire flight spectrum.

Maximum Lift and Lift Curve Slope Estimation

The estimation of the maximum lift coefficient was conducted using the methods presented in reference 1. Equation 3.12 was used to estimate the clean wing C_{Lmax}. A 2-dimensional airfoil maximum lift coefficient (C_{lmax}) of 1.60 was found from reference 6

$$C_{L\,max} = 0.9 \cdot C_{l\,max} \cdot \cos\Lambda_{0.25c} \qquad \text{(EQ 3.12)}$$

for the NACA 2412. From figure 3.2, the value of wing quarter chord sweep ($\Lambda_{0.25c}$) used was −0.2 deg, making equation 3.12 reduce to approximately 0.9 times the 2-D max lift coefficient. The 3-D, clean wing C_{Lmax} is, therefore, estimated at 1.44 (the full-scale aircraft C_{Lmax} is 1.55)

The maximum lift coefficient for max flap deflection (35 degrees) was estimated by using a ΔC_{Lmax} value found using equation 3.13. This equation is presented in

$$\Delta C_{L\,max} = \Delta C_{l\,max}\left(\frac{S_{flapped}}{S_{ref}}\right)\cos\Lambda_{HL} \qquad \text{(EQ 3.13)}$$

3.14

reference 1 for fowler type flaps. The ratio of flapped planform area to reference wing area denotes the extension of the flap rearwards that is characteristic of fowler type flaps. The angle of the flap hinge line (Λ_{HL}) is zero for the C172P. The increment in lift from equation 3.13 is estimated at 0.58 pushing the flapped C_{Lmax} up to 2.02. This estimated flapped maximum lift coefficient is believed to be an overestimate since the full-scale aircraft value for C_{Lmax} with full flaps is 1.92. For this reason, the full flaps maximum lift coefficient used throughout the analysis of the 1/3-scale C172P is 1.92.

An estimate of the three-dimensional lift curve slope was conducted using equation 3.14 (from reference 1). The 2-D lift curve slope was found from reference 6 to be 0.1046 deg^{-1} or 5.9982 rad^{-1}. The value of τ (0.03) used in this equation is a function

$$C_{L\alpha} = \frac{C_{l\alpha}}{1 + \frac{C_{l\alpha}}{\pi \cdot AR}(1+\tau)} \qquad \text{(EQ 3.14)}$$

of the wing taper ratio (c_t/c_r) of 0.679. Therefore, the 3-D clean wing lift curve slope is estimated at 0.1041 deg^{-1} or 5.9657 rad^{-1}.

Hinge Moment Estimation

Hinge moment estimations were made in order to properly size the servo actuators needed to drive the control surfaces. The author conducted this estimation for the elevator and rudder. The students who conducted the original wing structural analysis estimated the hinge moments for the aileron and flap.

The NACA 0009 airfoil is used for the tail surfaces. From reference 2, for a

NACA 0009 with a control surface chord to stabilizer chord ratio of 0.3, estimates of the

2-D hinge moment derivatives $c_{h\alpha}$ and $c_{h\delta}$ were made at -0.0075 and -0.013, respectively.

These values were then adjusted to account for 3-D effects for both stabilizers. The

adjusted derivatives were used then used in equation 4.15 to determine the estimated

hinge moments for the horizontal and vertical stabilizers. Therefore, the

$$ HM = C_h \cdot \frac{1}{2} \cdot \rho \cdot V^2 \cdot S_c \cdot \overline{c_c} \qquad \text{(EQ 4.15)} $$

elevator and rudder servos must be sized to accommodate control surface torques of 78.9

in-oz and 91.1 in-oz, respectively. The value given for horizontal stabilizer hinge

moment is per side since two servos are used to actuate the elevator.

Stability Axis Reference Frame

The reference frame used for the analysis of stability and control characteristics of

an aircraft is the stability axis. The stability axis differs in orientation from the body axis

by the angle of attack. By definition, the stability X-axis begins at the aircraft's CG and

points down the component of the velocity vector that exists in the body axis X-Z plane.

This causes the stability Z-axis to be rotated in the body axis X-Z plane also by the angle

of attack. The stability Y-axis and the body Y-axis both remain collinear and point

directly out the right side of the aircraft. Figures 3.5 and 3.5 show the stability and body

reference frames in their proper orientation.
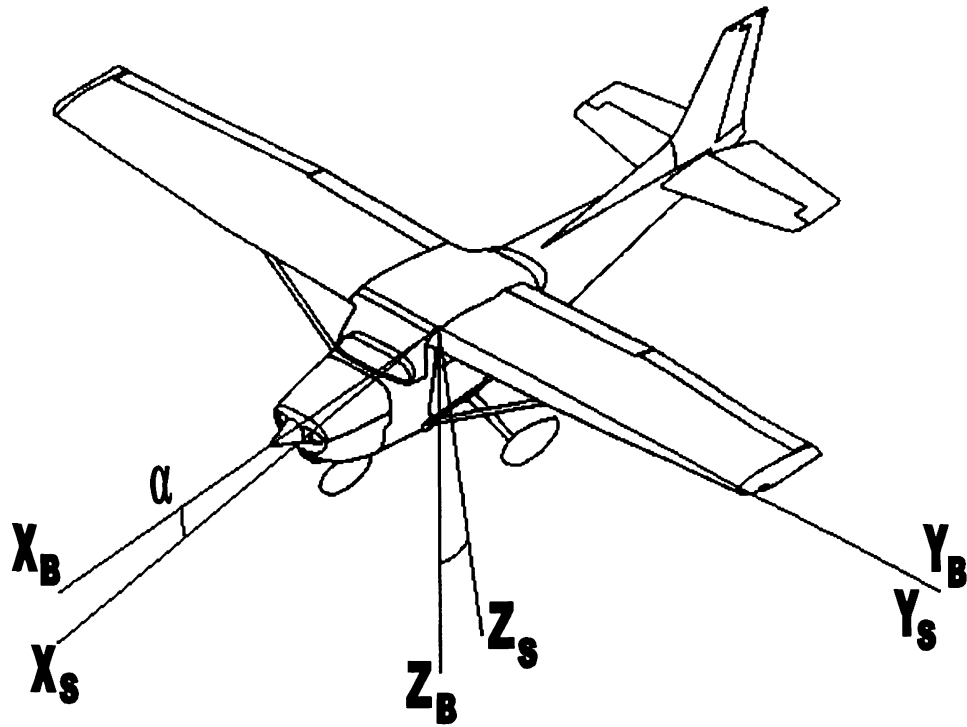
Figure 3.5: Stability and Body Axes Orientations – Orthographic Projection
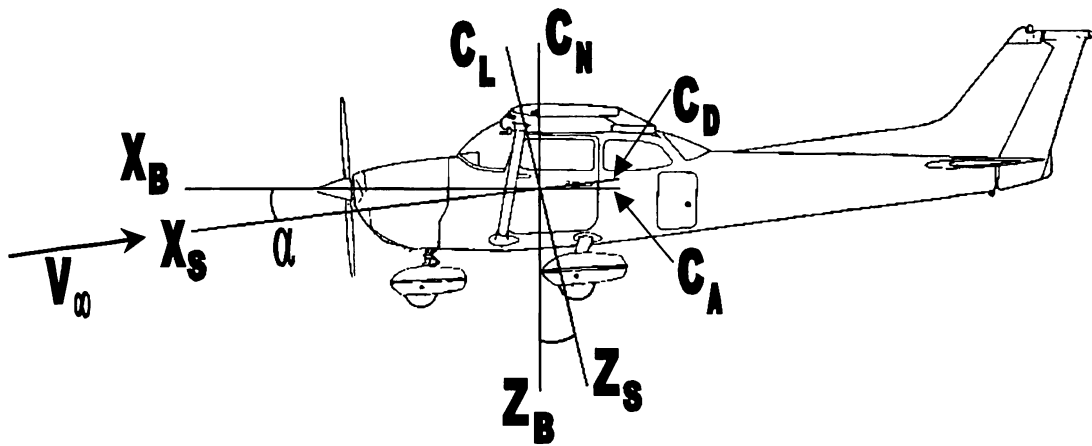
Figure 3.6: Stability and Body Axes Orientations – Side View

The advantage to the distinction between the body and stability reference frames

is seen in the basic summation of forces along each of the axis of each of the reference

frames. Since the stability axis is aligned with the relative wind vector, the summation of

forces in the stability Z-axis yields the lift coefficient. Summation of forces in the body Z-axis direction yields the normal force coefficient, which is usually not as easy to work with as the lift coefficient. Similarly, summation of the forces in the stability X-axis yields the drag coefficient while summation of the body X-axis forces yields the axial force coefficient. Since the stability and body Y-axes are collinear, summation of forces along these axes will both yield the side force coefficient. At an angle of attack of zero, the stability and body reference frames are aligned. In this specific case, the normal force coefficient equals the lift coefficient and the axial force coefficient equals the drag coefficient.

An example of the differences encountered in the use of dissimilar reference frames is found during the analysis of level flight performance. By definition, the thrust vector is fixed with respect to the body reference frame. Often, this thrust vector is aligned at an incidence angle with respect to the body X-axis, to help reduce pitching moments or gyroscopic effects. Only during straight and level flight, at an angle of attack equal to the negative of the incidence angle of the thrust vector, is the thrust truly equal to the drag. In straight and level flight, for angles of attack where the stability and body axes are not coincident, the stability X-axis component of thrust must equal the drag. Similarly, the body X-axis component of thrust must equal the axial force. In many cases, the small angle approximation can be applied during non-accelerated flight allowing the simplification of "thrust equals drag" to be applied.

Stability and Control Derivatives

The equations of motion for an aircraft in flight can be reduced to a set of simultaneous homogeneous differential equations with constant coefficients. The constant coefficients of these equations are the aircraft's flight characteristics such as velocity (u, v, w), orientation (θ, ϕ, ψ), mass moments of inertia (I_{xx}, I_{yy}, I_{zz}), and control surface deflections $(\delta_e, \delta_a, \delta_r)$. The derivatives in this system of differential equations are the stability and control derivatives.

The solution of the six-degree-of-freedom system of equations and the theoretical estimations of all of the stability and control derivatives is beyond the scope of this project and is not discussed here. Data collected during testing of a flight test vehicle (the 1/3-scale C172P included) can be used to quantify some of the stability and control derivatives in order to verify theoretical estimates. However, many of the derivatives can not be directly measured on an aircraft in flight due to the lack of physical constraints. For these parameters, estimates must be made from the effect they have on other flight characteristics.

The design of the data acquisition system on-board the 1/3-scale C172P will allow the determination of some of the key stability and control characteristics from data collected during flight testing. For example, derivatives, such as elevator power $(C_{m\delta e})$ and rudder power $(C_{n\delta r})$, can be found by measuring control surface deflections with the aircraft placed at trimmed pitch or yaw angles. Characteristics such as dynamic stability can be evaluated using time history plots of aircraft response to pilot induced

disturbances. Even the stick-fixed neutral point can be located by flying with the c.g. moved progressively further aft until the aircraft becomes neutrally stable (statically).

The remainder of this section describes how determinations of the acceptability of the aircraft's response can be made if the response to control input is known.

Longitudinal Control: Longitudinal controllability is characterized by the ability of the elevator to change the pitch attitude of the aircraft. Deflection of the elevator results in a pitching rate, about the center of gravity, denoted by q and given in radians per second (rad/s). A positive elevator deflection (trailing edge down) should cause a nose down pitching moment about the c.g. During flight, acceptable aircraft response to elevator input can be determined if, when trailing edge up deflection is commanded, a nose up pitching moment is generated causing the aircraft to also pitch up.

Static Longitudinal Stability: Acceptable static longitudinal stability requires that the aircraft move toward equilibrium when displaced by a vertical disturbance such as a wind gust. During flight, if a trailing edge up elevator input is commanded, the aircraft should pitch up (and decelerate). When the elevator input is removed, the aircraft must readily pitch down (and accelerate) towards the original trim attitude (and speed). The opposite must also be true for a trailing edge down input.

Dynamic Longitudinal Stability: When the aircraft encounters a wind gust or step control input (sometimes termed an elevator doublet), its response will be a function of the time

duration of the input signal. A short duration input should cause the aircraft to pitch up and down in a second-order, highly damped cycle. This is termed the short period mode of response. A long duration input will excite the aircraft's Phugoid (or long-period) second-order cyclic response.

During flight testing, a pitch doublet (short-period) should cause a cyclic pitch response that quickly dampens. A long-period pitch doublet should cause a Phugoid response that dampens to 1/10 amplitude after two complete cycles.

Lateral-Directional Control: The ability of the ailerons and rudder to change the roll and yaw attitudes, respectively, determine the lateral-directional controllability of the aircraft. Since the lateral and directional motions are closely coupled, they are often analyzed together. Aileron deflection results directly in a roll rate about the X-axis in the stability reference frame. Deflection of the rudder results in a yaw rate about the Z-axis (again in the stability reference frame). During flight, acceptable response to aileron control input requires that a positive roll (left wing up, right wing down) initiates due to positive aileron deflection (left aileron trailing edge down, right aileron trailing edge up). Acceptable rudder response will swing the nose to the right (positive sideslip) when the rudder is deflected trailing edge right.

Static Lateral-Directional Stability: Aircraft response to a displacement of roll or sideslip angle must be towards equilibrium. When the aircraft is displaced to a roll angle, ϕ, a restoring rolling moment must be generated that lowers the high wing and returns the

aircraft to its trimmed condition. Similarly, when the aircraft is displaced to a sideslip angle, β, a restoring yawing moment must exist to return the aircraft toward equilibrium. During flight, after a positive roll control input is applied, the aircraft will roll to the right. When the control input is removed, the aircraft should naturally roll to the left towards equilibrium. Positive rudder control can also be applied, displacing the nose to the right. Releasing the rudder input should result in immediate movement towards the left (towards equilibrium).

Dynamic Lateral-Directional Stability: An aircraft has multiple dynamic responses to aileron or rudder inputs (or wind gusts). The most notable of these is an occasionally mildly damped oscillation both laterally and directionally known as Dutch roll. Commanding a rudder doublet during flight can initiate a Dutch roll response. Similarly to the Phugoid response, the Dutch roll oscillations should dampen quickly to be considered acceptable. Due to the characteristics of the 1/3-scale C172P, excitation of the Dutch roll response may be difficult.

3.4: Component Weight Estimation

A preliminary estimation of the weight of each component of the 1/3-scale C172P was conducted. Knowledge of the individual component weights allows for the estimation of the moments of inertia that determine the aircraft's dynamic response. During the construction phase, the weight estimations presented here provided weight and tolerance goals for the individual pieces.

The procedure used to estimate the individual component weights came from pages 404-407 of ref. 1. Equations A.1 through A.11 in appendix A were used to determine the weights of the various components of the aircraft. Table 3.5 presents the values of the parameters used in these equations.

Table 3.5: Weight Estimation Parameters

Parameter	Value	Description	Parameter	Value	Description
S_w	19.33	Wing reference area (ft^2)	H_t/H_v	0.0	0.0 for conventional tail
W_{fw}	5.6	Weight of fuel in wing (lb)	S_f	20.2	Fuselage wetted area (ft^2)
A_w	7.29	Wing aspect ratio	L_t	4.76	Tail length (ft)
A_h	3.62	Horizontal tail aspect ratio	(L/D)	5.5	Fuselage fineness ratio
A_v	0.93	Vertical tail aspect ratio	W_{pres}	0.0	Weight of pressurization sys.
Λ_w	0.0035	Wing c/4 sweep angle (rad)	N_l	4.5	Ultimate landing load factor
Λ_h	0.0751	H. tail c/4 sweep angle (rad)	W_l	88.9	Landing gross weight (lb)
Λ_v	0.5707	V. tail c/4 sweep angle (rad)	L_m	5.85	Main gear length (in)
λ_w	0.657	Wing taper ratio	L_n	7.50	Nose gear length (in)
λ_h	0.571	H. tail taper ratio	W_{en}	7.1	Uninstalled engine weight (lb)
λ_v	0.519	V. tail taper ratio	V_t	1.5	Total fuel volume (gal)
$(t/c)_w$	0.12	Wing thickness to chord ratio	Vi/Vt	0.62	Fuel in wing/total fuel
$(t/c)_h$	0.09	H. tail thickness to chord ratio	N_t	3	Number of fuel tanks
$(t/c)_v$	0.09	V. tail thickness to chord ratio	L	7.32	Fuselage length (ft)
N_z	8.7	Ultimate load factor	B_w	12.0	Wing span (ft)
W_{dg}	88.9	Design gross weight (lb)	S_v	1.93	V. tail area (ft^2)
q	12.8	Cruise dynamic pressure (psf)	N_{en}	1	Number of engines
S_{ht}	4.12	H. tail planform area (ft^2)	W_{uav}	~10	Uninstalled avionics wt. (lb)

Table 3.6 shows the final calculated weights of each of the components of the 1/3-scale C172P. Notice that the final estimated empty weight of the aircraft constitutes 66.9% of the maximum takeoff weight (W_{dg}) of 88.9 lbs. The remaining 30.1% (29.42 lbs) is available for ballasting the aircraft to obtain the proper mass moments of inertia.

3.23

Table 3.6: 1/3-Scale C172P Component Weights

Component	Estimated Weight (lb)	Percentage of Max Takeoff Wt (%)
Wing	13.87	15.6
Horizontal Tail	1.13	1.3
Vertical Tail	0.73	0.8
Fuselage	6.67	7.5
Main Landing Gear	7.06	7.9
Nose Landing Gear	8.37	9.4
Engine (installed)	15.69	17.7
Fuel System	3.66	4.1
Flight Controls System	2.31	2.6
TOTAL	59.47 lb	66.9%

3.5: 1/3-Scale Structural Substantiation

Detailed structural analysis was conducted on various key components of the 1/3-scale C172P to ensure the proper sizing of these structural members. Professor Eastlake's Detail Design students during the fall semester 1997 completed the original analysis of the wing, fuselage, and tail. An engine mount was designed during the summer of 1998 by a group of students in Dr. Ladesic's detail design class. The final engine mount constructed for use on the 1/3-scale C172P differed slightly from this design (see section 4.2). This section discusses the procedures used in the structural design.

Loading Diagram (V-n)

The method used to determine the 1/3-scale C172P's loading diagram was similar to that which would be used for a full-scale aircraft. Reference 8 describes the procedure used in this project for constructing the V-n diagram. The following describes the analysis results.

The final loading diagram is actually a composite of the maneuver diagram and the gust load diagram. The maneuver diagram is used to show the maximum positive and negative static loads that the aircraft must be able to withstand. The gust load diagram is used to expand the maneuver diagram such that those loads that could be encountered during a wind gust in flight will not overstress the aircraft. The gust load lines used in the analysis of the 1/3-scale C172P were calculated with gust velocities of 50 ft/s up to cruise speed and 25 ft/s up to the design dive speed. The same gust velocity is not used at both points on the diagram because it is assumed that, should large turbulent gust velocities be encountered at the design dive speed, the pilot would slow down to a speed at which the gusts no longer threaten to overstress the aircraft.

The first step in constructing the V-n diagram was to determine the cruise and design dive speeds for the 1/3-scale C172P. At an altitude of 8000 ft., a full-scale C172P cruises at 138 mph. This speed, corrected to sea level, equates to 179.5 ft/s. Using the scaling laws discussed in section 2.1, the 1/3-scale C172P's cruise speed was calculated to be 103.8 ft/s, or 61.5 kts. (at sea level). The design dive speed, which is defined as $1.5V_{cruise}$, was determined to be 155.6 ft/s, or 92.2 kts.

Estimation of the maximum lift coefficients in clean and flapped configurations is discussed in section 3.3. The values of C_{Lmax} used here are 1.55 for the clean configuration and 1.92 for the aircraft in the landing configuration (flaps full). Equation 3.17 was used to construct the positive and negative load lines on the V-n diagram. To generate the gust load lines, equation 3.18 was used. Note that the units of the velocity

3.25

term in equation 3.8 are knots equivalent while the velocity term used in equation 3.7 is

expressed in ft/s. The total aircraft lift curve slope, $C_{L\alpha A}$, used in

$$L = n_z \cdot C_{L\max} \cdot \frac{1}{2} \rho \cdot V^2 \cdot S_{ref} \qquad \text{EQ (3.16)}$$

$$n_z = \left(\frac{W}{S_{ref}}\right)^{-1} C_{L\max} \cdot \frac{1}{2} \rho \cdot V^2 \qquad \text{EQ (3.17)}$$

After substitutions: $n_z = 0.0002584 \cdot C_{L\max} \cdot V^2$

equation 3.8 was determined in section 3.3 to be 5.97 rad/s. Equation 3.19 was used to

find the value of K_g. The gust velocities used in the generation of the loading diagram

were +/- 25 ft/s

$$n = 1 \pm \frac{K_g U_{de} V_e C_{L\alpha A}}{498\left(\dfrac{W}{S}\right)} \qquad \text{EQ (3.18)}$$

After substitutions: $n = 1 \pm 0.001543 \cdot U_{gust} \cdot V_e$

$$K_g = \frac{0.88\mu}{5.3 + \mu}, \text{ where } \mu = \frac{2\dfrac{W}{S}}{g\bar{c}\rho C_{L\alpha A}} \qquad \text{EQ (3.19)}$$

and +/- 50 ft/s, as stated earlier. No scaling factor was applied to the gust velocities since

the 1/3-scale C172P will fly through the same atmosphere as the full-scale C172P and,

therefore, will experience the same gust magnitudes. The low wing loading of the 1/3-

3.26

scale C172P increases the slope of the gust lines causing the loading diagram to be expanded, when compared to the full-scale aircraft. The expansion of the V-n diagram results in maximum and minimum load factors, for the 1/3-scale aircraft, that are greater in magnitude than the load factors used in the design of the full-scale aircraft. In the case of this project, the gust lines presented on the loading diagram in figure 3.7 stretched the maximum positive load factor from 3.8 to 5.8 g. The minimum load factor was found to be −3.8 g (down from −1.9 g). Table 3.7 contains the velocities and load factors at some of the important points on the loading diagram in figure 3.7.

Table 3.7: Key Velocities and Load Factors from the V-n Diagram

V-n Diagram Point	Velocity (kts)	Positive n_z (g)	Negative n_z (g)
Stall (flaps full), V_{S0}	26.8	0.9	-0.8
Stall (clean), V_S	29.8	1.2	-0.9
Max Full Flap Speed	38.9	2.0	-1.6
Max Partial Flap Speed	43.6	2.0	-2.0
Maneuver, V_A	60.0	3.8	-3.7
Cruise, V_C	61.5	5.7	-3.8
Design Dive, V_D	92.2	4.6	-2.6
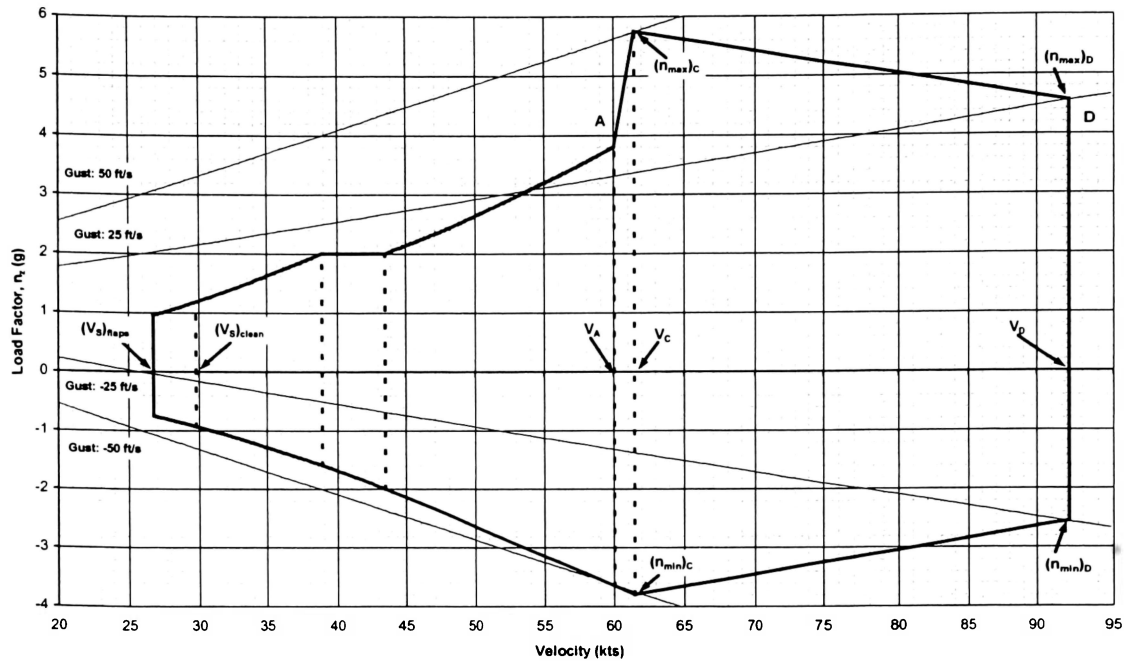
Figure 3.7: 1/3-Scale C172P Loading Diagram (V-n)

Materials Testing: Experimental Determination of the Allowables

The materials used to construct the 1/3-scale C172P were to be purchased from suppliers that may or may not be vendors of certified materials. Because of this, the theoretical stress allowables for each material type could not be guaranteed. Therefore, it was decided that experimental determination of the stress allowables for each material type would be conducted.

Six samples each of balsa, spruce, and birch plywood were fabricated and tensile tested in the Materials Testing lab at ERAU. The samples were sized in accordance with the configuration shown in figure 3.8. Figure B.1 shows a sample being tested in the Dillon Dynamometer at ERAU. Table 3.8 shows the results of this testing.
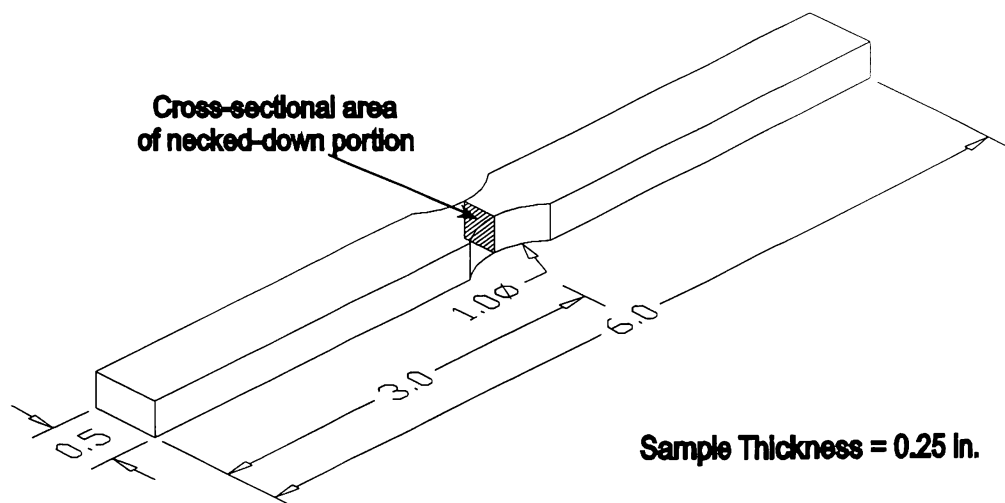
Figure 3.8: Tensile Test Sample Configuration

Table 3.8: Experimental Determination of Material Allowables – Results

Sample #	Neck Width (in)	Neck Thickness (in)	Neck Cross-Sectional Area (in^2)	Tested Ultimate Strength (lb)	Resulting Ultimate Tensile Stress (psi)
Balsa - 1	0.25	0.25	0.0625	130	2080
Balsa - 2	0.25	0.25	0.0625	244*	3904*
Balsa - 3	0.25	0.25	0.0625	108	1728
Balsa - 4	0.25	0.25	0.0625	101	1616
Balsa - 5	0.25	0.25	0.0625	220*	3520*
Balsa - 6	0.25	0.25	0.0625	108	1728
Spruce - 1	0.25	0.25	0.0625	1275	20400
Spruce - 2	0.25	0.25	0.0625	1100	17600
Spruce - 3	0.25	0.25	0.0625	1320	21120
Spruce - 4	0.25	0.25	0.0625	1160	18560
Spruce - 5	0.25	0.25	0.0625	1200	19200
Spruce - 6	0.25	0.25	0.0625	935	14960
Ply - 1	0.25	0.25	0.0625	900	14400
Ply - 2	0.25	0.25	0.0625	1400	22400
Ply - 3	0.25	0.25	0.0625	1075	17200
Ply - 4	0.25	0.25	0.0625	1025	16400
Ply - 5	0.25	0.25	0.0625	1150	18400
Ply - 6	0.25	0.25	0.0625	1050	16800

*NOTE: These samples exhibited grip failures rather than neck failures.

The results of this testing were both unexpected and promising. The majority of the samples ruptured ultimately at unexpectedly high tensile stress levels while the scatter of the data showed the irrepeatability of wood. Because the tested ultimate tensile stress

3.29

levels were higher than expected, confidence was gained in the final chosen values for the material allowables.

The balsa samples that failed as expected (1, 3, 4, and 6) resulted in an average ultimate tensile stress of 1788 psi. The average stress levels for the spruce and plywood samples were 18640 and 17600 psi, respectively. These average values correspond reasonably well with the accepted allowables for dry wood found ANC-18 (reference 7). The values from ANC-18 are given in table 3.9 for both wet and dry wood.

Table 3.9: Material Allowables from ANC-18

Wood Type	Moisture Content / Specific Gravity	Modulus of Rupture (Static Bending) (psi)	Shear Strength Parallel to grain (psi)
Balsa	Dry / 0.17	2,800	100
Sitka Spruce	Green / 0.37	5,700	760
Sitka Spruce	Dry / 0.40	10,200	1,150
Birch (Paper)	Green / 0.48	6,400	840
Birch (Paper)	Dry / 0.55	12,300	1,210

Notice that the allowable given in ANC-18 for balsa wood is higher than the experimentally determined value. For this, and other reasons, it was decided that balsa would not be used for structural components.

The values given for dry spruce and birch in table 3.9 are considerably lower than those found during testing. This can be attributed to the following: 1) the values given in ANC-18 represent minimum values, and 2) the tensile stress due to static bending (My/I) is less than that of pure tension (P/A) for a given load. Table 3.10 shows the final allowables used throughout this project. The values chosen correspond to the wet wood values found in ANC-18. The reason for this was to provide a high factor of safety to

3.30

help account for material defects and fastening inconsistencies. In the following sections, these allowables are further reduced, increasing the factor of safety. Even with all of the safety factor padding, it is not believed that the structural weight will become a limiting factor.

Table 3.10: Final Material Allowables

Material Type	Allowable Ultimate Tensile Stress (psi)	Allowable Ultimate Shear Stress (psi)
Spruce	5,700	760
Birch (plywood)	6,400	840

Analysis of the Tail

The structural analyses of the vertical and horizontal stabilizers were conducted using the same methodology and, therefore, are presented together in this section. The analysis of the wing, described in the next section, was done using a similar method

The structural analysis of the tail components started with a few basic assumptions as follows:

1. The maximum lift coefficient of each surface is 1.0
2. The lift distribution can be approximated using the Prandtl lifting line theory
3. The spar caps carry the entire bending stress load
4. The shear web carries the entire shear stress load
5. The front spar is capable of carrying the entire load of the surface (i.e. no load on the rear spar)

The analysis began by using Prandtl's Lifting-Line theory to determine the lift coefficient distribution on the lifting surface based upon inputs of key airfoil and

geometrical characteristics. Table 3.11 shows the characteristics that were used to describe the vertical and horizontal stabilizers. Table 3.12 shows the resulting lift coefficient distributions for these surfaces (at the angle of attack that produces an overall surface lift coefficient of 1.0).

Table 3.11: Vertical and Horizontal Stabilizer Characteristics for Lift Distribution

Characteristic	Vertical Stabilizer Value	Horizontal Stabilizer Value
Aspect Ratio	1.185	1.693
Taper Ratio	0.5337	0.5878
Centerline Chord (in)	18.53	17.66
Centerline Lift Curve Slope (1/rad)	6.1364	6.1364
Tip Lift Curve Slope (1/rad)	6.1364	6.1364
Centerline Zero Lift Angle (deg)	0.0	0.0
Tip Zero Lift Angle (deg)	0.0	0.0
Washout (deg)	0.0	0.0

Table 3.12: Lift Coefficient Distributions – Vertical and Horizontal Stabilizers

Spanwise Location (Y/b)	Vertical Stabilizer Lift Distribution	Horizontal Stabilizer Lift Distribution
1.0000	0.0000	0.0000
0.9969	0.1572	0.1544
0.9724	0.4507	0.4419
0.9239	0.6928	0.6785
0.8526	0.8714	0.8537
0.7604	0.9929	0.9762
0.6494	1.0637	1.0521
0.5225	1.0910	1.0867
0.3827	1.0870	1.0922
0.2334	1.0580	1.0734
0.0785	1.0063	1.0306
0.0000	0.9800	1.0200

The lift distributions from table 3.12 were then translated into shear and bending moment distributions to find the maximum value of each. The maximum values of shear and bending moment on the vertical spar are 21.8 lb. and 168.5 in.-lb., respectively. The similar maximums for the horizontal spar are 26.5 lb. and 253.7 in.-lb.

3.32

Using the equation for bending stress in a beam (equation 3.20), a relationship between bending stress and moment of inertia was found for each stabilizer surface (equations 3.21a and 3.21b).

$$f_{bend} = \frac{M \cdot y}{I} \qquad \text{(EQ 3.20)}$$

$$\left(f_{bend}\right)_{\text{Vert.Stab.}} = \frac{139.13}{(I)_{\text{Vert.Spar}}} \quad \text{(EQ 3.21a)} \qquad \left(f_{bend}\right)_{\text{Horiz.stab}} = \frac{199.67}{(I)_{\text{Horiz.Spar}}} \quad \text{(EQ 3.21b)}$$

The material allowables from the previous section were then used to specify the upper limit of bending stress for equations 3.21a and 3.21b. The value of allowable stress given for spruce (5700 psi) was first reduced by a knock-down factor of 0.99. A factor of safety of 2 was also used to further reduce the allowable to 2822 psi. Rearranging equations 3.21a and 3.21b (and using this material allowable) and then solving for I gives minimum values of moment of inertia for the vertical and horizontal stabilizer spars of 0.0430 and 0.0907 in^4, respectively.

A matrix of area moments of inertia was generated for each of the vertical and horizontal stabilizer spars using a series of nominal material dimensions (every 1/16 in) and the spar heights for each spar. The specified minimum moment of inertia values were then compared with this matrix until a suitable combination of spar cap thickness and width were chosen. The spar cap dimensions chosen for the vertical and horizontal stabilizers are shown in table 3.13.

The dimensions of the shear web were found in a similar fashion to the spar caps. The overall spar height at the root minus the cap thickness dictates the height of the web offering only web thickness as a variable. Equation 3.22 shows the formula used for determining the shear stress due to a bending load. The web thickness must be large enough to support this stress.

$$f_{H.Shear} = \frac{V \cdot Q}{I \cdot t}$$ (EQ 3.22)

The material allowable for birch plywood was used in sizing the shear web. The value given earlier (6400 psi) was reduced by both a 0.99 knock-down factor and a factor of safety of 2 yielding a new allowable of 3168 psi. Using this new value, the minimum thickness required for each shear web was calculated from equation 3.22 as 0.0167 in. for the vertical stabilizer and 0.0212 in. for the horizontal stabilizer. These minimum thickness values are each less than 1/32 in. For added stiffness, manufacturing ease, and overall shear web stability, a 1/8 in. thickness was chosen. Table 3.13 shows the final dimensions for the shear webs for the stabilizer front spars.

Table 3.13: Stabilizer Spar Dimensions

Dimension	Vertical Stabilizer	Horizontal Stabilizer
Overall Spar height (at root) (in)	1.651	1.574
Cap Thickness (in)	0.125 (1/8)	0.188 (3/16)
Cap Width (in)	0.500 (1/2)	0.500 (1/2)
Web Thickness (in)	0.125 (1/8)	0.125 (1/8)
Web Height (in)	1.401	1.195

Analysis of the Wing

Structural analysis of the wing followed much the same procedure as that of the stabilizers. A modified version of the list of assumptions given for the stabilizer analysis was used for the wing analysis. The following assumptions were used.

1. The lift distribution can be approximated using the Prandtl lifting line theory

2. The spar caps carry the entire bending stress load

3. The shear web carries the entire shear stress load

4. The front spar is capable of carrying the entire load of the surface (i.e. no load on the rear spar)

5. The wing struts are non-structural and do not contribute to the load carrying capacity of the wing

The wing of the C172P consists of a constant chord section inboard and a straight tapered section outboard as shown in figure 3.9. Since the MS Excel spreadsheet that was used to approximate the lift distribution is only capable of using a constant taper ratio, the lift distribution was estimated using a blend of the results of a wing of constant chord and a wing of constant taper.
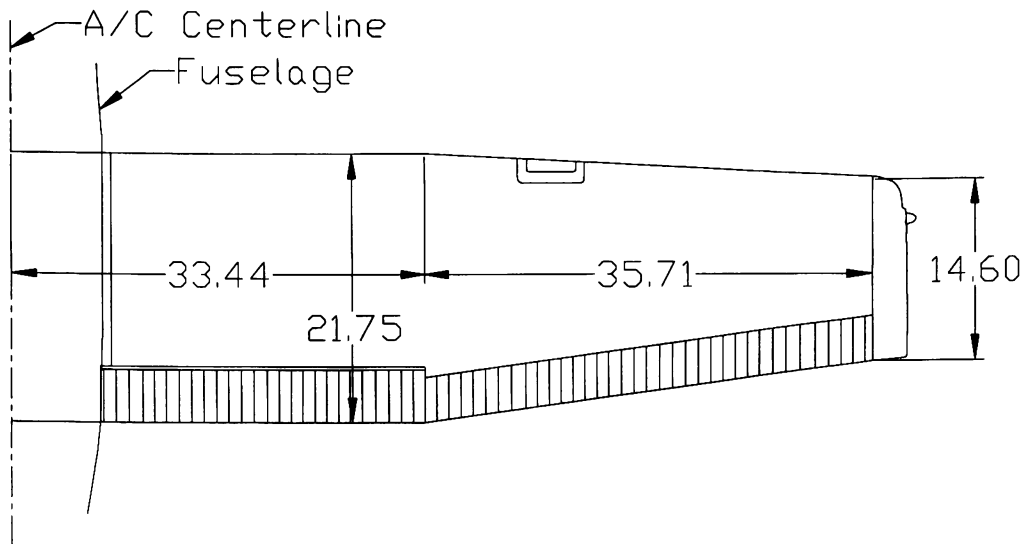
Figure 3.9: C172P Wing Planform

Table 3.14 shows the resulting lift distributions for a clean wing ($C_{Lmax} = 1.55$)

and for flaps deployed ($C_{Lmax} = 1.92$). The average lift distribution for each configuration

was then translated into a load distribution using the maximum load factor that

corresponds to that configuration. At 1g, the lift with flaps deployed is greater than the

lift for a clean wing. However, after examining the load distributions at the maximum

load factor corresponding to each configuration, the clean aircraft was shown to be the

worst case for this aircraft due to its maximum load factor of 5.8g.

Table 3.14: Wing Lift Distribution

$C_{Lmax} = 1.92$

y/b	$(C_l)_{l=1.0}$	$(C_l)_{l=0.682}$	Average C_l
1.000	0.000	0.000	0.000
0.997	0.313	0.354	0.334
0.972	0.867	0.969	0.918
0.924	1.284	1.401	1.343
0.853	1.570	1.660	1.615
0.760	1.781	1.842	1.812
0.649	1.938	1.966	1.952
0.522	2.040	2.023	2.032
0.383	2.125	2.067	2.096
0.233	2.194	2.093	2.144
0.078	2.225	2.060	2.143
0.000	2.235	2.037	2.136

$C_{Lmax} = 1.55$

y/b	$(C_l)_{l=1.0}$	$(C_l)_{l=0.682}$	Average C_l
1.000	0.000	0.000	0.000
0.997	0.250	0.282	0.266
0.972	0.692	0.772	0.732
0.924	1.026	1.119	1.073
0.853	1.256	1.327	1.292
0.760	1.428	1.476	1.452
0.649	1.558	1.580	1.569
0.522	1.645	1.630	1.638
0.383	1.719	1.671	1.695
0.233	1.780	1.697	1.739
0.078	1.809	1.674	1.742
0.000	1.815	1.665	1.740

For the clean wing at 5.8g, the maximum shear was found to be 271.2 lb. and the maximum bending moment was found to be 8447 in-lb. These were the values used in the remainder of the analysis.

Similarly to the analysis of the stabilizers, the spar caps were sized using the equation for stress due to bending (equation 3.20). The allowable used in the analysis of the wing differed from that used in the analysis of the stabilizers to reduce the amount of material. The allowable corresponding to spruce from table 3.10 was multiplied by a 0.99 knock-down factor and a factor of safety of 1.5 producing a final allowable for the wing

3.37

spar caps of 3762 psi. Unlike the stabilizers, it was decided that the wing would utilize a

tapered spar cap to further eliminate material and save weight. Table 3.15 shows the ten

wing stations used in the tapering calculations. The full spar height, local bending

moment, and minimum section moment of inertia are also given.

Table 3.15: Tapered Wing Spar Cap Sizing

Distance from root, y (in)	Full Spar Height at y (in)	Bending Moment at y (in-lb)	Minimum Moment of Inertia (in^4)
0.00	2.588	8446.6	2.905
5.62	2.588	6996.1	2.406
16.78	2.588	4543.3	1.563
27.58	2.588	2709.8	0.932
33.40	2.588	2000.0	0.688
37.58	2.500	1471.6	0.489
46.73	2.305	702.2	0.215
54.72	2.134	282.4	0.080
66.53	1.882	17.60	0.004
71.78	1.769	0.006	1.3×10^{-6}

A matrix of moments of inertia was again used to select the spar cap sizes for the

wing spar. Table 3.16 shows the chosen dimensions of the front spar caps. The

dimensions of the spar caps at any y-location between the points in specified in table 3.16

can be found by simple linear interpolation.

Table 3.16: Wing Front Spar Cap Dimensions

Distance from root, y (in)	Front Spar Cap Width (in)	Front Spar Cap Height (in)
0.00	2.375	0.625
7.91	2.125	0.500
33.40	0.750	0.375
71.78	0.500	0.250

3.38

The shear web of the wing's front spar was sized in similar fashion. The material allowable corresponding to plywood, given earlier, was used in conjunction with equation 3.22 to yield the values for minimum moment of inertia found in table 3.17.

Table 3.17: Tapered Wing Spar Shear Web Sizing

Distance from root, y (in)	Full Spar Height at y (in)	Shear at y (lb)	Min MOI due to Shear (in^4)
0.00	2.588	271.2	0.1308
5.62	2.588	245.4	0.1133
16.78	2.588	194.2	0.0863
27.58	2.588	145.3	0.0630
33.40	2.588	120.0	0.0513
37.58	2.500	102.1	0.0452
46.73	2.305	66.2	0.0318
54.72	2.134	38.9	0.0201
66.53	1.882	7.58	0.0044
71.78	1.769	0.05	0.1308

The width of the shear web was then determined from minimum moment of inertia values given in table 3.17. Table 3.18 shows the chosen front spar shear web thicknesses. The y-distances given in table 3.18 are notated with the superscripts '-' and '+' to show that the shear web thickness is constant up to that y location. It then changes to the smaller thickness discontinuously (although when constructed, a splice doubler on both sides of the shear web maintain a load path through the discontinuity).

Table 3.18: Wing Front Spar Shear Web Dimensions

Distance from root, y (in)	Front Spar Shear Web Thickness (in)
0.00	0.250
7.91$^-$	0.250
7.91$^+$	0.188
33.40$^-$	0.188
33.40$^+$	0.125
71.78	0.125

The sizing of the rear spar was done by assuming that a proportional amount of the load distribution was reacted on the rear spar. At low angles of attack, the center of lift resides at approximately 33% mac. Summing forces in the vertical direction yields the proportion of lift occurring on the rear spar. This proportion was then used to also ratio the bending moment. Solving for spar dimensions as shown above yields the rear spar sizes shown in table 3.19. The loads on the rear spar were significantly lower than those on the front spar, hence the much smaller spar sizes. Added confidence in the rear spar sizing comes from knowing that the front spar was designed to carry the entire load on the wing. Note that the caps of the rear spar are not tapered like the front spar.

Table 3.19: Wing Rear Spar Dimensions

Distance from root, y (in)	Rear Spar Cap Width (in)	Rear Spar Cap Height (in)	Rear Spar Shear Web Thickness (in)
0.00	0.500	0.250	0.125
7.91^-	0.500	0.250	0.125
7.91^+	0.500	0.188	0.125
33.40^-	0.500	0.188	0.125
33.40^+	0.500	0.125	0.125
71.78	0.500	0.125	0.125

Analysis of the Fuselage

The students of Mr. Eastlake's detail design class conducted the analysis of the fuselage structure during the fall semester, 1997. The author, both as a check of the work completed in 1997 and as a general exercise, conducted an analysis of the tail-cone portion of the fuselage in 1998.

The tail-cone portion of the fuselage was represented as a simple space-truss with an offset taper as shown in figure 3.10. Although the actual aircraft has a skin that is

3.40

designed to carry torsional loads, this analysis was conducted assuming that the loads were reacted by the stringers only. For the purpose of this analysis only, two bulkheads were assumed (one at each end of the tail-cone), to reduce the complexity. This analysis did not account for loads being reacted by the actual bulkhead rings that exist between the rear window and the leading edge of the horizontal stabilizer.
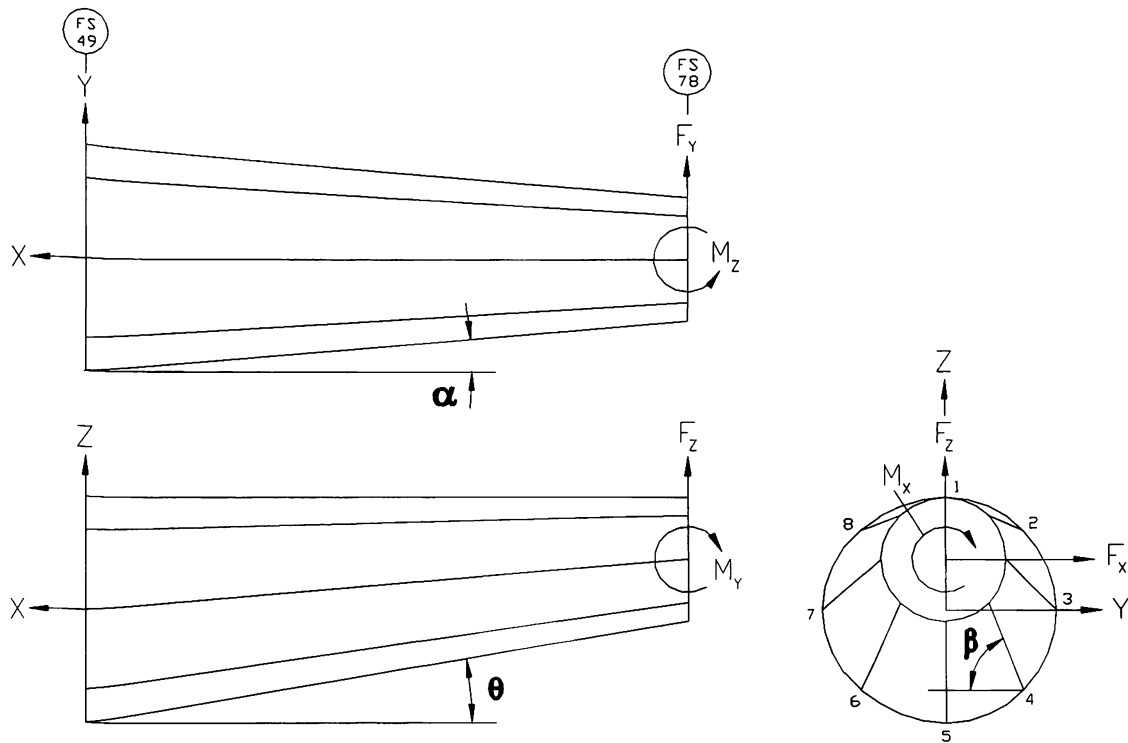

Figure 3.10: Structural Representation of the Fuselage Tail-Cone

As shown in figure 3.10, the structural representation of the tail-cone consisted of eight stringers arranged evenly spaced around an offset, tapered cone. Table 3.20 shows the relative distance along each axis, total length, and orientation angles for each of the eight stringers. The beginning and ending bulkheads were assumed to be circular, for simplicity, unlike the actual bulkhead rings. Three forces (F_x, F_y, F_z) and three moments

3.41

(M_x, M_y, M_z) were assumed to act on the aft bulkhead, which represents the spar

attachment point for the horizontal and vertical stabilizers. The values used in this

analysis for these forces and moments are presented in table 3.21.

Table 3.20: Fuselage Tail-Cone Stringer Distances

Stringer	Δx (in.)	Δy (in.)	Δz (in.)	Length (in.)	α (deg)	β (deg)	θ (deg)
1	29.00	0.000	0.000	29.00	0.00	--	0.00
2	29.00	1.733	0.717	29.06	3.42	22.5	1.42
3	29.00	2.450	2.450	29.21	4.83	45.0	4.83
4	29.00	1.733	4.183	29.35	3.42	67.5	8.21
5	29.00	0.000	4.900	29.41	0.00	90.0	9.59
6	29.00	1.733	4.183	29.35	3.42	67.5	8.21
7	29.00	2.450	2.450	29.21	4.83	45.0	4.83
8	29.00	1.733	0.717	29.06	3.42	22.5	1.42

Table 3.21: Tail-Cone Analysis Forces and Moments

Variable	Description	Value
F_x	Maximum lift force of the horizontal stabilizer	52.9 lb.
F_y	Maximum lift force of the vertical stabilizer	21.8 lb.
F_z	Drag force of horizontal and vertical stabilizers	-3.59 lb.
M_x	Pitching moment contribution of the vertical stabilizer	138 in.-lb.
M_y	Pitching moment contribution of the horizontal stabilizer	474 in.-lb.
M_z	Torsional moment caused by stabilizer lift (centers of pressure) existing at some distance from the surface root.	676 in.-lb.

The forces and moments in table 3.21 were resolved to the forward bulkhead

making the values of M_x, M_y, and M_z equal to 729, -1051, and 769 in.-lb., respectively

(no change to the forces). The translated loads were then evenly distributed over the eight

stringers and the associated stresses were computed. The stringers are made from spruce

and, therefore, the allowables used for tensile and shear strength were 2822 and 376 psi,

respectively (after a 0.99 knock-down and a factor of safety of 2).

3.42

Using the equations for bending stress, axial stress, shear stress, and torsional stress, a minimum stringer cross-sectional area of 0.045 in^2 was found. The "T"-styled stringer cross-section shown in figure 3.11 was chosen to provide a cross-sectional area of 0.063 in^2. The chosen stringer dimensions provide an additional safety factor of 1.4 over those imposed in the allowable knock-downs.
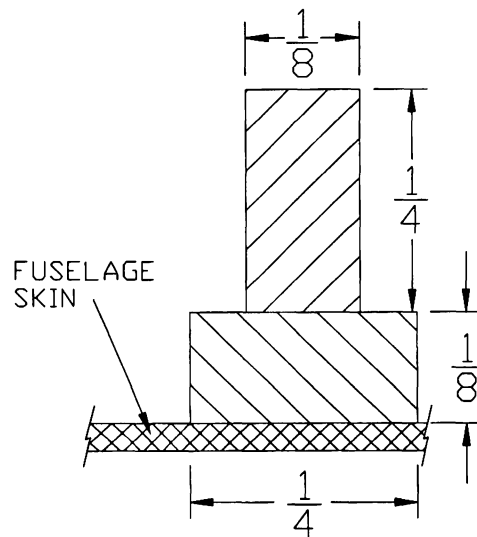
Figure 3.11: Fuselage Tail-Cone Stringer Cross-Section

Analysis of Other Aircraft Components

Various other structural portions of the aircraft required diligent design and analysis. Students in the Detail Design classes at ERAU conducted much of the analysis of these components. These students designed the following components of the 1/3-scale C172P. Details about the analysis and design of these components can be found in the corresponding final design reports. All of these items, with exception to the nose landing gear, were constructed in-house; the nose gear was purchased from Robart.

1. The engine mount,
2. The main landing gear,
3. The nose landing gear,
4. An engine test-stand

3.6: The On-Board Data Acquisition System

In order to conduct a complete analysis of the characteristics of the 1/3-scale C172P, a reliable means of collecting accurate data from the aircraft was needed. A data collection and transmission system, that resides on-board the aircraft, was designed and built for this purpose. The onboard data acquisition and telemetry system (ODATS) allows the real-time measurement of more than 65 parameters. The system also transmits the data to the ground via wireless modem in a constant stream during testing. The data collection station (section 3.7) will simultaneously store and analyze this stream of data. It is hoped that the real-time analysis of some of the incoming data will allow the pilot and flight test engineer the ability to conduct more productive testing. Section 3.7

describes in more detail, the manner in which the real-time analyzed data will be presented to the crew on the ground. The capability of performing real-time analysis of the incoming data stream should reduce the number of reflies required to acquire acceptable data. This will be accomplished by utilizing at least the following two characteristics of the ODATS and data collection station.

1. The pilot will have computer-generated instruments similar to those in a full-scale aircraft to aid in conducting precision maneuvers.
2. The test engineer will have the ability to determine the validity of the data through "instant" plotting of various characteristic curves to help determine the successfulness of a maneuver.

The design of the ODATS began with the layout of the sub-systems. Since the design, construction, and testing of the ODATS was deemed to be outside the scope of this project, help was requested and received from the Avionics Engineering Technology department at ERAU. With the aid of Dr. Albert Helfrick and the Avionics Engineering design class during the spring semester, 1997, a system was designed which would meet the needs of the 1/3-scale C172P and Aquilas flight test projects. The following items were considered necessary characteristics of the ODATS and, therefore, were adopted as the design specifications.

1. Light Weight: Weight is usually a consideration with aircraft, and the C172P and Aquilas are no exception. Although the bulk of the weight of the ODATS is in the batteries, lightweight sensors, boards, and components were sought after to keep the overall weight down.
2. Low Power Consumption: Since the entire ODATS system must be powered by on-board batteries, the systems were designed to minimize the power consumption and extend the up-time.
3. Low Cost: The available budget of the 1/3-scale C172P project did not allow for extravagance in the avionics systems. To reduce the overall cost, some

components and sub-systems were assembled by Avionics Engineering Technology students.

4. Portability: Upon completion of the flight testing of the 1/3-scale C172P, much of the ODATS is to be removed from the aircraft and placed into the Aquilas model. To allow for the portability required, components of sub-systems were mounted in easily accessible locations throughout the aircraft.

5. Upgradeability: The ODATS was designed with future expansions in mind. When the system is moved to the Aquilas model, it is planned that additional sensors and sub-systems will be added to help increase the understanding of the flight characteristics of the new model.

An overview of the entire system is given here, followed by a more detailed description of the sub-systems and their components. Descriptions of the sub-systems to the level of detail which would include characteristics such as brands and specifications of the individual components, is left to the final reports of the Avionics Engineering Technology design students.

The ODATS system is designed to accommodate four major sub-systems that operate simultaneously. The system design was conducted with both the C172P and the future Aquilas in mind. The four major sub-systems and their respective sub-systems include the following:

1. Video Transmission,
2. Ballistic Recovery,
3. Data Collection,
    a. Safe-Life Monitoring,
    b. Power Plant Monitoring,
    c. Global Positioning,
    d. In-Flight Loads Monitoring, and
4. Aircraft Control.

Figure 3.12 shows a flow chart of the sub-system connectivity and interaction. Although the ODATS system was designed to accommodate all four of the major sub-systems, the Ballistic Recovery, Safe-Life Monitoring, and Global Positioning sub-systems were excluded from construction to minimize complexity and cost during the C172P project. The hardware components for the remaining sub-systems, however, were built with provisions for the excluded systems to be added later. Each of the four major sub-systems are described here.

Audio/Video Transmission System

The video transmission system consists of a high-resolution microvideo color camera and wireless transmitter that will stream live data to the ground station during flight. The video and audio signals will be relayed to the ground using a 910 MHz, 450 mW transmitter. On the ground, the signal will be displayed on a TV monitor and recorded on a VHS video cassette recorder.
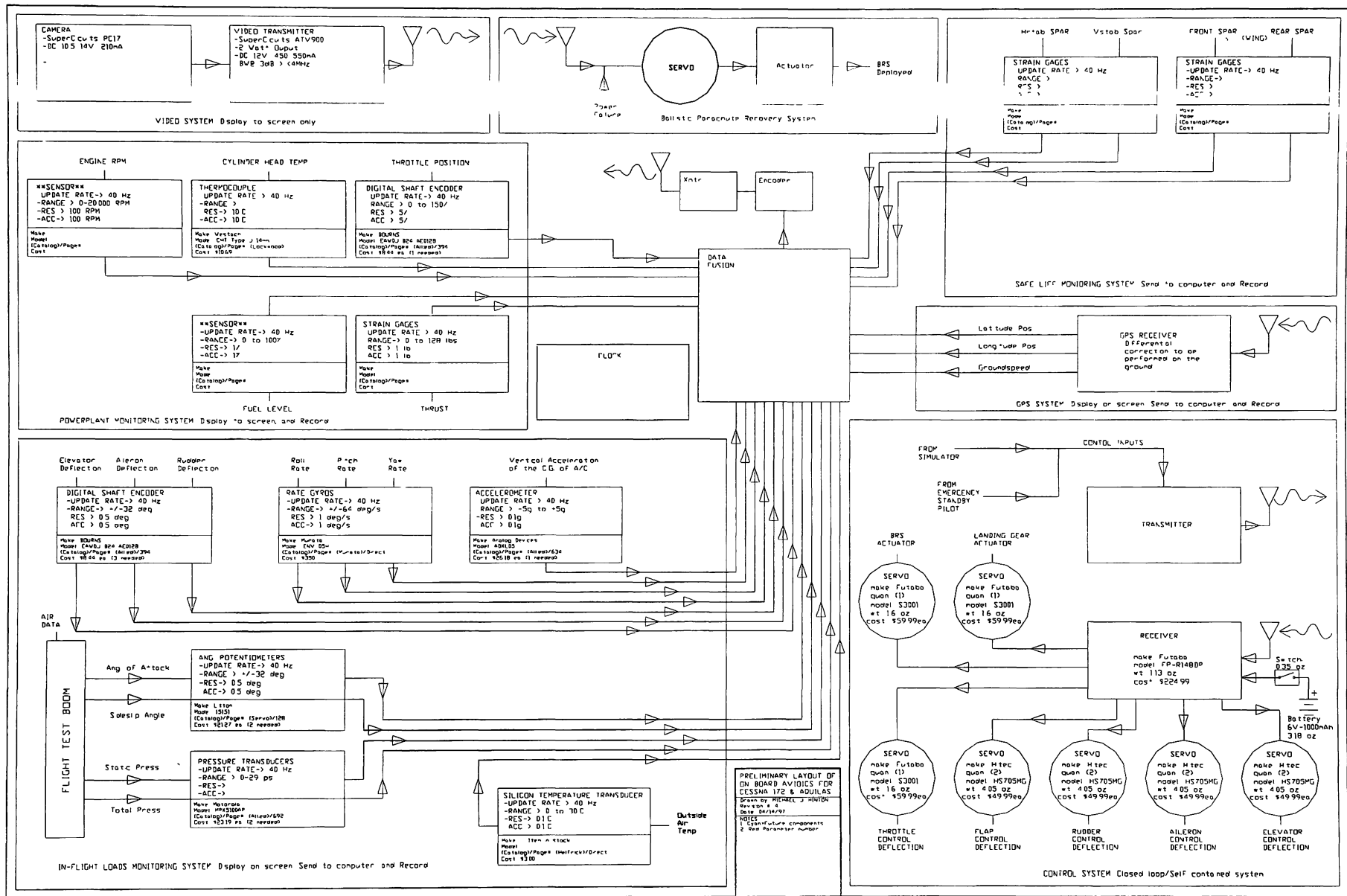
Figure 3.12: 1/3-Scale C172P Aircraft Systems Flowchart

3.48

The video system uses its own transmission and receiving hardware and carrier frequency and, therefore, operates independently from all other systems. The 910 MHz carrier frequency resides in the amateur television (ATV) frequency band as designated by the Federal Communications Commission (FCC). For this reason, it may be required that some individual be present during all flight testing who maintains an ATV license.

Ballistic Recovery System

A ballistic recovery parachute system (BRS) is included in the ODATS to give peace-of-mind in the event of a catastrophic failure. When activated, a parachute will be deployed from the aircraft allowing the injured airplane to float to safety. Since the BRS is not to be included into the 1/3-scale C172P, much of the detail design has been left incomplete.

This sub-system is designed to be triggered either by a total loss of power, loss of the ground-to-aircraft control link, or by servo commanded actuation. If the system is commanded to fire, the signal that actuates the servo will be supplied through the Aircraft Control sub-system. Should the aircraft loose its control signals (from the ground) for an undetermined length of time, then the system would activate the parachute deployment.

Examples of BRS systems exist on full-scale aircraft through the general aviation and ultralight communities. BRS systems have also been designed for smaller aircraft such as military drones and remotely guided reconnaissance/surveillance aircraft. Many of the manufactured models of BRS packages available during the design of these sub-

systems were either too large, too heavy, too bulky, or just designed for much larger

aircraft. The cost of a pre-assembled BRS package is also quite substantial. For these

reasons, incorporation of a BRS package was deemed not feasible for the 1/3-scale

C172P.

Data Collection System

The data collection system is comprised of four sub-systems as listed below. A

description of each of these sub-systems follows below, followed by a description of the

data collection and transmission portion of the system that compiles the data stream and

sends it to the ground.

1. Safe-life monitoring,
2. Global positioning,
3. Powerplant monitoring, and
4. In-flight loads monitoring systems.

Safe-Life Monitoring: The safe-life monitoring components allow for the

continuous tracking of stresses on key components of the structure. Through the AGATE

effort at ERAU, a new concept was explored that would allow a variable amount of time

between major aircraft structural inspections. A core package of monitoring sensors

could be installed on an aircraft to keep track of stress loads on the structure. This data

could then be used to determine whether the airframe was in need of structural

inspections, either earlier or later than the scheduled maintenance time, due to its time

history of stress loadings.

The concept of safe-life monitoring was explored as part of the AGATE effort and, in-turn, the Aquilas. The safe-life monitoring system is not included on the 1/3-scale C172P.

Global Positioning: A GPS receiver can be incorporated into the data collection package. The purpose of using the GPS receiver is two-fold: 1) to verify/rationalize the airspeed calibration of the airdata boom airspeed, and 2) to aide in maneuver precision for maneuvers which require certain ground-tract characteristics. The global positioning sub-system uses a differential GPS receiver (or a normal GPS receiver with differential corrections made in the ground station) to receive the satellite signals and then passes the latitude, longitude, and groundspeed magnitude along to be transmitted to the ground.

The global positioning sub-system is not included on the 1/3-scale C172P.

Powerplant Monitoring: Monitoring of key engine operating parameters is crucial in characterizing aircraft performance. The powerplant monitoring sub-system collects the engine rpm, cylinder head temperature, throttle position, and fuel level. Also accommodated are provisions for manifold pressure, and strain gages (for calculating thrust). However, manifold pressure is not available on the Quadra Aerrow Q100XL engine that is used on the 1/3-scale C172P and, therefore, was not included during the construction of the ODATS. Similarly, the engine mount strain gages intended to be used to measure thrust were not included in the 1/3-scale C172P system.

3.51

After being transmitted to the ground, the data collected from the engine will be recorded and simultaneously displayed to the pilot and flight test engineer via computer-generated gages on the ground data station (see section 3.7).

One of the parameters within the powerplant monitoring sub-system is engine rpm. Rotational speed of the engine is useful for many reasons, the largest of which is to the pilot in setting power for maneuvers. Since the Quadra Aerrow Q100XL uses an electronic ignition system to deliver the spark to the engine, reading the engine rpm is as straightforward as reading the spark delivery signal and patching it into the data stream. The electronic ignition controller receives a signal from a magnet mounted on the crankshaft which it uses to adjust its timing. This signal will be spliced into and fed directly into the data gathering portion of the system.

The cylinder head temperature will help to ensure adequate cooling of the engine. The cylinder head temperature is measured using a type-K thermocouple. A thermocouple was chosen over a thermistor due to its high temperature capabilities. The sensor is attached to a flat washer allowing it to be mounted to the engine by placing the washer portion between the spark plug and the engine.

The throttle position is measured using a precision potentiometer mounted to the throttle control servo. A precision potentiometer was chosen for its continuous relationship of output signal to shaft rotation. Originally, a digital shaft encoder was considered but was eliminated due to its stair-stepped output signal. Although the output

signal from a digital shaft encoder does not require analog-to-digital conversion, the resolution of ±1 deg was determined to be unacceptable.

Providing an accurate, safe, and compact method of sensing fuel level became a difficult problem. No desirable method was found by the spring of 1999. An early iteration of the design called for a capacitive device that uses the fuel itself as a dielectric between two electrically charged plates. Due to complexity and cost, this idea was replaced with a fuel flow integration method using a flow meter mounted in the fuel supply line. This newer method requires that the fuel flow sensor be quite accurate to provide reliable fuel quantities. Fuel flow meters of with the accuracy required that would sense flows in the range required were found to be rather expensive. It was decided that the errors associated with fuel flow integration method (using an affordable fuel flow meter) could result in large enough errors in remaining fuel quantities as to cause an unexpected in-flight engine shutdown. As a temporary solution to the problem, test would be conducted to determine the shortest run time for a full fuel tank at the maximum fuel flow rate (max power). The fuel tanks would always be completely filled before each flight and this run time would never be exceeded while in flight. Meanwhile, the ODATS has been built to accommodate a fuel level sensor once a suitable one is found.

The ODATS is designed with provisions for measuring thrust via a set of strain gages mounted to the engine mount. The thrust measuring system, however, is not included as part of the system installed in the 1/3-scale C172P.

3.53

Provisions are also included in the ODATS for measuring manifold pressure. The sole reason for including this parameter is to help match 1/3-scale flight test data with full-scale flight test data. Since the power output of the engine on the full-scale aircraft is directly related to the manifold pressure, then it is believed that the 1/3-scale engine power output could similarly be predicted. The Quadra Aerrow Q100XL does not, however, provide a means to measure manifold pressure. This parameter, therefore, has been excluded from the system built for the 1/3-scale C172P and 1/3-scale Aquilas.

In-Flight Loads Monitoring: The in-flight loads monitoring sub-system consists of the sensors required to determine flight speed, aircraft attitude, accelerations, and control deflections. This sub-system utilizes twelve sensors throughout the aircraft to measure the following required parameters.

1. Total Pressure
2. Static Pressure
3. Angle of Attack
4. Angle of Sideslip
5. Vertical Acceleration of the CG
6. Rate of Pitch
7. Rate of Roll
8. Rate of Yaw
9. Outside Air Temperature
10. Elevator Deflection
11. Aileron Deflection
12. Rudder Deflection

The total and static pressure values will be collected using a pitot-static probe mounted on the airdata boom fastened to the left-hand wing tip. The design of the airdata

boom is detailed in section 3.8. Total and static pressures are important for determining such characteristics as airspeed and altitude. The pressures will be sensed using absolute pressure transducers mounted in the wing.

The angle of attack and angle of sideslip help determine the aircraft orientation with respect to the relative wind. These parameters will be measured using precision potentiometers mounted in the airdata boom (see section 3.8).

Vertical acceleration of the aircraft's center of gravity is measured using a solid state, piezo-electric accelerometer. The accelerometer is mounted to a circuit board as near to the aircraft's center of gravity as possible. To help assure that the accelerometer is mounted at the aircraft's c.g., the circuit board will be mounted on an adjustable mounting device. This will allow the board to be shifted forward or back to account for a more forward or more aft loading distribution.

Aircraft pitch rate, roll rate, and yaw rate will all be measured using angular rate gyros. Similarly to the accelerometer above, it is desired that these devices be mounted as close to the aircraft's c.g. as possible. At the time of the construction of the ODATS, a suitable rate gyro could not be found at a reasonable price. For this reason, the current data collection system does not contain the rate gyros but spare data channels have been provided to accommodate them once suitable ones are found.

Outside air temperature will be measured via a silicon temperature transducer. The transducer will be mounted on the side of the fuselage of the aircraft and will measure static air temperature. A silicon temperature transducer was chosen over a thermocouple or thermistor because it offers the proper resolution and accuracy over the anticipated range of outside air temperatures. The sensor itself is also very compact and inexpensive.

Elevator, aileron, and rudder deflections are measured using precision potentiometers that are mounted to the controlling servos. The potentiometers are mounted to the servos via a bracket designed to align the potentiometer shaft with the servo actuator shaft. As the servo rotates, the potentiometer is also turned allowing the measurement of the control surface deflection. Although the ailerons and elevator are actuated using two servos each, the precision potentiometer used to measure control surface deflection is attached to only one of the available servos.

Data Collection and Transmission: The data fusion block seen in figure 3.12 gathers the measurements from the sensors into a data stream that can be transmitted to the ground station. This portion of the system has three primary steps in gathering the data: 1) condition the signal, 2) convert the signal (if required), and 3) multiplex the many channels of data into a single data stream.

The data fusion's first task, signal conditioning is required to amplify weak signals and degrade strong signals to a point where all the signals from all the sensors are

3.56

similar in magnitude. As an example, if the output of a sensor is ±1 volt, and the system operates on ±5 volts, then the sensed signal must be amplified before continuing. The signal conditioners in the ODATS are mounted as close to the sensors as possible to minimize the effects of voltage drops and interference that can be present over long stretches of cable. Four separate sensor boards were built to serve as data collection stations throughout the aircraft. The sensors in the tail (elevator and rudder deflection) are collected by a board mounted in the aft tail cone just beneath the mounting points for the horizontal and vertical stabilizers. Another board mounted in the left hand portion of the wing is used to collect the signals for aileron and flap deflection, total and static pressure, and angle of attack and angle of sideslip. The third board, mounted in the back of the firewall, collects cylinder head temperature, throttle position, and engine rpm. The forth board is mounted near the c.g. and processes the remaining parameters.

The next function of the data fusion block, signal conversion, also occurs at the collection boards throughout the aircraft. Since the data stream that is transmitted the ground is a digital stream, the signals from the various sensors must converted to digital before being compiled into the stream. Almost all of the signals collected on the 1/3-scale C172P are analog and must be converted. Only the engine rpm can be sensed without requiring conversion.

The conversion of the signal from analog to digital occurs via a separate analog-to-digital (A/D) converter for each sensor. The A/D converters are mounted on the signal collection board located nearest the sensor.

The ODATS was designed to condition and convert the signal as close to the sensor as possible to minimize any interference and ensure data quality. Under normal operations, the 1/3-scale C172P will be using three simultaneous wireless transmissions along with a high voltage spark ignition. Any of these systems could introduce interference into the ODATS. Prompt conditioning and conversion of the sensed signals was determined as a way to minimize possible interference from these sources.

Each of the conditioned and converted signals is next sent to the multiplexers to be compiled into the data stream. Details, such as the order in which the data is compiled into the stream, can be found in the final reports of the Avionics Engineering Technology detail design course from spring 1997.

The final steps in the data collection system include encoding the signal and transmitting it to the ground. Originally, an FCC compliant transmitter was to be designed and built for this project. Although more expensive than building a transmitter/receiver pair in-house, an off-the-shelf set was purchased to minimize the project's complexity and schedule risks.

Aircraft Control System

The aircraft control system allows the pilot on the ground maneuver the aircraft through control surface deflections. The pilot uses a hand-held transmitter to send requested control inputs to an on-board receiver. The receiver then translates the signal and passes the requested control inputs onto the respective servo actuator.

The initial step in the design of this system was to determine how many possible control actions would be needed. The needs of the Aquilas model were considered simultaneously so that only one transmitter/receiver set would need to be purchased for both projects. Table 3.22 shows the control actions required for each aircraft.

Table 3.22: Aircraft Control System Actuators Required

	1/3-Scale C172P	Aquilas
1	Aileron Deflection	Aileron Deflection
2	Elevator Deflection	Elevator Deflection
3	Rudder Deflection	Rudder Deflection
4	Flap Deflection	Flap Deflection
5	Throttle Position	Throttle Position
6	Main Gear Brake Actuation	Main Gear Brake Actuation
7	--not used--	Landing Gear Retraction
8	--not used--	BRS Actuation

Figure 3.12 shows the conceptual layout of the aircraft control system. Contained within the sub-system box are the primary components of the radio system needed to control the aircraft. The radio system requires a transmitter (with internal battery), a receiver, a battery on-board the aircraft, and servo actuators. Since the aircraft control system has its own transmitter/receiver pair then this sub-system operates independent of all other sub-systems.

A radio system capable of supplying eight channels of control was required to accommodate the needs of the two aircraft. The radio system chosen was the model FP-8UAP from Futaba. This system uses pulse code modulation (PCM) to code the data onto the carrier frequency offering a more secure/interference-free signal. The frequency modulated (FM) carrier frequency used by this radio is in the 72 MHz band. This frequency band does not require a special license for operation; however, it is

3.59

recommended that the pilot and back-up pilot be registered with the Academy of Model Aeronautics (AMA).

The transmitter output is 750 mW giving a range under normal atmospheric conditions of well over a mile. A 500 mA battery is supplied in the transmitter and nominal power consumption is rated at 250 mAh. The receiver draws a constant 14 mA from the battery pack on-board the aircraft. The FP-8UAP radio system comes with four model S3001 ball bearing standard-size servos. These servos can be used in the 1/3-scale C172P for low-torque control requirements such as throttle position and brake actuation. To actuate the aerodynamic control surfaces (ailerons, elevator, rudder, and flaps), high-torque servos are needed. The servos chosen for these surfaces are the model HS705MG from Hitec. These high-torque servos have metal gears and double ball bearings to withstand the higher loads. Table 3.23 shows some specifications of these two servo models.

Table 3.23: Servo Actuator Specifications

	Futaba S3001	Hitec HS705MG
Dimensions	1.6" L x 1.4" H x 0.78" W	2.0" L x 2.3" H x 1.10" W
Weight	1.59 oz.	4.05 oz.
Output Speed	0.22 sec for 60° rotation	0.27 sec for 60° rotation
Output Torque	42 in-oz	161 in-oz

The flowchart diagram (fig 3.12) shows two possible control request generators; the pilot flying from a simulator and a back-up pilot flying within visual contact from the ground. The 1/3-scale C172P is intended to be flown only by a pilot on the ground with visual contact with the aircraft. This is the traditional style of R/C aircraft control. The

simulator concept evolved out of the AGATE effort at ERAU during 1996 and 1997. It is unknown whether the Aquilas will have the ability to be flown via sit-in simulator with mocked-up controls and live visual feed.

3.7: The Data Collection Station

A data collection station is necessary to a) receive and store the streaming data from the aircraft, b) conduct real-time data analysis, and c) present the pilot and flight test engineer with details about the flight required to conduct accurate flight test maneuvers. As discussed earlier, two streams of data will be simultaneously transmitted from the aircraft in flight to the ground station. One of the data streams will carry audio and video signals from the on-board camera while the other stream will carry the data from the ODATS.

The data collection station consists of two primary devices, a laptop computer and a TV/VCR set. The laptop is responsible for the collection, storage, and manipulation of the data stream from the aircraft while the TV/VCR will collect, display, and store the signal from the camera. Each of the two devices at the ground station uses its own receiver, power source, and storage device and is, therefore, not reliant upon the operability of the other. Following is a description of each of these devices.

Laptop Computer: The laptop computer must be connected to the ODATS data receiver in order to collect the data stream from the aircraft. The transmitter/receiver pair chosen for this project is a wireless computer modem and transmits the data in a common

modem protocol. Since a wireless modem and common transmission protocol were chosen, no special hardware or software requirements were placed on the laptop computer (most computers come standard with the tools needed).

The computer chosen was is made by Toshiba and was selected for its speed, reliability, and cost. The computer has a dual-boot capability allowing it to run either Microsoft Windows 98 or Red Hat Linux 5.2. The capability of reading the data stream from the wireless modem is available in both operating systems, however, a special program to conduct the real-time data analysis and presentation was designed that would require a UNIX-like operating system (Linux).

During the data collection stage of a test (aircraft streaming data to the computer), the custom data analysis program would decipher the incoming data stream, store a copy to the hard disk, and analyze and display the results. Currently, only preliminary ideas exist about the final display and the data it presents. As the project evolves, however, the display can be modified to provide the required data.

The current design for the output display of the streamed data can be seen in figure 3.13. The output currently has graphical displays of the parameters such as engine rpm, angle of attack, angle of sideslip, and control surface and throttle positions. Currently, strip-chart type graphs are used for the first three parameters while bar chart type indicators are used for the position readouts. Also included on the display are numerical indications of outside air temperature, and total and static pressure. The

aircraft icon in the middle of the display is designed to move in response to changes in angle of attack and angle of sideslip. The region notated as "big empty space" will be filled with analyzed data such as airspeed, altitude, and vertical acceleration. These parameters will be supplied in the form of dial gages similar to those found in full-scale aircraft.
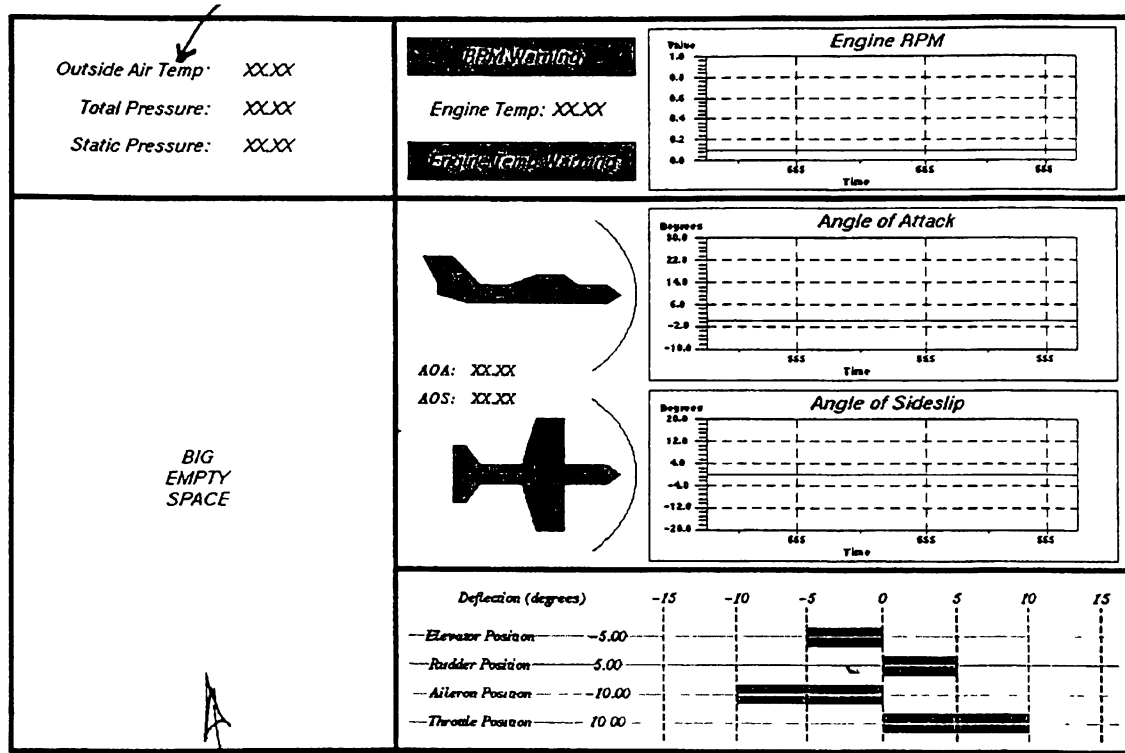
Figure 3.13: Real-Time Data Display – Ground Station

TV/VCR Set: As mentioned in section 3.6, a 910 MHz receiver receives the audio/video signal on the ground. This signal is displayed and recorded simultaneously using a television and videocassette recorder.

3.63

A few requirements governed the choice of a TV and VCR set to perform the task. The first was portability. The units chosen must be easily moved to the flying site and, preferably, placed where the pilot can easily use the display to aide in performing maneuvers. The second and third requirements were DC power supply capability and low power consumption. The need to operate the TV and VCR on DC power stems from the lack of AC power at the original proposed flying site. Operating on DC power only (supplied by a 12 VDC auto battery), the units must have low power consumption to preserve battery charge.

A TV/VCR combination unit with a 9-inch diagonal screen was purchased. The unit operates on AC or DC power and satisfies the portability and low power consumption requirements.

The audio/video system was temporarily installed in an SAE cargo lift competition aircraft to test system operability. The author piloted the aircraft through ground maneuvers at ERAU using the visual cues from the video display on the TV/VCR set only. The video system was found to work flawlessly and the aircraft was found to be surprisingly easy to maneuver in this manner.

3.8: The Airdata Boom

The airdata boom is used to collect the total and static pressures and angle of attack and angle of sideslip on the aircraft. The boom is mounted to the left-hand wing tip. The design of the airdata boom is similar to the boom used on ERAU's full-scale

C172P flight-test aircraft. The original boom used on the full-scale aircraft was designed and built by Mike Stevens (a former ERAU graduate student). The final design used on the 1/3-scale C172P can be seen in figure 4.14 in section 4.3.

The airdata boom consists of two primary sections. The forward section of the boom is the pitot-static probe for measuring total and static pressure. The aft section of the boom has two fins attached to precision potentiometers for measuring angle of attack and angle of sideslip. The fins weathervane to align with the relative wind as the aircraft moves through the air. The position of the potentiometers is then used to determine the orientation angles of the aircraft.

The airdata boom for the 1/3-scale aircraft needed to have all the functionality of the boom that was used on the full-scale aircraft. However, due to the relatively small size of the 1/3-scale C172P model, the airdata boom designed for the full-scale aircraft could not be used directly without modifications. At first, the 1/3-scale airdata boom was sized according to the traditional scaling techniques discussed earlier. This design was found to be non-viable because of difficulties in locating cost-effective precision potentiometers small enough to fit inside the tube.

The second stage in the design of the airdata boom called for the tube sizing to be large enough to fit an optical digital shaft encoder similar to the ones originally considered for determining the control surface deflections. The shaft encoders, however, had a very coarse resolution when used with the 8-bit system (ODATS). The angle

measurements read from these digital encoders would be no more precise than ±1.5 deg. This was clearly not precise enough for measurements of either angle of attack or angle of sideslip.

The diameter of the aft tube was again increased until it would accommodate a precision potentiometer. The potentiometer chosen was smaller than that used in the full-scale airdata boom. Although the 1/3-scale airdata boom was not as small as desired (1/3-scale), this allowed the boom for the 1/3-scale C172P to be smaller than the full-scale boom.

The pitot-static probe that encompasses the front of the boom was designed primarily for ease of manufacture. The shape of the nose of the probe, however, was chosen to minimize the sensor error due to the flow misalignment that occurs at angles of attack (and sideslip) other than zero. For a subsonic aircraft such as the 1/3-scale C172P, a hemi-spherical nose shape gives reasonably accurate pressure readings at flow angles up to about ±5 deg. Beyond the ±5 deg band, a hemispherical nose also give reasonably repeatable errors that can be used to correct for the flow misalignment.

The pitot-static probe was designed to have a single hole in the nose for reading total pressure and a series of holes further down the shaft for measuring static pressure. The static pressure ports open into a plenum inside the probe. This is to equalize the pressures on all sides of the probe before a measurement is taken. The total and static pressures are measured via a pair of single-port, absolute pressure transducers. Due to the

3.66

size limitations of the boom, the pressure transducers could not be mounted in close proximity to the pressure sources (the total and static pressure ports). The pressure transducers, therefore, must be mounted in the wing and have tubing run from the ports to the transducers.

The airdata boom was originally designed to be mounted to the aircraft on the left-hand wing strut. Difficulties in configuring the mounting hardware and routing the wiring for the sensors forced the mounting location to be changed to the left-hand wing tip. With the boom mounted to the wing tip, the wires from the potentiometers to the A/D converters is much shorter offering a reduced chance of interference. The shorter distance from the total and static pressure ports to the pressure transducers also reduces the sensor lag for those components. Section 4.3 describes the construction and testing of the airdata boom.

Chapter 4: Construction of the Aircraft and its Systems

This chapter describes some of the processes used during the construction of the 1/3-scale C172P model. Fabrication of the aircraft began in the fall of 1997 and, by the spring of 1999, was approximately 75% complete. This thesis is intended to cover the portion of fabrication completed by the author; the completion of the project has been left to future students at ERAU.

4.1: Construction Plans

The construction of the 1/3-scale C172P began with a search for an adequate set of building plans. The author searched for plans from regular suppliers of large-scale model (R/C) aircraft. Cessna 172 model kits were found in different scales (other than 1/3), in different models (other than the "P" model), and different years (other than 1986). With the regular resources exhausted, the decision then was made to fabricate an original set of plans from which to build. The construction of this model would be unlike an ordinary radio-controlled model due to its complexity, weight, and structural requirements. The 1/3-scale C172P weighs more than 2½ times that of a comparable 1/3-scale high-wing single propeller recreational R/C aircraft and must be able to sustain 5.8 g's.

Both 2-D drawings and 3-D solid models were constructed to help in building the airplane. The 2-D drawings serve two main purposes: 1) planning structural layout and 2) working drawings that were used to construct pieces of the aircraft like the engine mount, landing gear, and airdata boom. The 3-D solid models were used to make building jigs

and composite lay-up molds used during construction. The building jigs were used to hold assemblies in place while building and the molds were used for the fiberglass lay-up of the skin panels of the aircraft.

The 2-D Drawings

Two-dimensional drawings of the 1/3-scale C172P were developed using AutoCAD. To begin the plans, a 3-view drawing of the 1986 C172P was located, scanned into the computer, and converted into a working AutoCAD drawing. The drawing was continuously modified throughout the construction of the aircraft as items, such as structural members, were appropriately sized and located.

In addition to the aircraft drawing, 2-D working drawings of other components were also developed using AutoCAD. Table 4.1 shows the filename and a description of each drawing. These files are the source for many of the drawings in this document.

Table 4.1: 2-D Drawing Descriptions

Filename	Description
cessna.dwg	Full aircraft with structural components and layout.
airdata.dwg	Airdata boom construction drawing – includes assemblies.
flowchart.dwg	Aircraft systems flowchart – used in initial design and layout of systems
Q100XL.dwg	The 1/3-scale C172P and Aquilas engine: The Quadra Aerrow Q100XL
engmnt.dwg	The drawing of the engine mount used on the 1/3-scale C172P
break_in.dwg	The drawing for the mount used to attach the engine to the break-in stand.
brakes.dwg	Contains the components of the braking system for the main gear.

The 3-D Solid Models

Three-dimensional solid models were constructed using the a software package called Varimetrix. The solid models were built using the 3-D solid modeling module. Solid models were made of the wing, fuselage, and horizontal and vertical stabilizers. The 3-D models were primarily used in the construction of composite lay-up molds and building jigs. Using the manufacturing module of Varimetrix, tool paths were generated on each of the surfaces of the solid models. The tool paths were then used to control ERAU's 3-axis computer numerically controlled (CNC) milling machine in the construction of the molds and jigs (see section 4.2-*The Jigs and Molds*).

In addition to the components mentioned above, 3-D models were made of the wing main spar. These models were used to generate tool paths for cutting the double-tapered spar caps (see section 4.2-*The Wing*).

4.2: Construction of the Aircraft Components

The 1/3-scale C172P is constructed using mostly traditional modeling materials and techniques. Unlike traditional modeling practice, however, balsa wood was not used in building structural components of the aircraft. The majority of the aircraft's structural components are made from spruce and birch plywood. The skin of the aircraft is constructed of 6 oz. bi-directional fiberglass cloth and epoxy resin in varying numbers of layers. The wing main spar was constructed of Douglas fir because of the material's straight, uniform fiber structure and moderately light weight. The following sections describe the construction of the various pieces of the aircraft in more detail. Section 3.4

4.3

describes the material testing which was conducted to determine the allowable values for use in the structural substantiation.

Jigs and Molds

To aid in the construction of the aircraft, building jigs were used to hold the various pieces in place during fabrication. Jigs were used in the construction of the wing and the horizontal and vertical stabilizers. The fuselage was built in halves and did not require a jig.

The jigs were cut from high-density polystyrene (blue foam) using ERAU's 3-axis CNC milling machine. Tool paths, which were generated from the 3-D solid models described earlier, were used to drive the CNC machine. Both the jigs and molds were cut using a zigzag cutting pattern. To reduce time when cutting the building jigs, a relatively coarse resolution between consecutive cutting tool passes was used (approximately 10-15% of the tool diameter). To ensure dimensional accuracy of the finished jig, however, the exact stop functionality of the CNC machine was utilized. This function ensures that the cutting tool reaches the exact (X,Y,Z) dimension specified before continuing to the next location. Although the exact stop function increases cutting time, the dimensional accuracy of the part is guaranteed.

Molds were constructed for use during the composite skin lay-up process. These molds were also cut from blue foam using the CNC milling machine. To ensure a smooth surface on the skin panels, a fine cutting tool resolution was used (approximately 2-5% of

the tool diameter). As with the building jigs, the exact stop functionality was used to ensure dimensional accuracy.

The cutting tool used for the molds was a ball-end mill and, even though a tool step value of 2-5% of the diameter was used, the finished cut surface displayed noticeable tooling marks. Therefore, the lay-up molds were lightly sanded to remove the cutting tool marks. After sanding, the molds were treated using a spray on latex enamel paint. Latex enamel was required for two reasons. First, latex paint does not require a propellant that dissolves blue foam. Second, the enamel characteristics of the paint provide a durable finish that resists punctures and dimples. Three light coats of this paint were required to produce the desired finish. Light sanding was also done following each coat of paint.

Done properly, a lay-up mold finished with this method could produce 3-5 parts before expiring. The molds made for the 1/3-scale C172P are geometry specific enough that only one part per mold was needed. After all the skin panels were finished, the molds were stored in case another panel would be needed.

Construction of the Empennage

The first component built was the vertical stabilizer. Two vertical stabilizers were eventually made; the first became the victim of a static test to failure, and the second was placed on the aircraft. The first vertical stabilizer was also a study in building materials and techniques. Lessons learned from this first stabilizer were carried throughout the construction of the entire aircraft.

The first vertical stabilizer built was a full sized (1/3-scale) stab constructed using spruce spar caps, balsa shear webs, balsa ribs, and balsa leading and trailing edges. The method used in building the all of the major components of the 1/3-scale C172P was developed during the construction of this first vertical stabilizer. The first step was the fabrication of the building jig, as discussed earlier. For the vertical stabilizer, only one jig was required. Eventually, both of the vertical stabs made, were built in this jig.

Next, rib profiles were plotted on paper in full-scale. Figure 4.1 shows the plot layouts used for the vertical stabilizer and the left and right horizontal stabilizers. These rib profiles were then bonded (using spray-on adhesive) to sheets of wood (balsa for the first vertical stabilizer; plywood for all other components) of appropriate thickness.
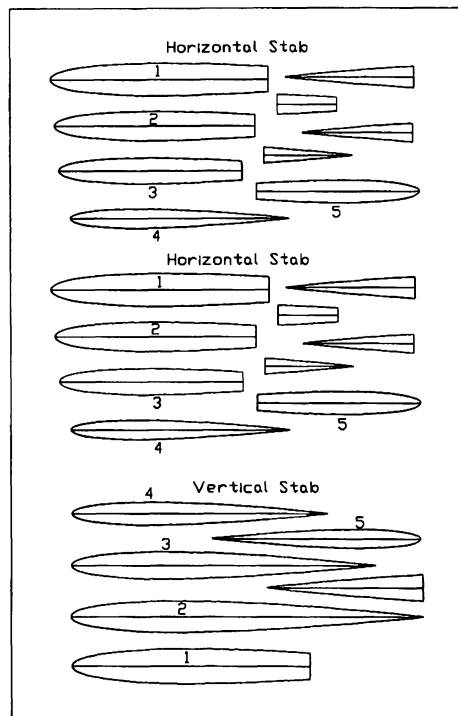
Figure 4.1: Vertical and Horizontal Stabilizer Plot Layouts

Once the individual ribs were cut from the plywood, provisions for the spars, leading and trailing edges, and servos were marked and removed. The pieces were then assembled in the jig. Figure B.4 shows the ribs in place in the vertical stabilizer jig. The ribs were placed approximately 2 inches apart and the entire stabilizer was bonded using cyanoacrylate ester (CA) and epoxy resin as would be expected in a traditionally constructed R/C aircraft. Figure B.5 shows the completed original vertical stabilizer.

Upon completion of the stabilizer, an ultimate strength test was conducted to determine the maximum strength of the stabilizer using these materials and technique. The test article was clamped to a solid table and then loaded using trapezoidal loading distribution as shown in figure B.5. Failure resulted at 90.4 lbs. This represents a side load on the vertical stabilizer in excess of 4 times the maximum expected load. Although the stabilizer was capable of withstanding loads greater than those expected in flight, a revision to the building techniques and materials was made when the failure was more closely examined. The failed piece showed distinct evidence of bond failure at some CA joints and delamination of some of the shear web pieces. For these reasons, two changes were made to the construction technique. It was decided to 1) use epoxy (instead of CA) to join structural members due to its greater strength and resilience, and 2) use plywood shear webs (instead of balsa) to reduce or eliminate the tendency for delamination.

Using the revised building materials and techniques specified, a new vertical stabilizer was constructed (using the existing jig). The new stabilizer had only five ribs (made of plywood) and a plywood shear web. The structural layout of this vertical

stabilizer can be seen in figure 4.2. Provisions for the rudder servo were provided, between the front and rear spars, in rib #2. The leading and trailing edges were made of balsa since they are not considered load-bearing members. Three rudder hinge mounting points were also incorporated into the rear spar. Additionally, the main spar caps were left extending below the root chord to be used in mounting the vertical stab to the fuselage.
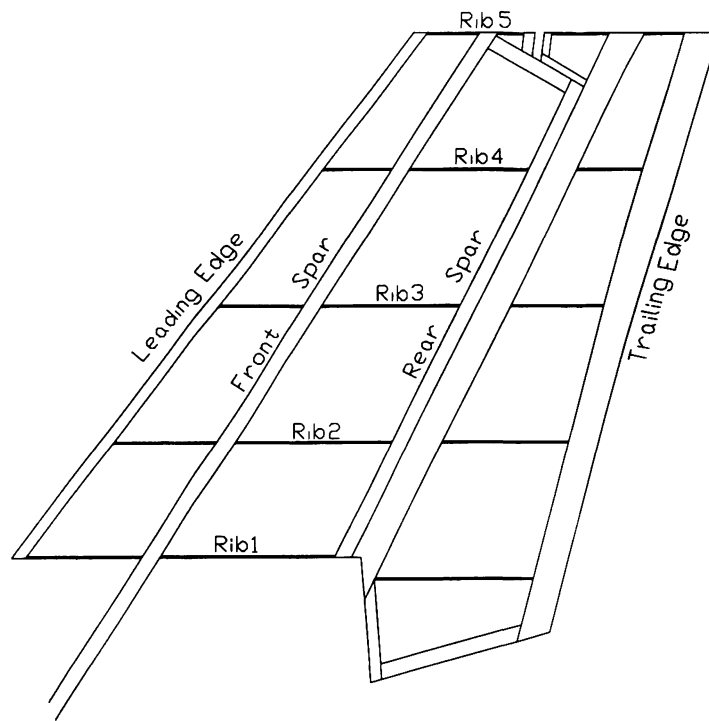
Figure 4.2: Vertical Stabilizer Structural Layout

The next item constructed was the horizontal stabilizer. The procedure used for this component was very similar to that used on the second vertical stabilizer described above. The building jig used for the horizontal stabilizer was a semi-span jig requiring the stabilizer to be built in two pieces. Once the left and right halves were finished, they were joined together and carry-through structure was added to maintain the load paths.

4.8

Figure 4.3 shows the structural layout of the horizontal stabilizer. Similarly, to the vertical stabilizer, the leading and trailing edges were constructed of balsa and the spars and ribs were made from spruce and plywood. The four circles noted in the figure (near the center of the stab) are the bolt locations for the mounting the stabilizer to the fuselage. Six elevator hinge points (not shown in figure 4.3) were also provided on the rear spar. Accommodations for elevator control servos (one for each side) were provided between ribs 2 and 3.
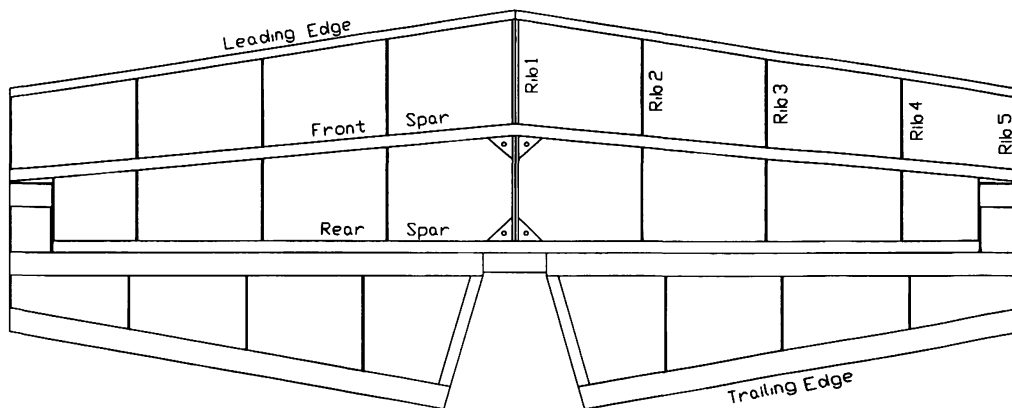
Figure 4.3: Horizontal Stabilizer Structural Layout

During the construction of the empennage components, the bond between the balsa leading and trailing edges and the thin ribs was found to be quite weak. To improve these joints and add structural rigidity, triangular gussets (not noted in figures 4.3 and 4.2) were placed in many of the acute corners. These gussets were made from light plywood, 1/4 in. thick, for its high strength-to-weight characteristics. Figure B.7 shows the horizontal stabilizer partially complete. At the time of this picture, the fiberglass skin panel had been bonded to the lower surface of the stabilizer.

4.9

Construction of the Wing

Unlike the horizontal stabilizer, the full span of the wing was constructed at once. Building jigs were fabricated for the left and right wing panels and then joined to make one, 12-foot long jig. The building jig for the wing had geometrical characteristics such as washout (wing twist) built into it allowing the assembly of the wing to be more accurate. The materials used in building the wing are consistent with those used in the horizontal and vertical stabilizer. Figure 4.4 shows the plot layout used to make the wing ribs.
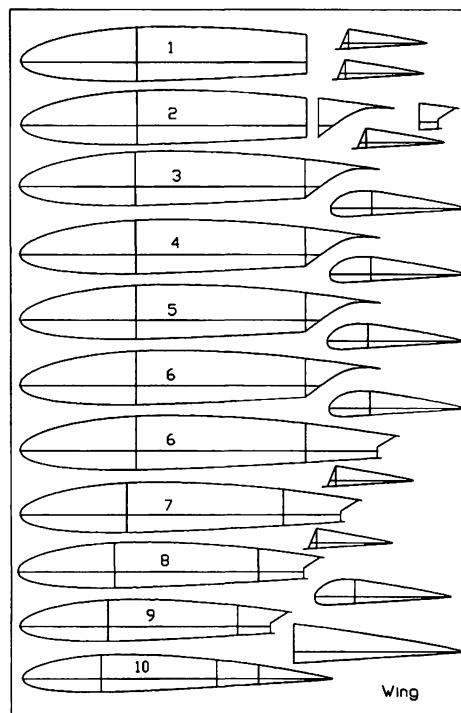
Figure 4.4: Wing Plot Layout

Notice that rib 6 has two profiles in figure 4.4. The only difference between these profiles exists aft of the rear spar. It can be seen from the structural layout presented in figure 4.5 that rib 6 is located at the junction of the inboard (rectangular) section and the

outboard (straight-tapered) section. The rib profiles aft of the rear spar and inboard of

this junction have provisions for the flap panel while the profiles outboard of this junction

have provisions for the aileron.

Leading Edge

Main Spar

Rib 1 Rib 2 Rib 3 Rib 4 Rib 5 Rib 6 Rib 7 Rib 8 Rib 9 Rib 10

Rear Spar

Aileron

Flap

Trailing Edge
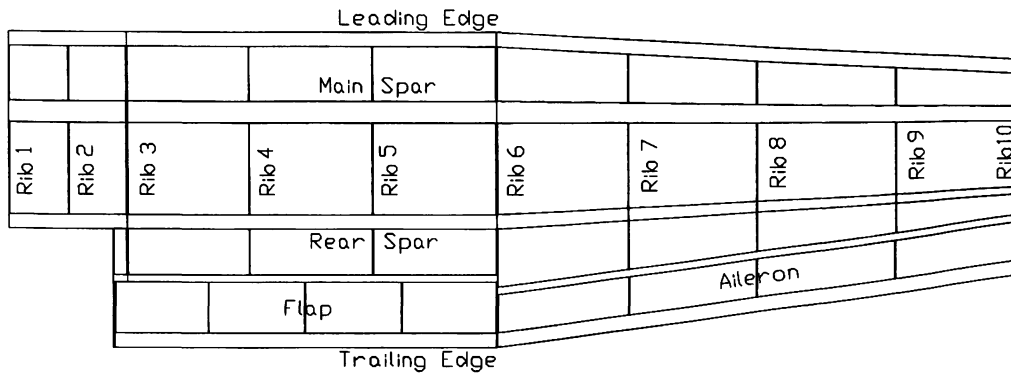
Figure 4.5: Wing Structural Layout

The ribs used in the outboard wing panels were made from 1/8 in. plywood while

the inboard panel (not including ribs 1-3) used 3/16 in. ribs. The center section (rib 3 of

the left panel through the center to rib 3 of the right panel) has 1/4 in. thick ribs.

The main spar of the wing was built from Douglas fir. The change in material

from spruce to fir was a last minute decision caused by the unavailability of large-

dimensioned, clean-grained spruce stock. Douglas fir was chosen because of its similar

specific gravity to spruce (0.43 for fir vs. 0.37 for spruce), higher allowable strength

(3366 psi), and cleaner grain structure. Although the finished Douglas fir wing spar

would weigh as much as 16% more than a spruce spar, the weight change was considered

negligible because the overall quantity of material used in the spar is low.

The spar caps were cut from the fir stock using ERAU's 3-axis CNC milling machine. Three-dimensional models of the spar caps were used to generate the tool paths for the CNC machine. Unlike the horizontal and vertical stabilizers, the wing's spar caps require tapered cuts along both the y and z axes. Using the CNC machine to cut the spar caps guaranteed that the tapers were cut accurately.

Each of the wing's upper and lower main spar caps were divided into five pieces for cutting: two outboard (left and right), two inboard (left and right), and a single center piece. All of the spar cap pieces were cut in similar fashion to that shown in figure 4.6. The first pass of the cutting tool was used to define the face of the spar cap (green dashed lines). After the face is cut, a profile cut is usually performed to detach the part from the stock (blue dashed line).
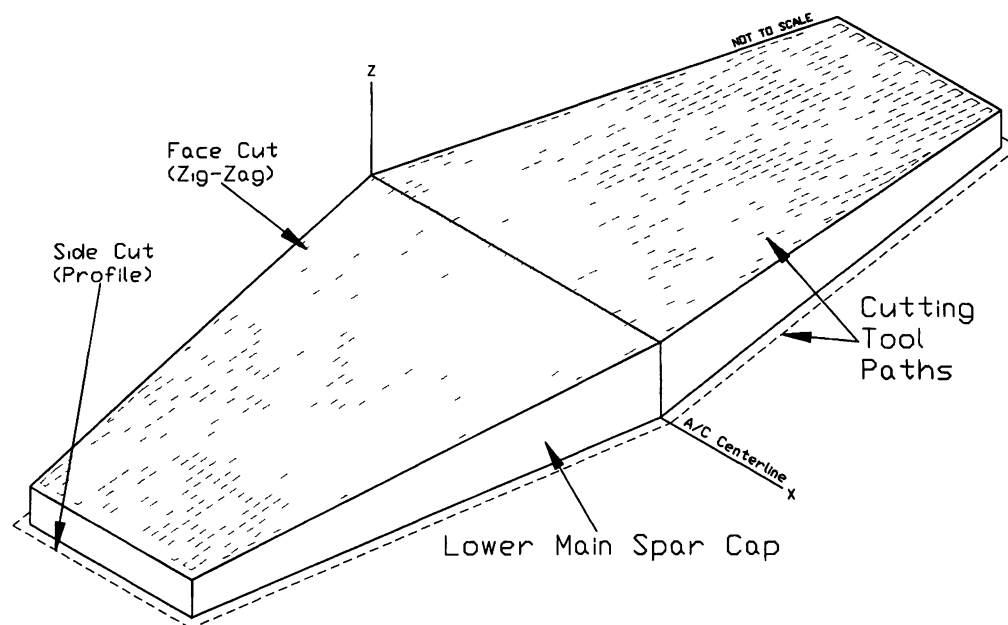
Figure 4.6: Wing Main Spar CNC Tool Paths

4.12

Cutting the spar pieces, however, required provisions to ensure that the finished cap would not break free from the stock before the cutting was complete. To guarantee that the part would not break free during cutting, two steps were taken. First, the stock was bonded to the cutting table using both screw fasteners and high strength spray adhesive. Second, the depth of the profile cut was set such that the part was not completely cut free from the stock. The remainder of the material, normally detached by the profile cut, was later removed by hand.

The assembly of the wing began with the lower main spar cap. Following the spar cap was the shear web, then the ribs, then the rear spar, and finally, the upper spar cap. Discontinuities exist in the spar caps and shear webs at both intersections of 1) the center section and the inboard panel and 2) the inboard panel and the outboard panel. To maintain load paths through these areas, doublers were used on the shear web. Plywood doublers were placed on the front and back of the shear webs for both the main spar and rear spar. The doublers extend from rib 4 of the left wing half to rib 4 of the right wing half, and from rib 5 to rib 7 of both wing halves. The doublers were sized such that the sum of the thickness of the front and back doublers equals the thickness of the shear web.

In an effort to save weight, the ribs in the outboard panel of the wing were outfitted with lightening holes. The majority of the portion of the ribs between the spars was removed. Also, the "D"-section portion of the ribs ahead of the main spar throughout the entire span of the wing were lightened.

Accommodations for four control servos were required in the wing. The flap servos were placed in the bay between ribs 4 and 5 and the aileron servos were placed between ribs 7 and 8. The flaps and ailerons were constructed after the wing structure was removed from the jig, simply for ease of construction.

The full-scale C172P has Frise type ailerons to reduce control forces and adverse yaw. To maintain similarity, Frise style ailerons were built for the 1/3-scale C172P. Figure 4.7 shows the actuation of the ailerons by the servo. The hinge line of the Frise ailerons is located on the upper surface of the wing. For the 1/3-scale aircraft, this hinge was constructed from miniature piano hinge. Figure B.20 shows the right-hand aileron mounted to the wing. As can be seen in figure B.20, three equal length portions of piano hinge were used on each aileron.

Figure 4.7 shows the range of aileron deflections can be quite large if the servo is actuated to its mechanical stop. Although the figure shows a very large deflection range, the radio controller used with the 1/3-scale C172P is equipped with functionality to limit the available control throw to the desired amount.
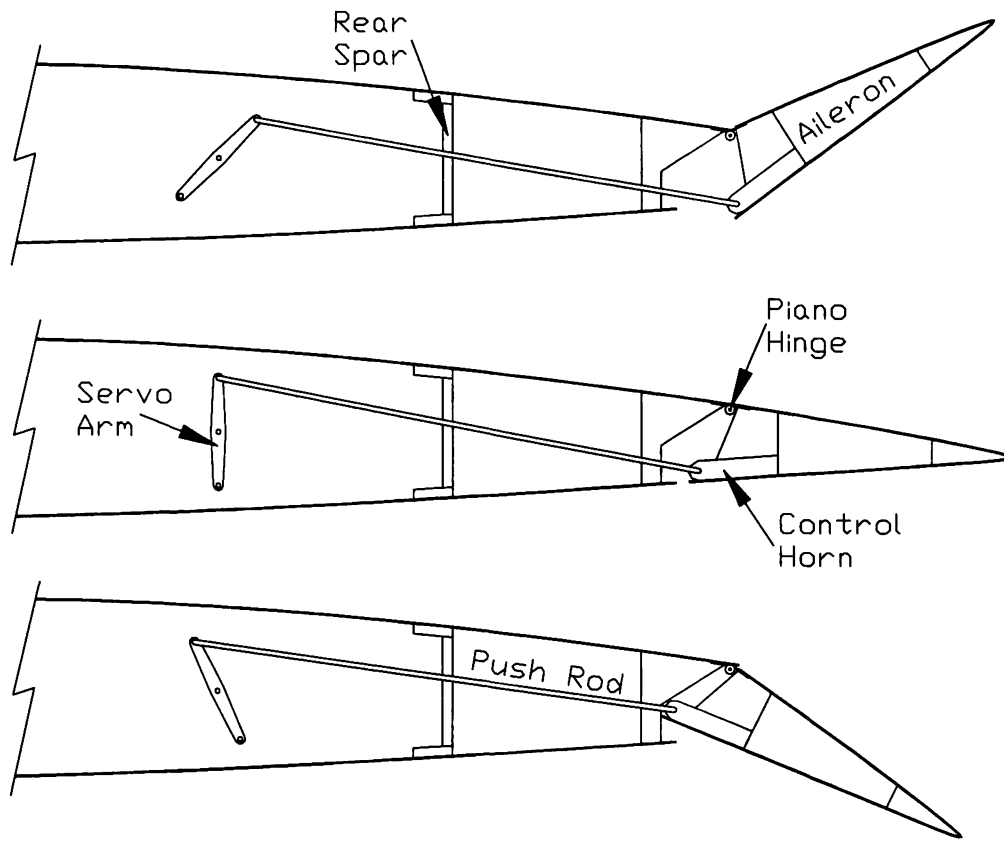
Figure 4.7: Aileron Control Linkage

The motion of the 1/3-scale C172P's flaps is similar to that of the full-scale aircraft. The flaps are single-slotted Fowler type and, therefore, require a somewhat sophisticated design to allow smooth operation. To achieve the desired action, the mounting of the flaps to the 1/3-scale aircraft was conducted similarly to the full-scale airplane. Figure 4.8 shows the two rib profiles, the "wing profile" and the "flap profile", that make up the flap mounting system. The wing profile is mounted to the rear spar of the wing and has two curve channels, or flap tracks. A pair of the flap profiles are mounted alongside the existing flap ribs (separated by the thickness of the wing profile). A pair of guide pins passes between the pair of flap profiles, through the flap tracks of the

4.15

wing profile. Figure 4.8 also shows the relative mounting locations of these flap

mounting components.
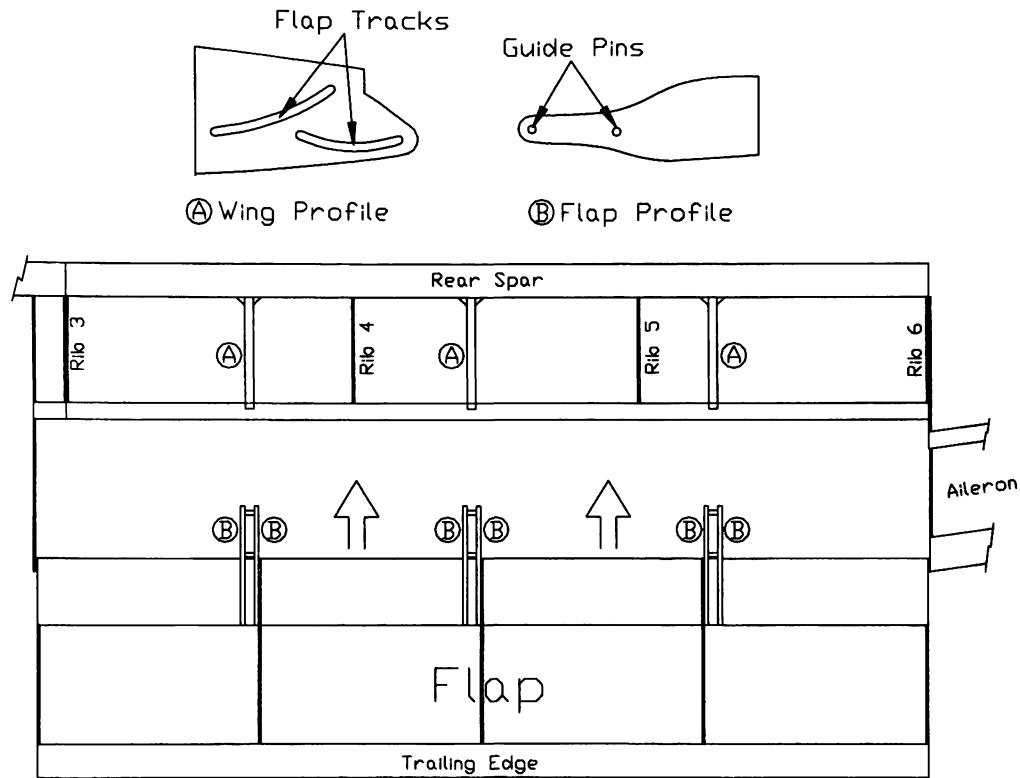
Figure 4.8: Fowler Flap Track Detail

Figure 4.9 shows side views of the completed flap mounting assembly at various

flap deflections. Notice that a continuous range of flap deflections is available from 0 to

35 degrees. This flap mounting design requires that the servo attachment point to the flap

be located mid-way between the guide pins of the flap profile. This allows for minimum

binding during flap extension and retraction. Figures B.21, B.22, and B.23 show the flap

mounting in detail.
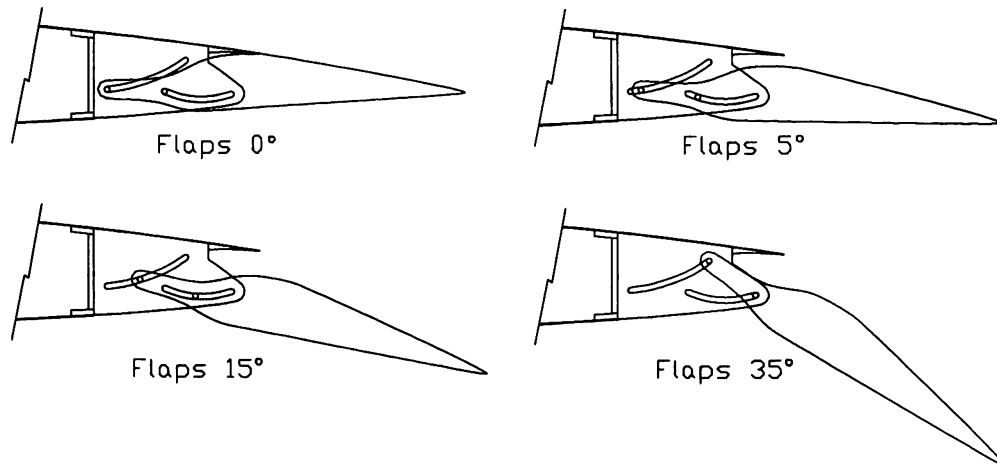
Figure 4.9: Flap Deflections

The full-scale C172P has been designed to use the wing strut as a major load bearing member for the wing. The 1/3-scale aircraft, however, does not require that the wing strut be capable of carrying any portion of the lift load on the wing. At this time, details about the design and the construction of the wing struts have not yet been addressed.

Construction of the Fuselage

Construction of the fuselage occurred in two stages. First the tailcone portion was built, followed by the cabin portion. Unlike the components described to this point, the fuselage did not require a building jig for construction. Instead, the portions were built in left and right halves and then joined together during final assembly.

Figure 4.10 shows cross-sections of the fuselage and their respective locations. These profiles inputted into the computer and were used to develop a 3-D solid model of the fuselage. Using the computer model, new cross-sections were developed at the

desired fuselage stations (FS). Figure 4.11 shows the structural layout of the fuselage and, hence, the locations of the bulkhead rings used for construction.
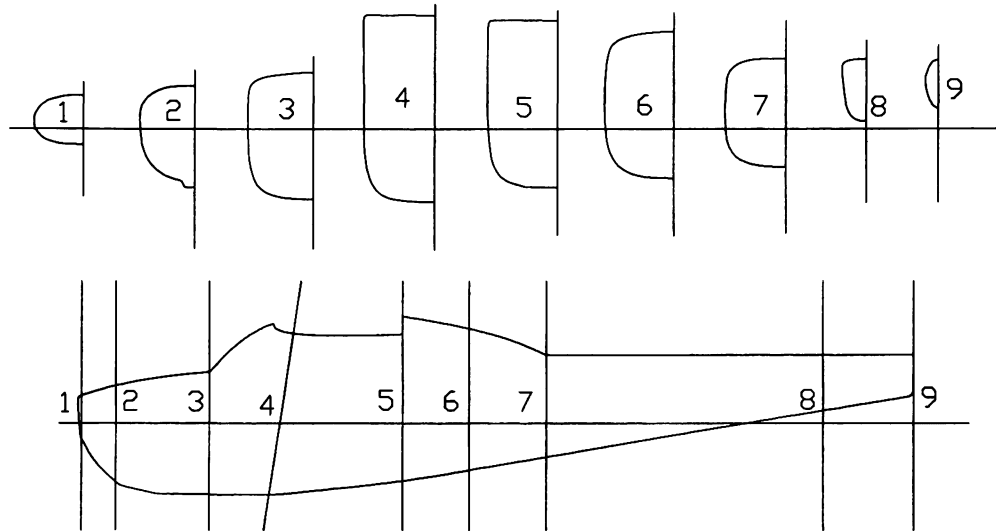
Figure 4.10: Fuselage Cross-Sections

Similarly to the wing and tail components, the fuselage rings were plotted on paper before being cut from plywood stock. Each ring was cut in two halves (left and right) similar to the profiles in figure 4.10.

Construction of each portion of the fuselage began first with a dorsal stringer and a keel stringer (see figure 4.11). The portion of the fuselage from ring 7 on is considered the tailcone section and was built first. The dorsal and keel stringers for this section were laid out on a flat surface and rings 7 through 12 were attached (perpendicular to the stringers). The finished assembly of the left half of the tailcone was then attached to the finished assembly of the right half of the tailcone.
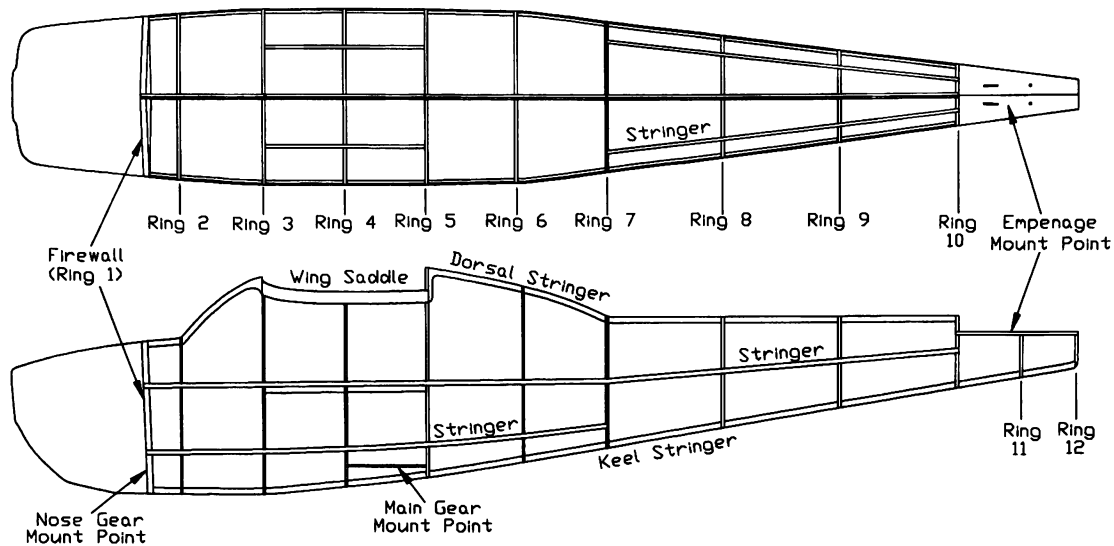
Figure 4.11: Fuselage Structural Layout

Once the tailcone assembly was complete, the additional six stringers specified in section 3.5 were added. Figure B.10 shows the finished assembly of the tailcone. This assembly process was repearted for the cabin portion of the fuselage resulting in the structure in figure B.11.

The forward-most fuselage ring shown in figure B.11 is ring 2. The firewall, or ring 1, was added forward of ring 2 (at the end of the dorsal and keel stringers shown). Instead of using a single thickness of plywood, the firewall was constructed of a sandwich of plywood and carbon fiber. Three layers of 1/8 in. plywood were used, between which, two layers of bi-directional weave carbon fiber was used. This five-layer sandwich was secured using epoxy resin.

A significant structural problem was the design of the wing attachment structure. This structure is required to transfer the lift loads from the wing into the fuselage rings

and stringers. Section 4.4 describes the wing-fuselage interface structure in more detail. Each of the joints in this region (and the entirety of the cabin portion of the fuselage) was not only bonded using epoxy resin, but also pinned with hardwood dowels for additional strength. Figure B.24 shows the wing, mounted to the fuselage, from the right, rear of the aircraft.

Figure B.13 shows the mounting interface for the empennage components to the fuselage. The fuselage structure provides a platform onto which the horizontal stabilizer is attached. Also, the vertical stabilizer main spar caps pass through the horizontal stab and attach to this platform. The portion of the skin that covers this section of the fuselage must remain removable to allow access to the bolts that hold the vertical stabilizer on.

Support structure was also provided in the cabin portion of the fuselage for the main landing gear. Mounting platforms were provided on both sides of the aircraft between ribs 4 and 5 (see figure 4.11 above).

The full-scale C172P has been designed to utilize a vertical tail extension (strake) for increased directional stability and improved spin characteristics. The construction of the 1/3-scale aircraft also includes this tail strake. At this time, however, details about the design and the construction of the strake have not yet been addressed.

The Landing Gear

Nose Gear: The nose gear of the 1/3-scale C172P was built by Robart Manufacturing, Inc. Originally, a design was developed which was to be built in-house. However, the product offered by Robart was determined to be more viable. The time savings due to out-sourcing the nose gear assembly made up for the increased cost of the part.

Figure B.15 shows the complete nose gear assembly mounted to the firewall. Located at the top of the assembly is a steering arm, which is used to turn the gear. The arm extends laterally on both sides of the gear and each side is attached to a servo, located directly behind the firewall.

Housed within the upper portion of the assembly is a coil spring to absorb shock. The nose gear has approximately 1 1/4 in. of travel. The nose gear tire (not shown in figure B.15; see figures B.29 and B.30) is 5.0 in. in diameter and has a cast aluminum rim.

Main Gear: The main gear structure was designed and built at ERAU. The tires and brakes, however, were purchased from Glennis Aircraft. The structure of the main landing gear centers on a 3/4 in. OD, 4000-series steel tube that extends, continuously, from the left side to the right. The sizing of the steel tube and design of the overall main gear system was coordinated by a group of students in the detail design class at ERAU during the fall semester, 1998.

Figure 4.12 shows the final assembly layout of the outboard portion of the main gear. The braking system for the 1/3-scale C172P is pneumatically actuated via a release valve in the center of the fuselage. Pressing the release valve (using a servo) releases pressurized air to both the left and right brakes, pushing the brake pads against the wheel rim. As mentioned previously, the brake unit and wheel tire and rim were purchased from Glennis Aircraft. The tire diameter used for the main gear is 6.0 in. The maximum diameter of the brake unit is 2.0 in. Figures B.29 and B.30 show the assembled aircraft fully supported on its landing gear.
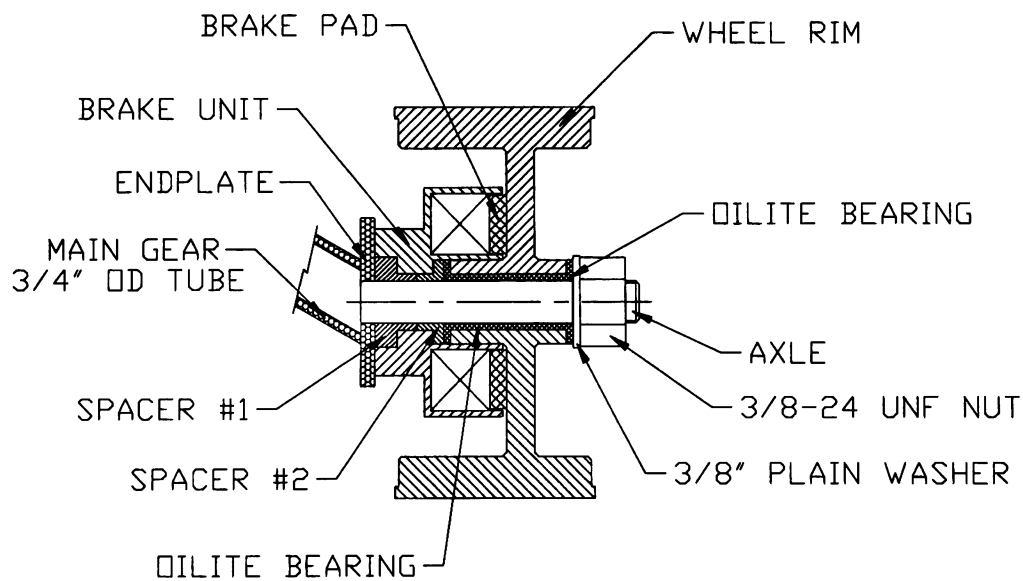
Figure 4.12: 1/3-Scale C172P Main Landing Gear Pneumatic Brakes

The Engine Mount

The engine mount used for the Quadra Aerrow Q100XL was designed and constructed at ERAU. Figure 4.13 shows the final layout drawing used for construction. The engine mount is a space frame structure built from 1/4 in. OD 4130 steel tubes. The wall thickness used for the main members is 0.022 in. The engine mount bolts to the firewall at four locations using 1/4 in. in diameter steel bolts. All of the engine mount structure is joined using Tungsten Inert Gas (TIG) welding for added strength.

The mounting plate that the engine bolts to contains four cups designed to accommodate rubber bushings for vibration damping. Figures B.16 through and B.18 show the engine, and engine mount secured to the firewall.
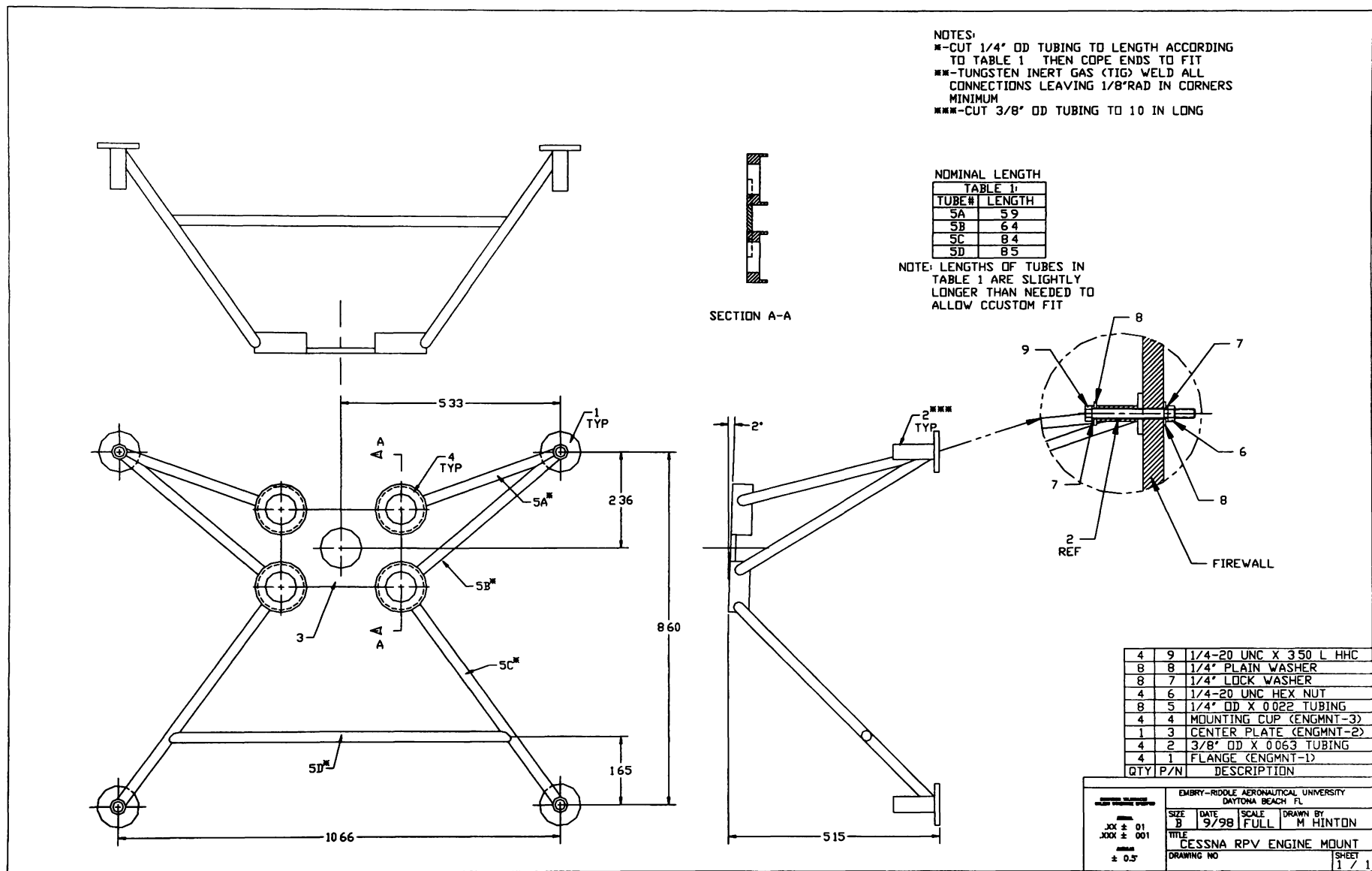
Figure 4.13: 1/3-Scale C172P Engine Mount

4.24

The Fiberglass Skin Panels

The external skin used on the 1/3-scale C172P was made using 6 oz. per square foot, bi-directional weave fiberglass. The vertical stabilizer, horizontal stabilizer, wing, and fuselage were all covered using fiberglass panels of varying layer count. The number of layers used depended only on the component; for example, the skin for the wing used four layers of fiberglass, while the stabilizers used only three. The cabin portion of the fuselage has four-layer panels while the tailcone portion has three-layer panels.

The lay-up of the fiberglass panels began with the fabrication of female molds (see *Jigs and Molds*, above). The molds were prepared for lay-up by applying a release agent (automobile wax) to the finished latex-enamel surface. The fiberglass cloth layers were then added along with the remainder of items necessary for the lay-up process. The entire assembly was then placed in a vacuum bag until cured.

The completed skin panels were trimmed to fit the respective surface and then applied using West Systems Slo-Cure epoxy resin (same resin used during lay-up). In some locations, bonding structure was unavailable and was, therefore, added. Before permanently attaching the panels, access panels were removed for the wing data collection location and the servos for the rudder (1 panel), elevator (2), flaps (2), and ailerons (2). These access panels are attached to the aircraft using small wood screws. The access panel for the rudder servo can be seen in figure B.19. Figures B.25 through B.27 show the access panels (panels removed) for the aileron servo (B.25), tailcone data collection board (B.26), flap servo (B.27), and wing data collection board (B.27).

4.3: Integration of the Aircraft Systems

Each of the many systems on-board the 1/3-scale C172P must be integrated into the aircraft with minimal impact on the operation of each of the other systems. This section is divided into the three major systems: control, ODATS, and audio/video. Each of the following sub-sections describes the considerations taken in integrating these systems.

Control System Integration

As mentioned previously, the control system components on-board the aircraft include ten servo actuators, a wireless receiver, and a battery pack. The receiver and battery were placed in the cabin portion of the fuselage. The servos were placed throughout the aircraft as close as possible to the item they control.

For the rudder, elevator, and nose gear, a pull-pull type connection was used between the servo and the item's control horn. This means that each end of the servo's control arm is connected to its own side of the controlled item's control arm. Figure B.19 shows the control linkages attached for the right-hand side of the rudder and upper right-hand side of the elevator. Using pull-pull type actuation is advantageous because it 1) reduces slop in the connection (that could lead to flutter or reduced control response) and 2) increases redundancy.

All the servos placed on the aircraft (except the brake servo) use push rods to manipulate the item they control. High tensile strength steel push rods (piano wire) were

used in all cases to reduce the possibility of bending under load. Each push rod/control horn connection (servo end and control item end) was made using a clevis connector. The clevis connectors were secured closed by sliding a small length of plastic tubing over the connection.

Many of the servos were located too far away from the receiver unit to allow the supplied connector cable to be used. Therefore, cable extensions were spliced into the lines between the servos and the receiver. The wire used for these splices was chosen to minimize the voltage drop from receiver to servo and, hopefully, maintain signal clarity. Also, connectors (located in the aft tailcone) were added in the signal lines for the elevator and rudder allowing the horizontal and vertical stabilizers to be completely removed from the aircraft.

Audio/Video System Integration

The micro camera has not yet been installed in the aircraft. However, during construction, provisions have been made to allow the audio/video components to be easily installed.

Provisions have been made for the camera to mounted in the aircraft looking forward from the front of the cockpit, giving a pilot's-eye-view. The forward and rear "windows" of the 1/3-scale C172P are not windows at all. Due to the difficulty in reproducing the complex curves of the windows of the full-scale aircraft, blocks of high density foam have been placed in these regions and carved into the proper shapes. A

small portion of the foam in the forward "window" will be removed to let the video camera look out.

The wireless transmitter antenna will protrude from the lower surface of the fuselage, between the main gear. This location was chosen to maximize signal strength below the aircraft when in flight.

The location of the battery needed for system operation has not yet been determined. The battery purchased for use with the audio/video system is a 6-volt DC, 7000 mAh, wet cell battery. Significant consideration will be needed in determining the mounting location of this battery due to its size and weight.

The Airdata Boom

Figure 4.14 shows the construction drawing used in building the airdata boom. Each of the components of the boom were manufactured at ERAU in the engineering machine shop. The assembled boom can be seen in figure B.2 during testing in ERAU's low speed wind tunnel.

The pitot-static portion of the boom was constructed first. The tubing used inside the probe was brass and was bonded in place using epoxy resin. The remainder of the pitot-static probe was also bonded together using epoxy resin.
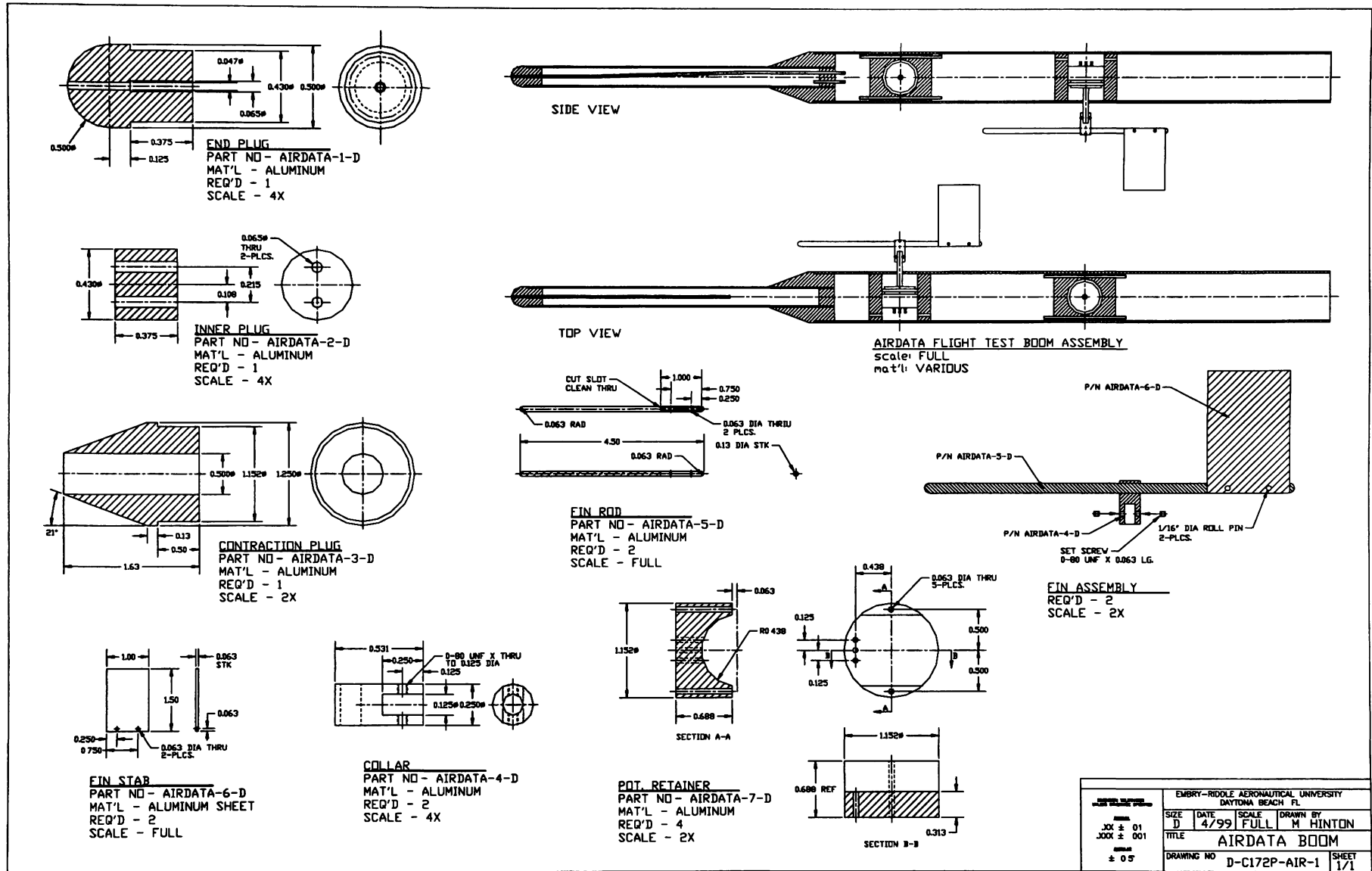
Figure 4.14: The Airdata boom

4.29

Tygon tubing was used to carry the pressure information from the total and static ports, through the remainder of the boom, to the data collection station in the wing. To pass the pressure data through the pot retainers, brass tubing was inserted, onto which the Tygon tubing was attached.

The cluster of three holes in the potentiometer retainers (seen in figure 4.14) is used to pass the potentiometer signal wires through. Each of these holes is sized such that two wires can pass through (one for each potentiometer, which itself requires three signal wires).

As mentioned earlier, the airdata boom has been tested and calibrated in ERAU's low speed wind tunnel. Figure B.2 shows the airdata boom mounted to the 6-component, pyramidal force balance in the low speed section of the wind tunnel. Pressure and angular data was collected from the boom's sensors and used to calibrate the airdata portion of the ODATS. The airdata boom worked completely as expected and gave good correlation during testing. The final results of the testing and calibration are presented in the final documentation of the ODATS.

The On-Board Data Acquisition System (ODATS)

The construction of the ODATS for the 1/3-scale C172P was conducted as a thesis project for Matti Hirvonen, an engineering student at ERAU specializing in avionics. During Matti's involvement with the project, all necessary components were purchased and assembled for the ODATS. The system was also powered up, tested, and

4.30

temporarily installed in the aircraft. Successful demonstration of streaming data from the aircraft to the ground station (laptop) was shown.

As mentioned in section 3.6, *Data Collection System*, the conditioned and converted data signals are compiled into a final data stream by the data fusion block in figure 3.12. A micro controller was purchased to control this assembly of the data stream. The controller can be programmed via software loaded onto the ground station computer. During operation, the micro controller orchestrates the reading of the data through control of a series of multiplexers. A data reading order was determined and programmed into the controller. The controller then switches from multiplexor to multiplexor reading each data word in the pre-defined order. The individual data pieces, along with error checking codes and time data, are then assembled into the data stream. Once it reaches the last piece of data, it starts again at the first data item. The completed data stream is then sent to the wireless modem for transmission to the ground.

At $2250 (in 1998), the 2.4 GHz wireless modem kit for the ODATS was, by far, the most expensive single item purchased for the 1/3-scale C172P project. The modem kit includes a remote wireless transmitting modem (on-board the aircraft), a dipole antenna, a base station receiving modem, and all other components necessary for operation. The base station modem interfaces with the ground station computer via standard RS-232 (serial) port cable. The software supplied by with wireless modem pair is also loaded onto the ground station computer.

The micro controller and wireless modem will be mounted in the cabin portion of the fuselage. The wireless modem antenna will also be mounted on the lower surface of the fuselage to maximize signal clarity below the aircraft.

The Pneumatic Braking System

As mentioned previously, the braking system on the 1/3-scale C172P operates on air pressure. This pneumatic system is surprisingly simple and was easy to install in the aircraft. Figure 4.15 shows the general system arrangement. All of the components of
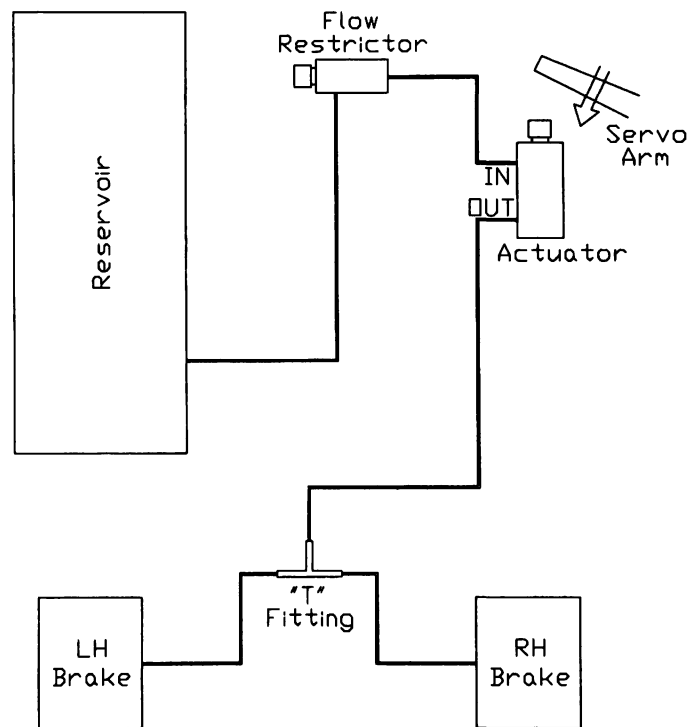
Figure 4.15: The Pneumatic Braking System

the brake system shown in figure 4.15 (except the reservoir and servo) were purchased from Glennis Aircraft. The reservoir, like the nose gear assembly, was purchased from Robart Manufacturing, Inc..

The pneumatic braking system operates on a 30-40 psi reservoir pressure. When the brakes are engaged, the servo arm is moves toward the brake actuator, pressing the pressure release switch. This releases the air to the "T"-fitting which sends pressurized air to both main gear brakes. The flow restrictor is placed in the system to keep from draining the reservoir too quickly.

The entire braking system is installed in the cabin portion of the fuselage and is mounted to the keel stringer between fuselage rings 4 and 5. The pressure reservoir can be refilled by following these five steps.

1. Disconnect the pressure line on the upstream side of the "T"-fitting,
2. Bleed excess pressure from the system by depressing the brake actuator switch,
3. Connect pump to disconnected line,
4. Depress brake actuator switch and back-pump the system/reservoir to desired pressure,
5. Reconnect the line to the "T"-fitting.

Although the brake system has been completely installed and functionally tested, powered taxi tests will need to be completed to adjust the brake "feel." System pressures below 30 psi can be used to soften the braking action at the expense of system operation cycles. Pressures above 40 psi may be needed in this case, however, due to the large aircraft weight.

The Engine Ignition and Fuel Systems

Ignition System: The Quadra Aerrow Q100XL uses an electronic ignition module to control the spark delivery to the engine. The Electronic Ignition Subsystem (EISS) has

the capability of controlling the timing of the engine as a function of engine rpm to optimize the engine performance. At engine speeds in the range of 0-1000 rpm, the unit fires the ignition at 0° top-dead-center (TDC). By 6000 rpm the EISS has advanced the timing (linearly) to 26-32° before top-dead-center (BTDC).

The electronic ignition module is mounted directly behind the engine on the forward side of the firewall. The unit is powered by a 6.0 VDC battery pack mounted just below it on the back side of the firewall. These components can be seen in figure B.18.

Fuel System: Fuel, in the 1/3-scale C172P, is contained in a pair of 20 fl. oz. fuel tanks located in the forward cabin portion of the fuselage. Permanent mounting structure has not yet been provided for the fuel tanks. The fuel supply line from each fuel tank will be attached to a "T"-fitting that supplies the carburetor. In-line fuel filters and check valves will be added to ensure proper and consistent system operation. Care must be taken in mounting the fuel tanks such that the fuel quantity is located above the carburetor to provide positive pressure. If the system is found to starve itself of fuel, then the crankcase can be outfitted with a pressure tap and a line can be routed from the engine back to the fuel tanks, pressurizing the tanks.

4.4: Aircraft Assembly/Disassembly

The 1/3-scale C172P utilizes a somewhat modular design allowing it to be easily disassembled for storage, transportation, or repair. Currently, the aircraft can be disassembled into four major components: 1) horizontal stabilizer, 2) vertical stabilizer,

3) wing, and 4) fuselage. Two more components will be added to the overall assembly once the aircraft is complete: 5) wing struts and 6) tail strake. This section describes how the tail surfaces and wing are attached to the fuselage.

The horizontal stabilizer is secured to the empennage mounting plate with four bolts. As shown in figure 4.16, the bolts pass through the upper surface of the stab, through the reinforcing blocks mounted to the lower surface, and into blind nuts in the empennage mounting plate. The incidence of the horizontal stab is set using a block of wood attached to the aft end of the empennage mounting plate. The incidence block can be replaced with an appropriately sized (taller or shorter) spacer depending upon a needed change to the tail incidence angle.
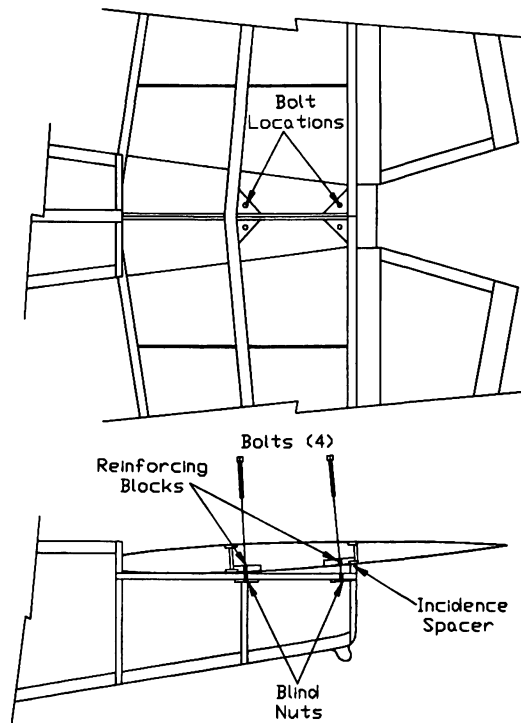
Figure 4.16: Horizontal Stabilizer Mounting Detail

The vertical stabilizer mounts to the aircraft only after the horizontal stabilizer is in place. Figure 4.17 shows the vertical stab mounting detail. The main spar caps of the vertical stabilizer pass through both the horizontal stab and the empennage mounting plate and are bolted to bracket structure below. The vertical stab also has a pair of bolts just in front of the rear spar that tie into blind nuts mounted under the upper surface skin of the horizontal stab.

FRONT VIEW
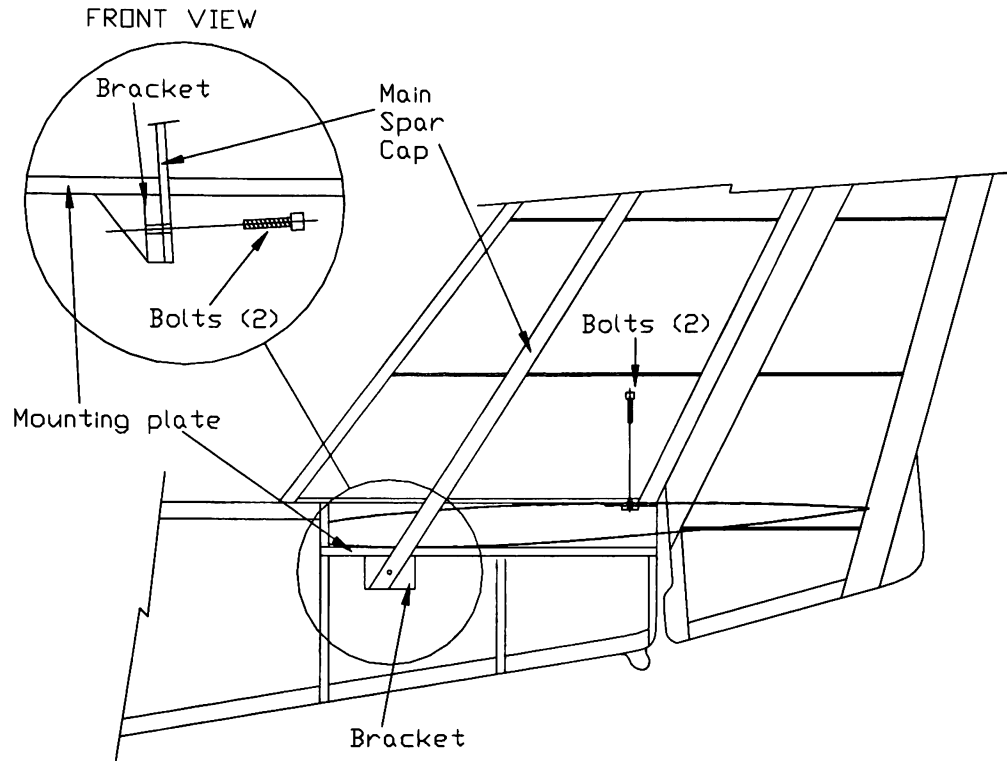
Figure 4.17: Vertical Stabilizer Mounting Detail

Figure 4.18 shows top, front, and side views of the wing attachment structure. Attached to each side of ribs 1 and 2 (of each side of the wing) are 1/4 in. plywood brackets that extend below the lower surface of the wing. These brackets are spaced such that they slide down over the sides of corresponding sub-ribs located below the wing ribs. A 1/4 in. bolt passes through the brackets and sub-ribs, holding the front of the wing down.

Protruding from the rear spar, between ribs 1 and 2, are a pair of 1/2 in. dowel pins. These dowels acts as alignment tools when bolting the wing to the fuselage. Between ribs 2 and 3, a 1/4 in. bolt passes through the rear spar into fuselage ring 5, securing the rear spar.

4.37
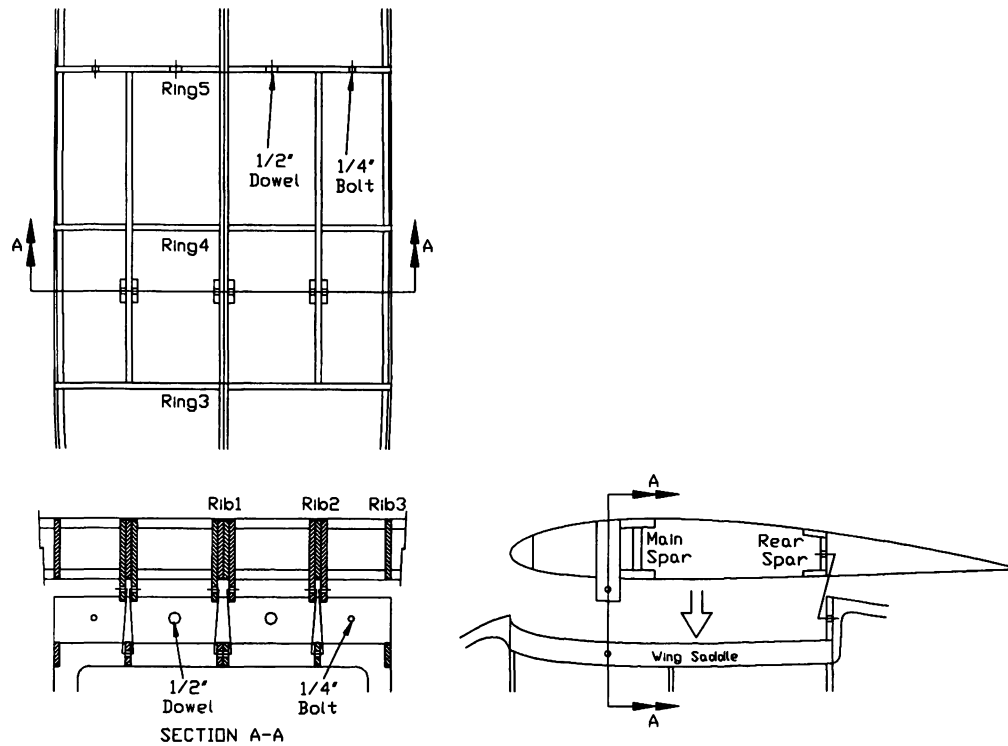
Figure 4.18: Fuselage-Wing Interface

The wing-fuselage attachment structure has been designed with multiple

redundancies applied. Each of the 1/4 in. bolts used throughout the attachment interface

exceeds the load carrying capacity required. Should one of the bolts fail, the increased

stresses would be easily shared amongst the remaining structure.

Chapter 5: Conclusions

The design and construction of the 1/3-scale C172P flight test aircraft was a large and multi-faceted project. Each facet of the project included engineering elements of design, aerodynamics, structures/stress, and manufacturing. The design phase of the project began in the early spring of 1997. Figure B.30 shows the culmination of the author's efforts during the construction phase of the project in late spring 1999.

Much was accomplished during the author's involvement in this project. Although the aircraft is not entirely complete, many of the systems and sub-assemblies are. The horizontal and vertical stabilizers, wing, and fuselage have been constructed. The landing gear, engine mount, and airdata boom were also completed. Functionality has been shown of the control system, audio/video system, ODATS, and braking system. Assembly of the components and most of the systems into the final aircraft has also been accomplished.

Each component or system on-board the 1/3-scale C172P was a project in itself, requiring, among others, detailed consideration of its contribution to the overall aircraft. Along with the design and construction, it was necessary to evaluate the effect each part had on the remainder of the aircraft. The completed aircraft will be a well integrated flight test vehicle capable of measuring the necessary parameters required to correlate full-scale and 1/3-scale flight characteristics. The verification of the scaling laws presented in chapter 2 will aid in future efforts with scaled flight test aircraft.

Many lessons were learned over the course of this project. Most notably, the process of moving from a design to a finished item can be a slow one. In this case, the magnitude and complexity of this project were largely underestimated, causing the construction phase to stretch out much longer than originally scheduled. Even with the unanticipated delays, the overall design, and resulting physical aircraft will provide a good platform for conducting the testing necessary for verifying the scaling technique.

Chapter 6: Recommendations for Future Work

By the end of the spring semester, 1999, the 1/3-scale C172P had not yet flown. In fact, figure B.30 shows the level of completion of the aircraft at approximately one week before the end of the author's involvement with the project. Following figure B.30, a handful of additional tasks were completed such as the bonding of the upper wing skin to the wing structure.

In general, it is recommended that the aircraft be completed and flown. It is also recommended that data be taken and analyzed so that correlations to predictions can be made. However, before these more obvious steps can be accomplished, the following items need to be completed or addressed.

1. Complete the engine cowling: The molds for the engine cowling have been fabricated but the fiberglass skins have not yet been completed. Provisions for attaching the cowling to the fuselage have been provided by stopping the fuselage skins at the first ring aft of the firewall (ring 2 in figure 4.11).

2. Complete the ground station: The completion of the design and the writing of the code for the ground station's data processing software are still required. Efforts in this area up to now have produced a very basic design (see section 3.7). It may be desired to evaluate off-the-shelf data acquisition and analysis software, such as LabView, to expedite this process if an individual with adequate programming skills cannot be found.

3. Design and build the tail strake and wing struts: The design and construction of the tail strake and the wing struts has not been accomplished. These components have not yet been considered because they are not necessary for the structural integrity of the aircraft.

4. Complete installation of fuel system: The necessary components of the fuel system have been purchased, but not installed in the aircraft.

5. Complete installation of audio/video system: The audio/video system has been tested for functionality but has not been installed in the 1/3-scale C172P. The mounting locations have been determined as specified in section 4.3.

6. Address center of gravity problem: A problem with the aircraft's c.g. was noticed during the later stages of construction. The tail-heavy characteristic of the 1/3-scale C172P suggests that the tail surfaces and/or fuselage tailcone may be heavier than planned. Modifications to these items may be needed once the remainder of the aircraft's components and systems are installed and a more accurate measurement of the c.g. is taken. An effort was made during construction to keep the overall empty weight of the aircraft significantly below the 89 lb takeoff weight in order to have margin for ballasting. Should the final aircraft empty weight be below the 89 lb limit, (and the aft c.g. problem still exist) ballasting the forward fuselage to compensate would be recommended.

7. Construct aerodynamic fairings: The full-scale C172P has a number of components solely for aerodynamic purposes including: 1) streamlined wheel pants on the nose and main gear, 2) streamlined main gear strut tube covers, 3) drooped wing tips, 4) horizontal and vertical stabilizer tip round-outs, and 5) wing trailing edge to upper fuselage fairings. All of these components benefit the aerodynamics of the aircraft and are non-structural components. The construction method proposed for these items is to hand shape high-density (blue) foam to the desired contour and then bond in place.

In addition to the seven items described above, a few items need to be accomplished once the aircraft is complete. Taxi tests must be conducted to properly adjust characteristics such as braking action. The proper camera angle should also be set during taxi tests.

Finally, it is recommended that a clear, complete, and concise set of flight test plans be made before beginning the testing program. A good description of the type of test, including the type and definition of each maneuver, will minimize the risk of collecting unusable data. Proper definition of the procedures and expectations of the testing will result in more highly productive flights. The results of the flight testing phase of the project must culminate in, at minimum, two items: 1) procedural recommendations to be used in follow-on scaled flight test projects and 2) verification/correlation of the scaling technique via comparisons to the full-scale C172P.

Appendix A

Weight Estimation Equations

(Taken from pages 404-407 of reference 1)

Wing:

$$W_{wing} = 0.036 S_w{}^{0.758} W_{fw}{}^{0.0035} \left(\frac{A}{\cos^2 \Lambda} \right)^{0.6} q^{0.006} \lambda^{0.04} \left(\frac{100 t/c}{\cos \Lambda} \right)^{-0.3} \left(N_z W_{dg} \right)^{0.49}$$ (EQ A.1)

Horizontal Stabilizer:

$$W_{h.tail} = 0.016 \left(N_z W_{dg} \right)^{0.414} q^{0.168} S_{ht}{}^{0.896} \left(\frac{100 t/c}{\cos \Lambda} \right)^{-0.12} \left(\frac{A}{\cos^2 \Lambda_{ht}} \right)^{0.043} \lambda_h{}^{-0.02}$$ (EQ A.2)

Vertical Stabilizer:

$$W_{v.tail} = 0.073 \left(1 + 0.2 \frac{H_t}{H_v} \right) \left(N_z W_{dg} \right)^{0.376} q^{0.122} S_{vt}{}^{0.873} \left(\frac{100 t/c}{\cos \Lambda_{vt}} \right)^{-0.49} \left(\frac{A}{\cos^2 \Lambda_{vt}} \right)^{0.357} \lambda_v{}^{0.039}$$ (EQ A.3)

Fuselage:

$$W_{fuse} = 0.052 S_f{}^{1.086} \left(N_z W_{dg} \right)^{0.177} L_t{}^{-0.051} \left(L/D \right)^{-0.072} q^{0.241} + W_{pres}$$ (EQ A.4)

Main Landing Gear:

$$W_{MLG} = 0.095 \left(N_l W_l \right)^{0.768} \left(L_m / 12 \right)^{0.409}$$ (EQ A.5)

Nose Landing Gear:

$$W_{NLG} = 0.125 \left(N_l W_l \right)^{0.566} \left(L_n / 12 \right)^{0.845}$$ (EQ A.6)

Installed Engine:

$$W_{inst.engine} = 2.575 W_{en}{}^{0.922} N_{en}$$ (EQ A.7)

Fuel System:

$$W_{fuelsys} = 2.49 V_t{}^{0.726} \left(\frac{1}{1 + V_i/V_t} \right)^{0.363} N_t{}^{0.242} N_{en}{}^{0.157}$$ (EQ A.8)

Flight Controls:

$$W_{flightcntls} = 0.053 L^{1.536} B_w{}^{0.371} \left(N_z W_{dg} \times 10^{-4} \right)^{0.80}$$

(EQ A.9)

Electrical System:

$$W_{electrical} = 12.57 \left(W_{fuelsys} + W_{avionics} \right)^{0.51}$$

(EQ A.10)

Avionics:

$$W_{avionics} = 2.117 W_{uav}{}^{0.933}$$

(EQ A.11)

Appendix B
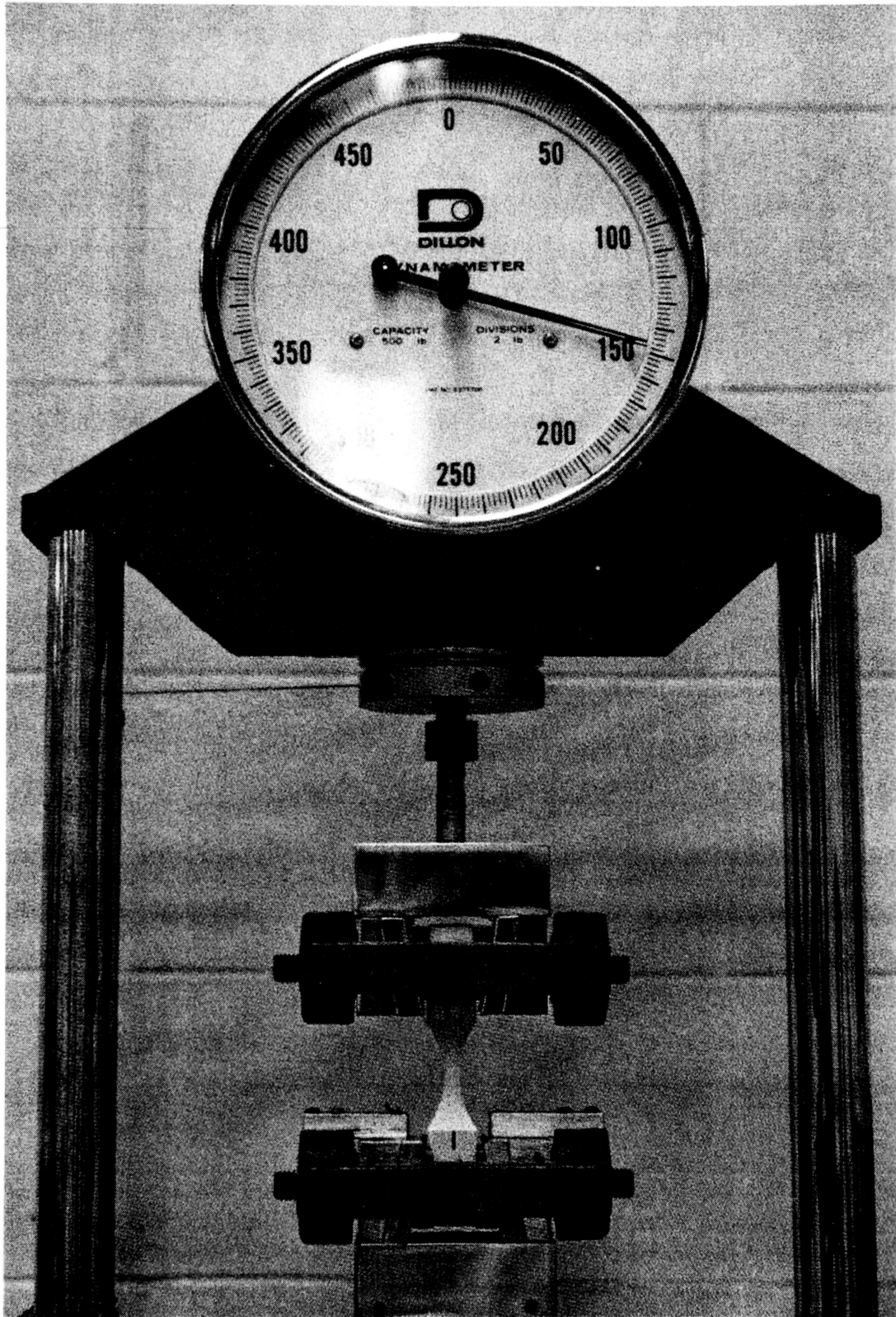
Figure B.1: Testing of Tensile Sample Using ERAU's Dynamometer
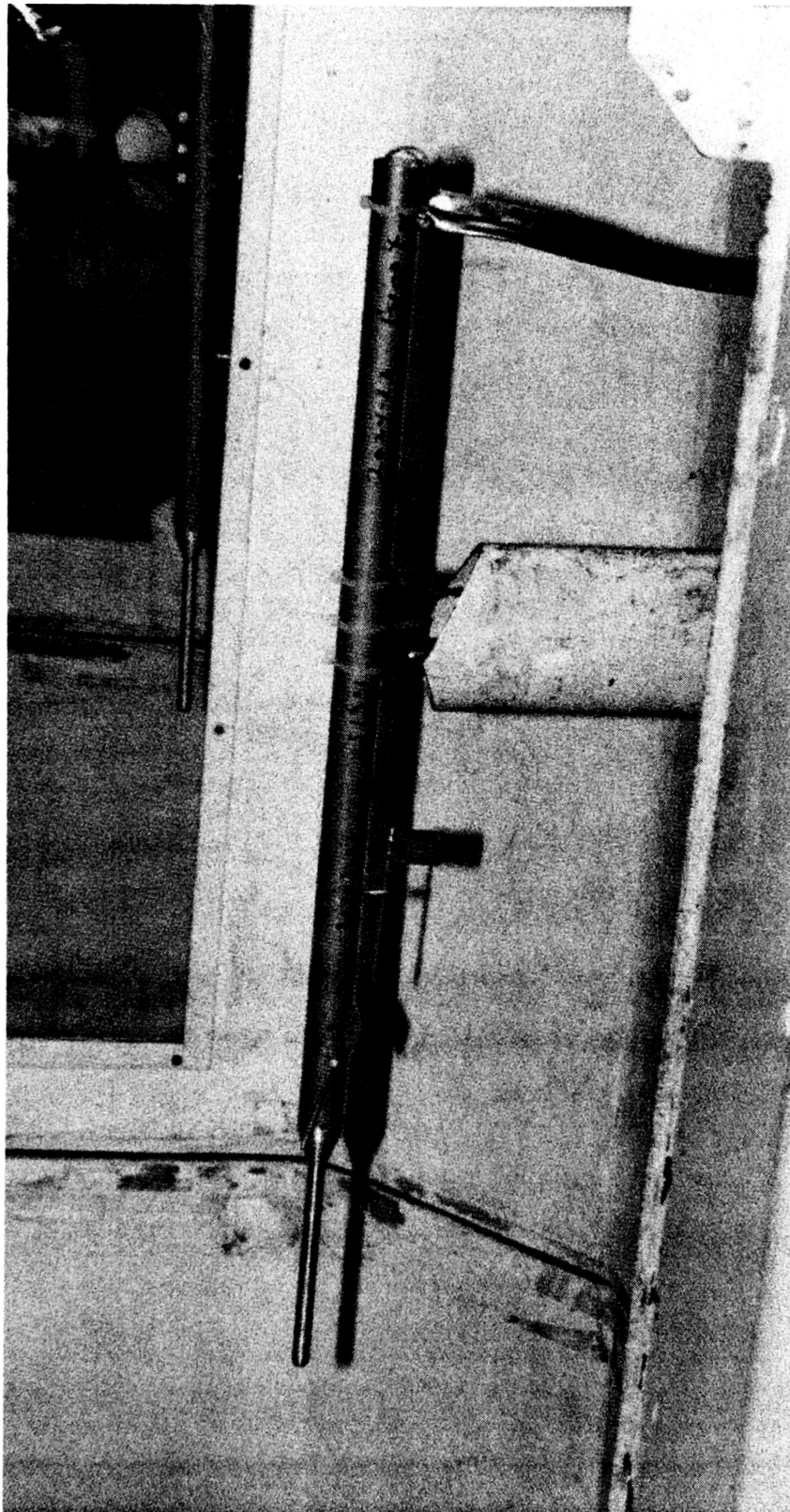
Figure B.2: Testing the Airdata Boom in ERAU's Low Speed Wind Tunnel
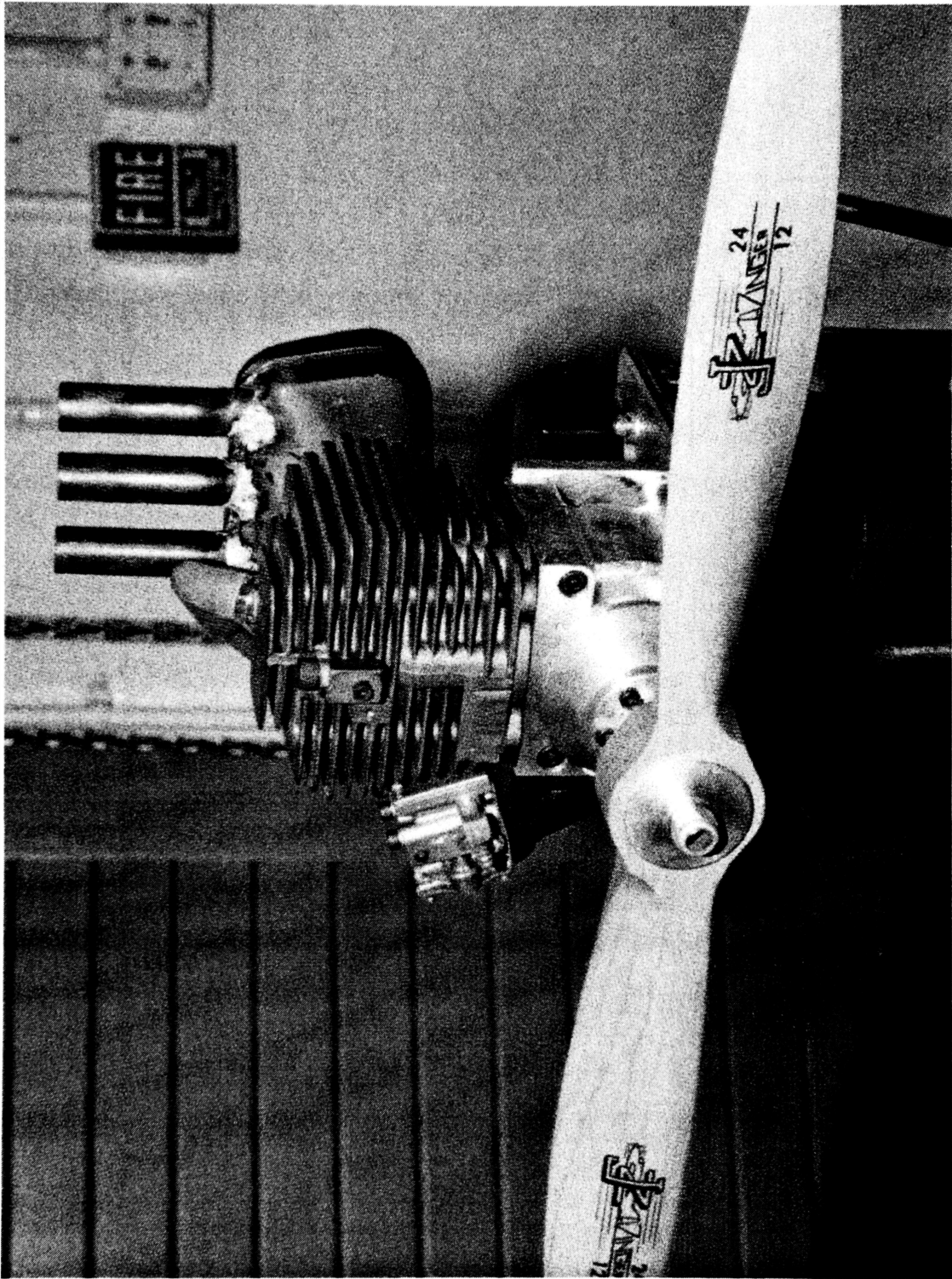
Figure B.3: Quadra Aerrow Q100XL with 24x12 Wooden Propeller
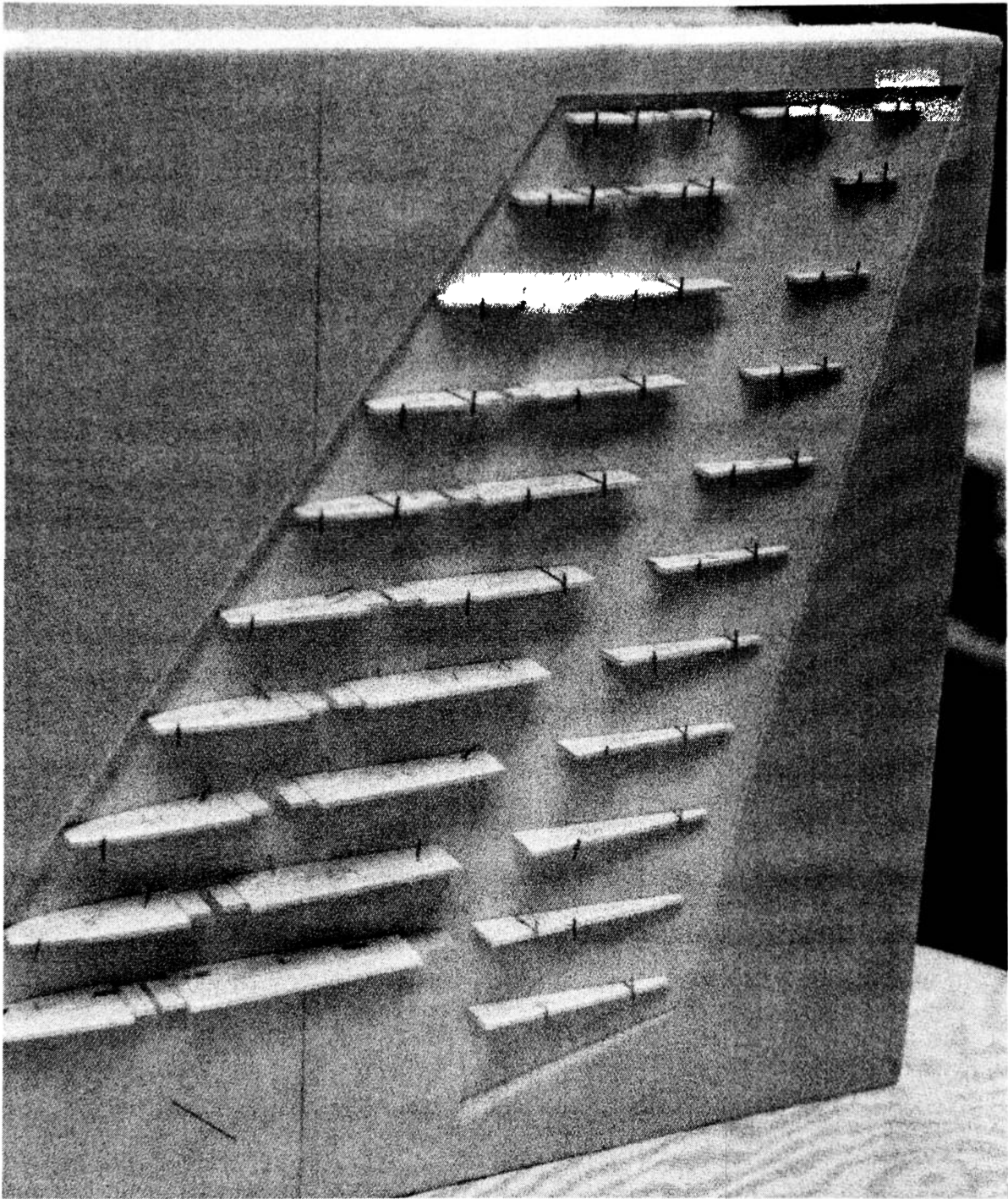
Figure B.4: Vertical Stabilizer Ribs in Building Jig Prior to Assembly
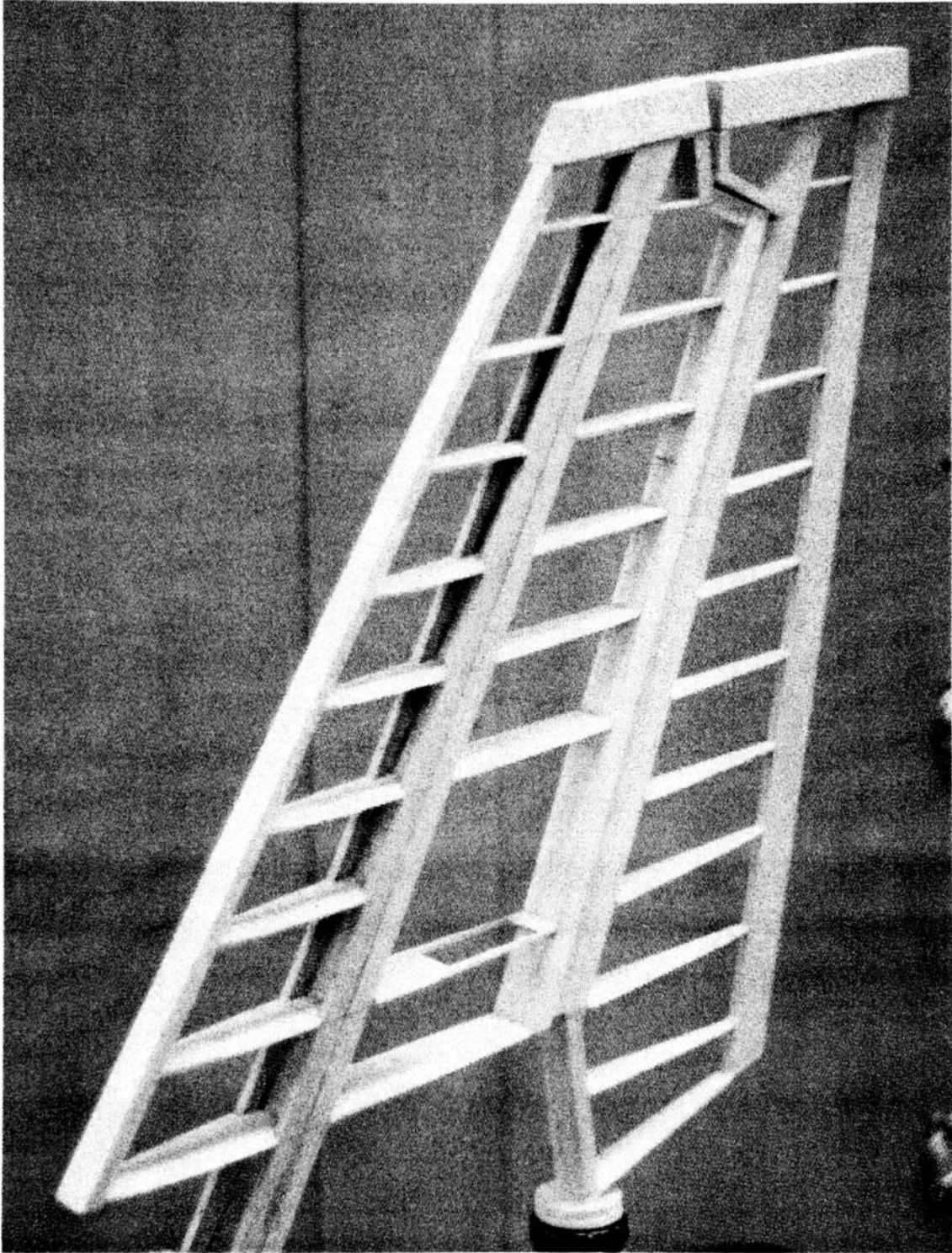
Figure B.5: Original Vertical Stabilizer Final Assembly
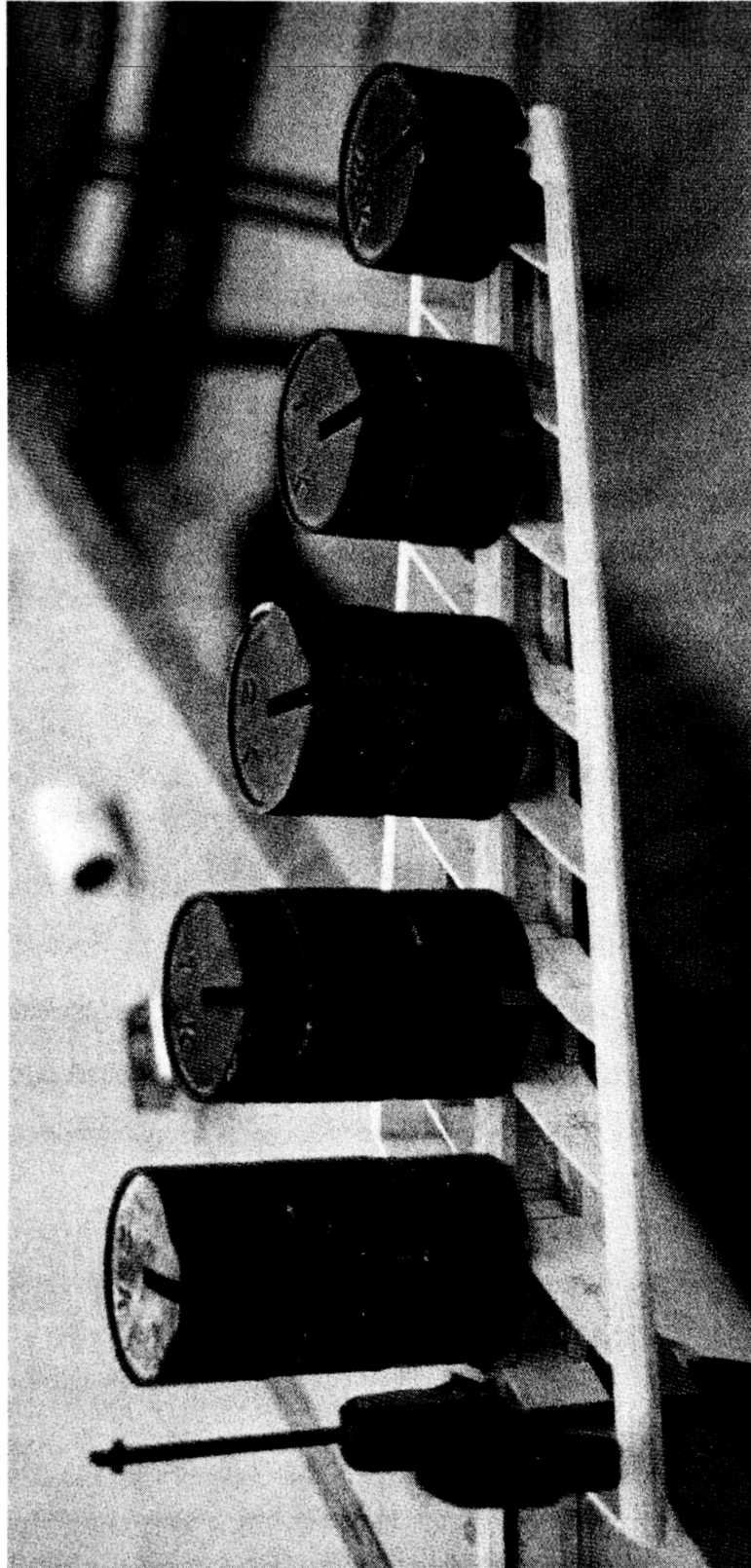
Figure B.6: Original Vertical Stabilizer Ultimate Load Test
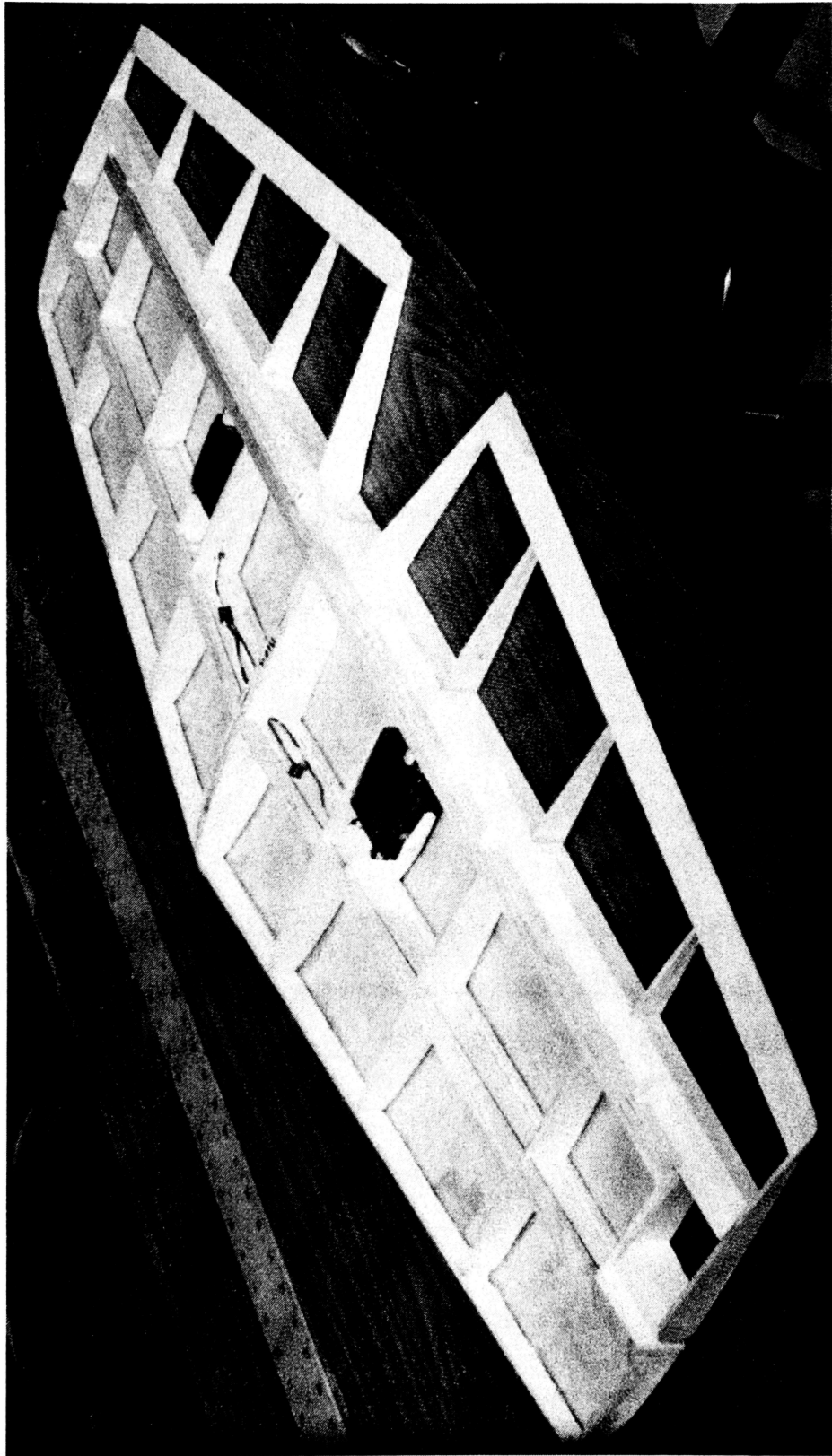
Figure B.7: Horizontal Stabilizer Assembly
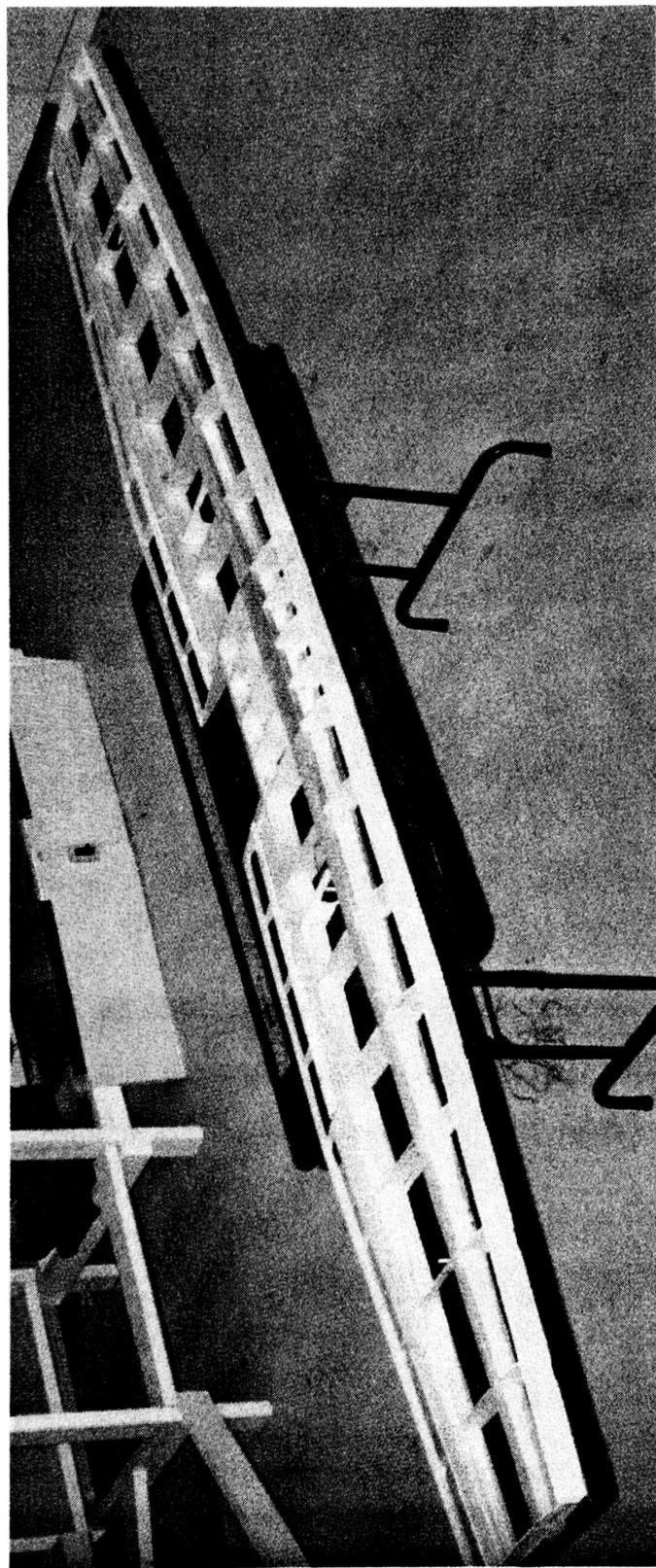
Figure B.8: Wing Assembly - 1

Figure B.9: Wing Assembly - 2

Figure B.10: Fuselage Tailcone Assembly
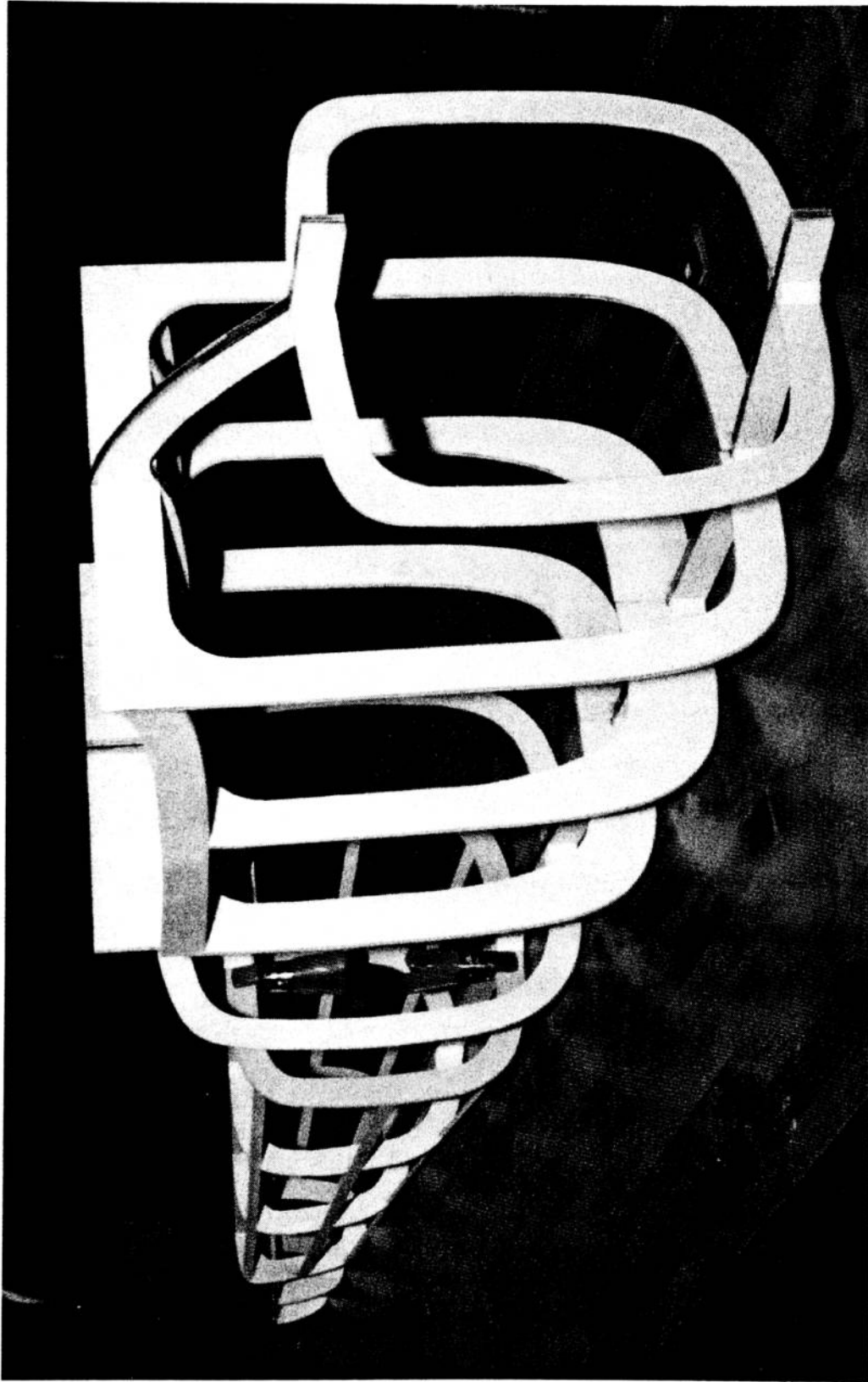
Figure B.11: Fuselage Assembly – All Rings in Place

Figure B.12: Vertical and Horizontal Stabilizers Mounted to Aft Fuselage Tailcone
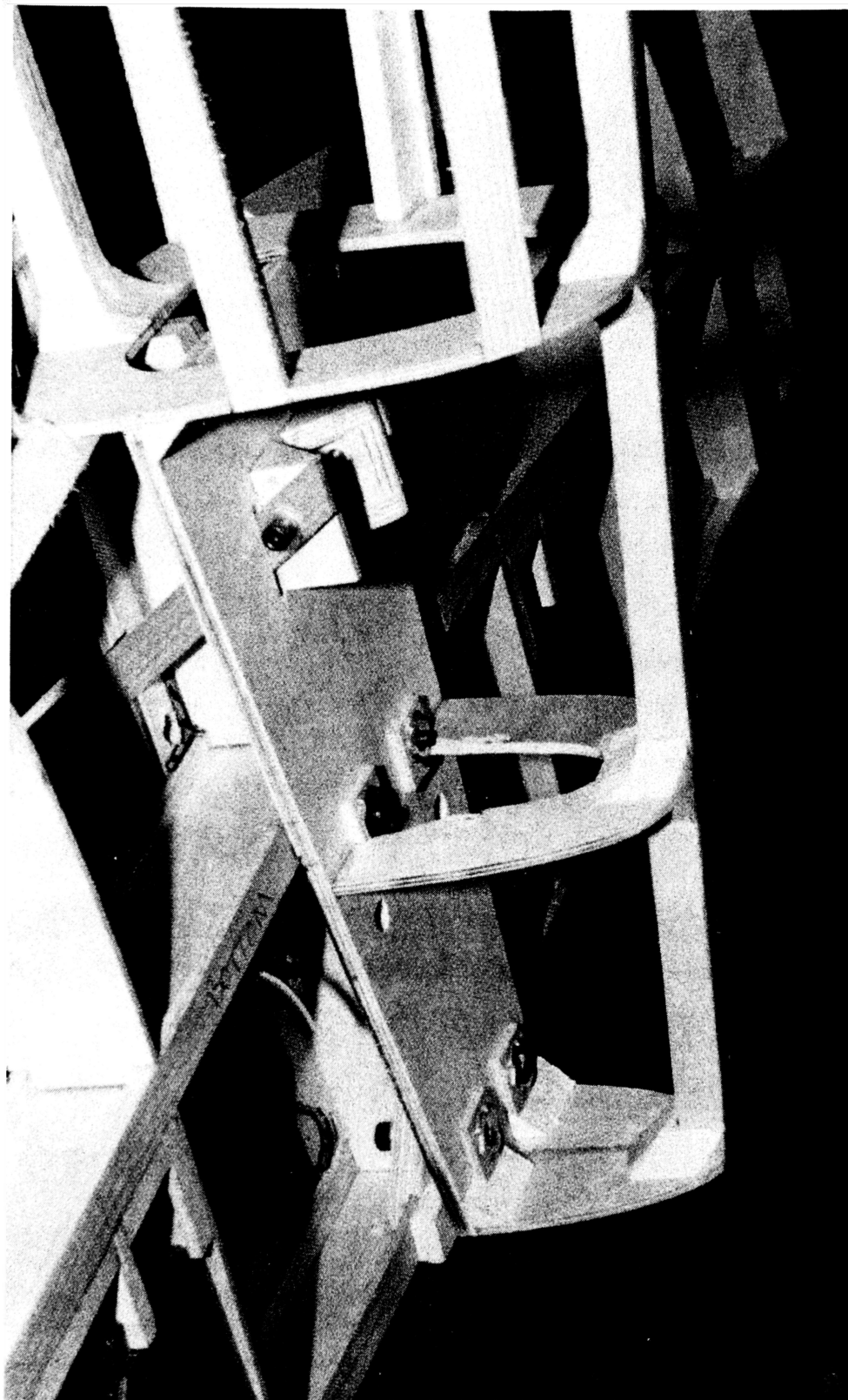
Figure B.13: Vertical and Horizontal Stabilizer Mounting Detail - 1

Figure B.14: Vertical and Horizontal Stabilizer Mounting Detail - 2
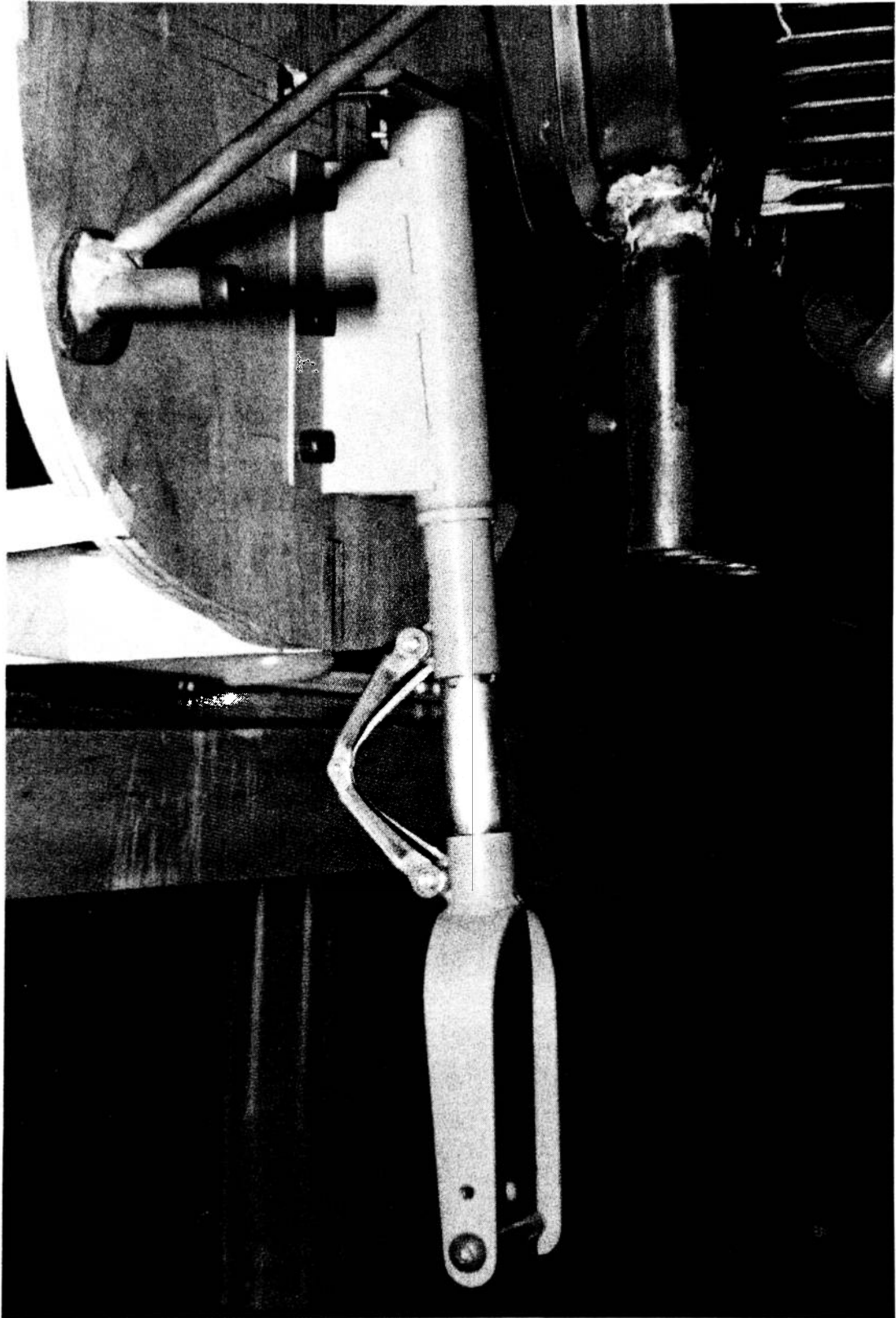
Figure B.15: Nose Gear Mounted to Firewall

B.16
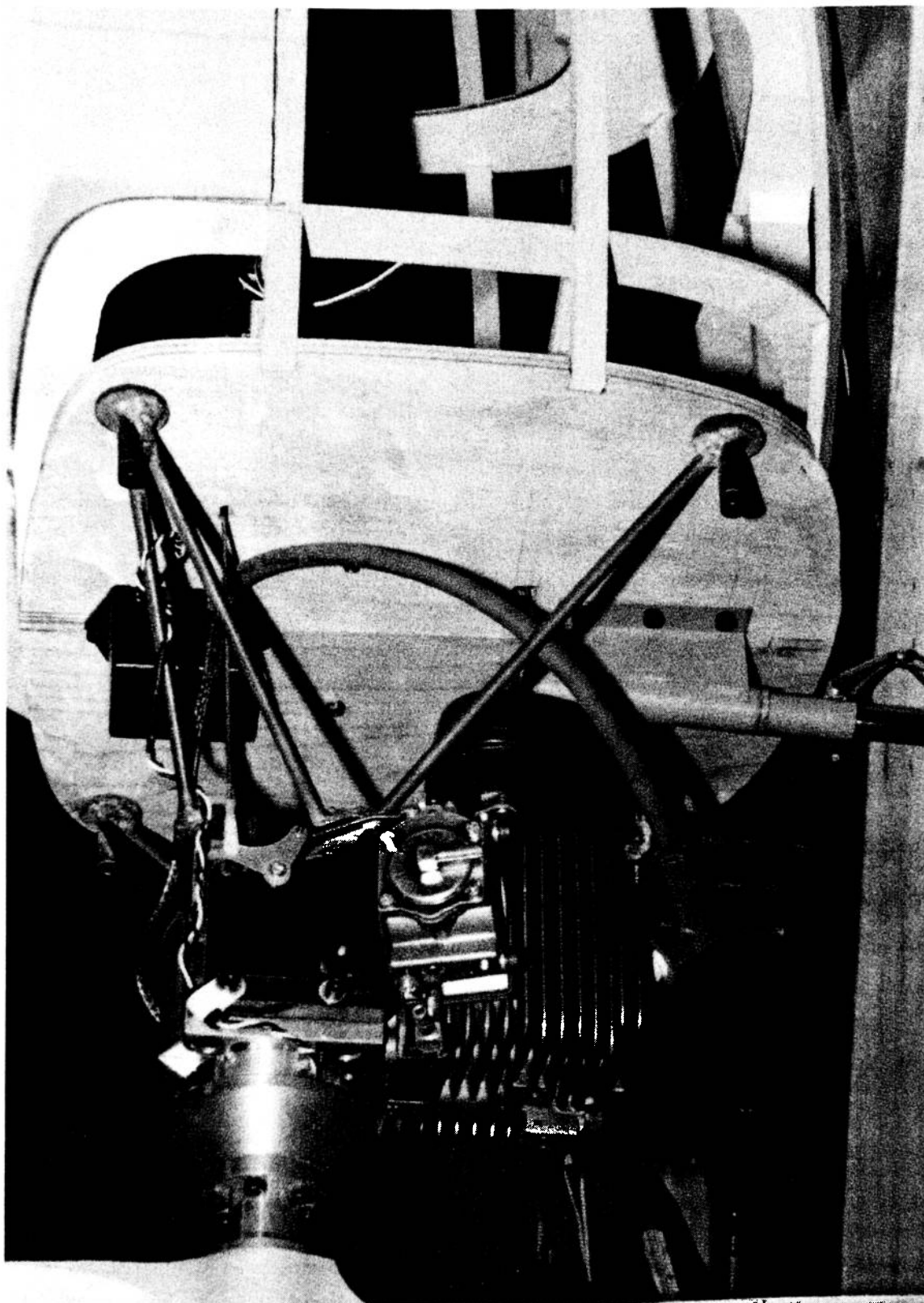
Figure B.16: Engine, Engine Mount, and Nose Gear Mounted to Firewall
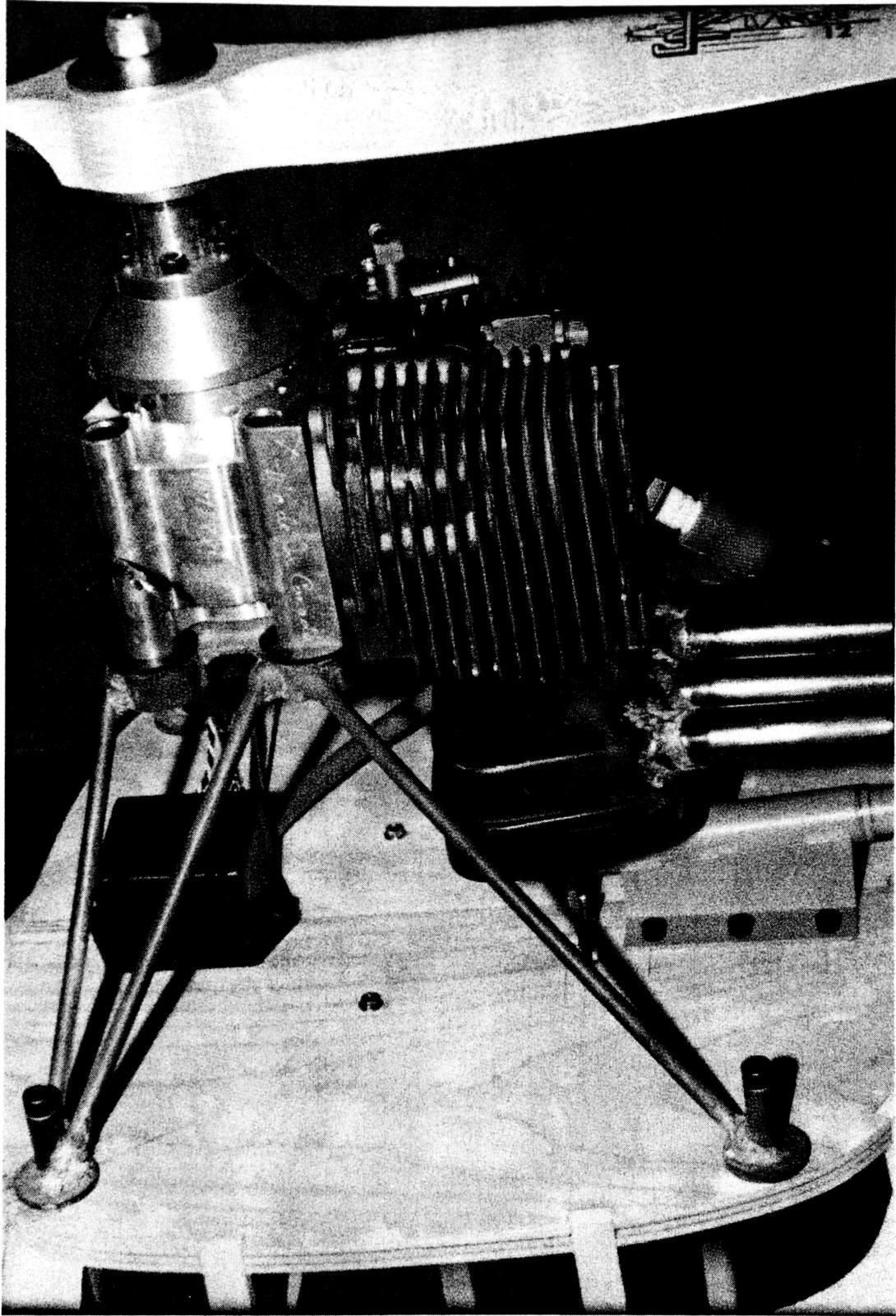
Figure B.17: Engine/Engine Mount Detail
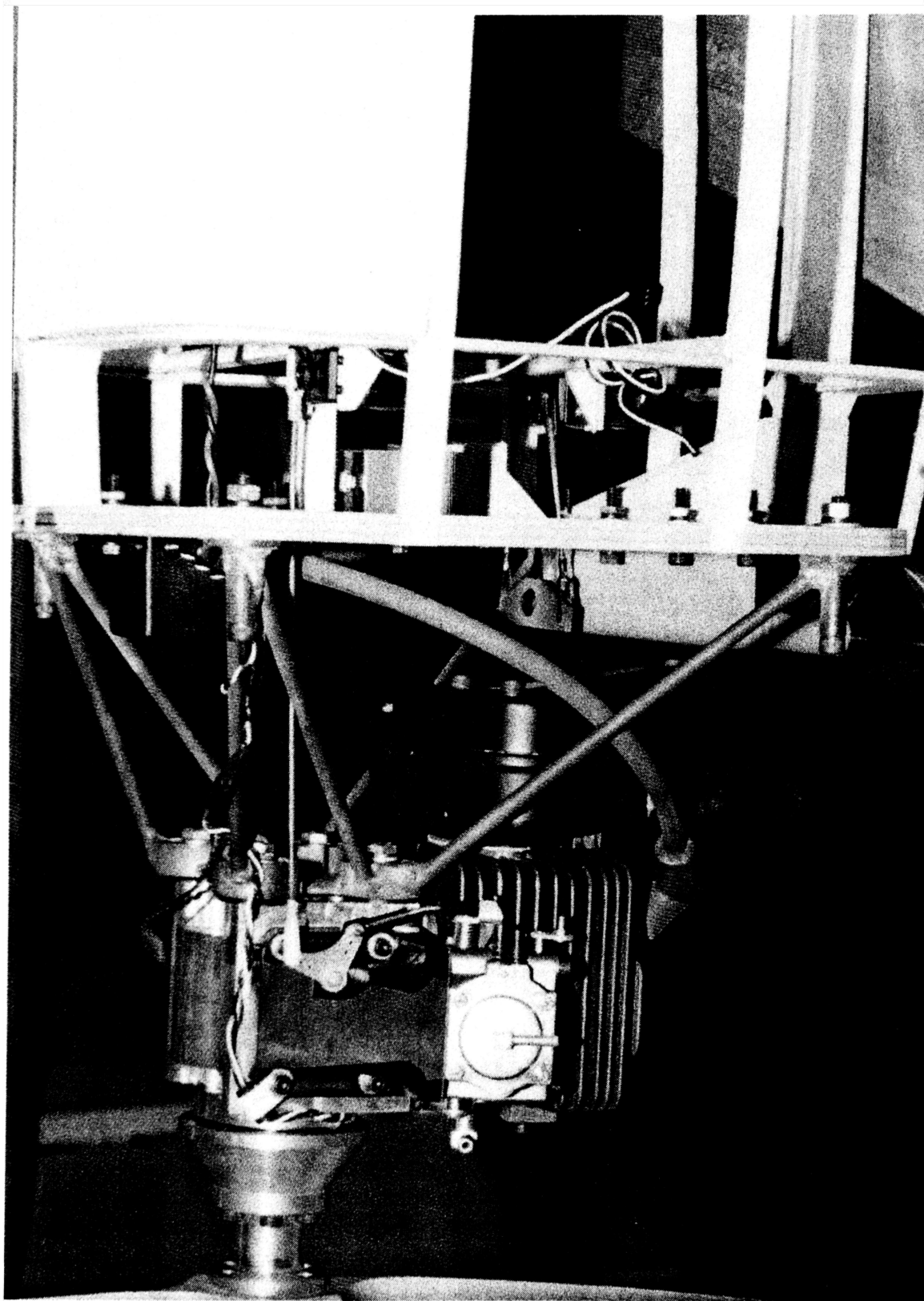
Figure B.18: Firewall Detail
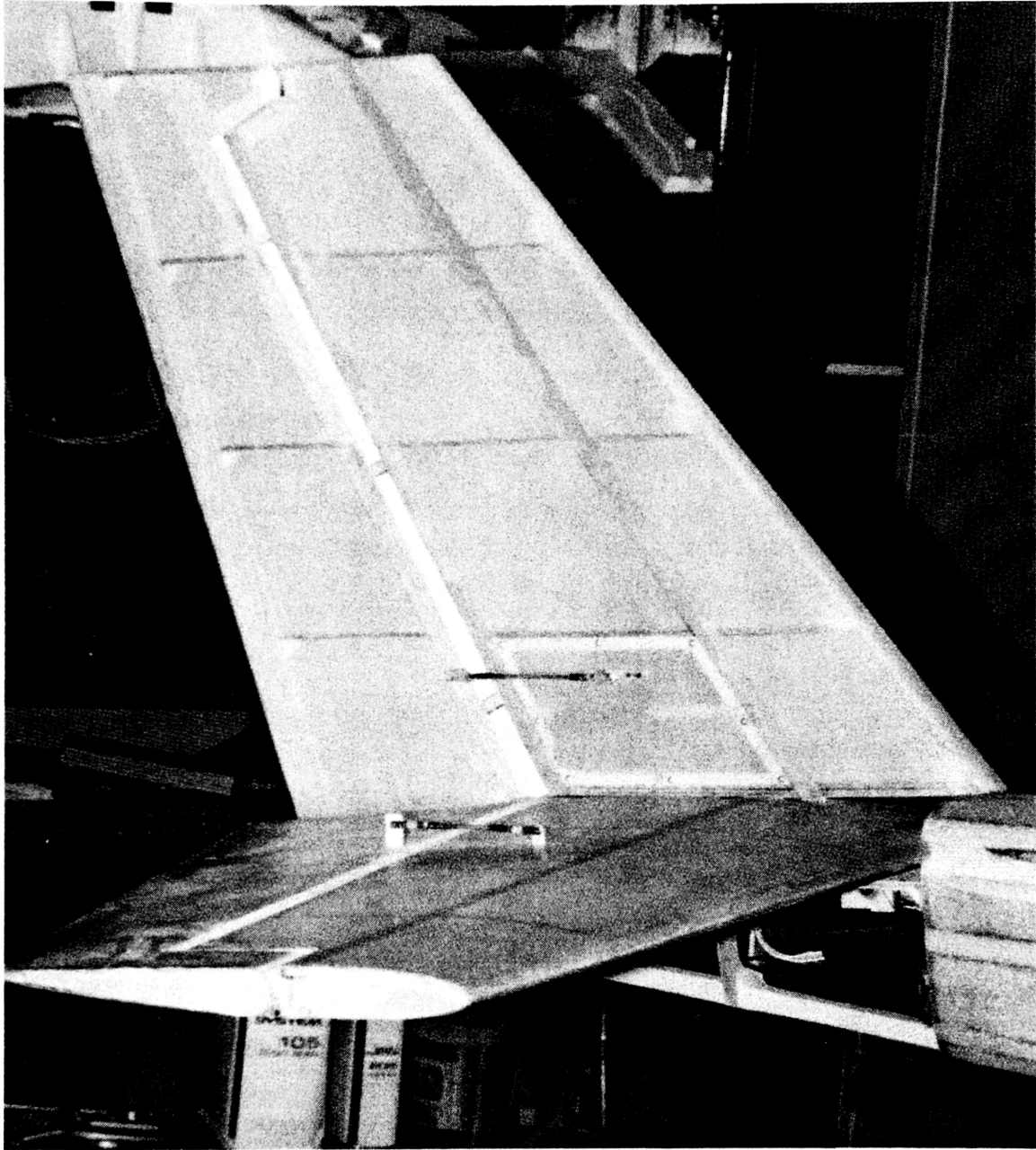
Figure B.19: Skinned Tail Surfaces Mounted to Aft Fuselage Tailcone

Figure B.20: Aileron Hinge Mounting Detail
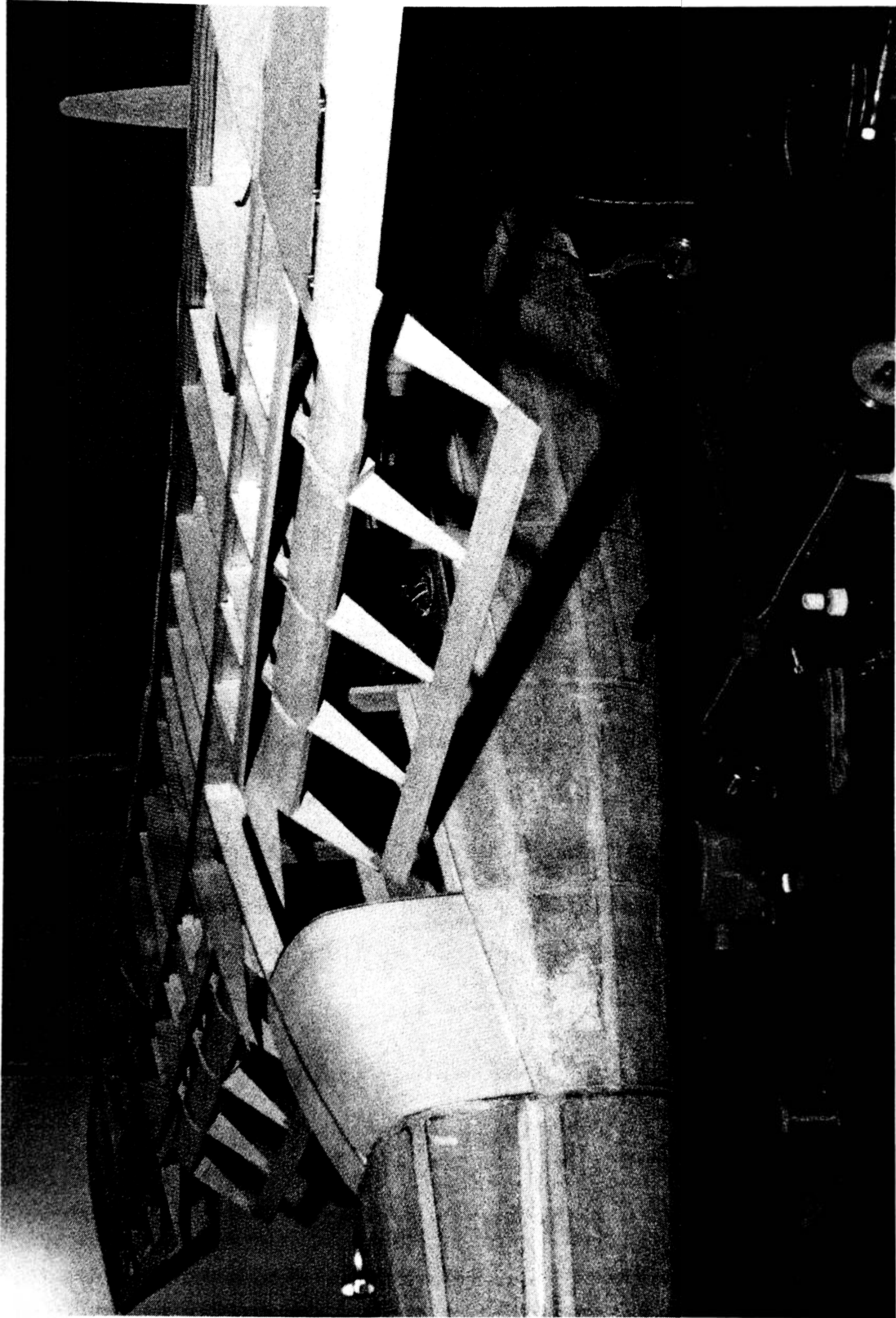
Figure B.21: Fowler Flap Action Detail
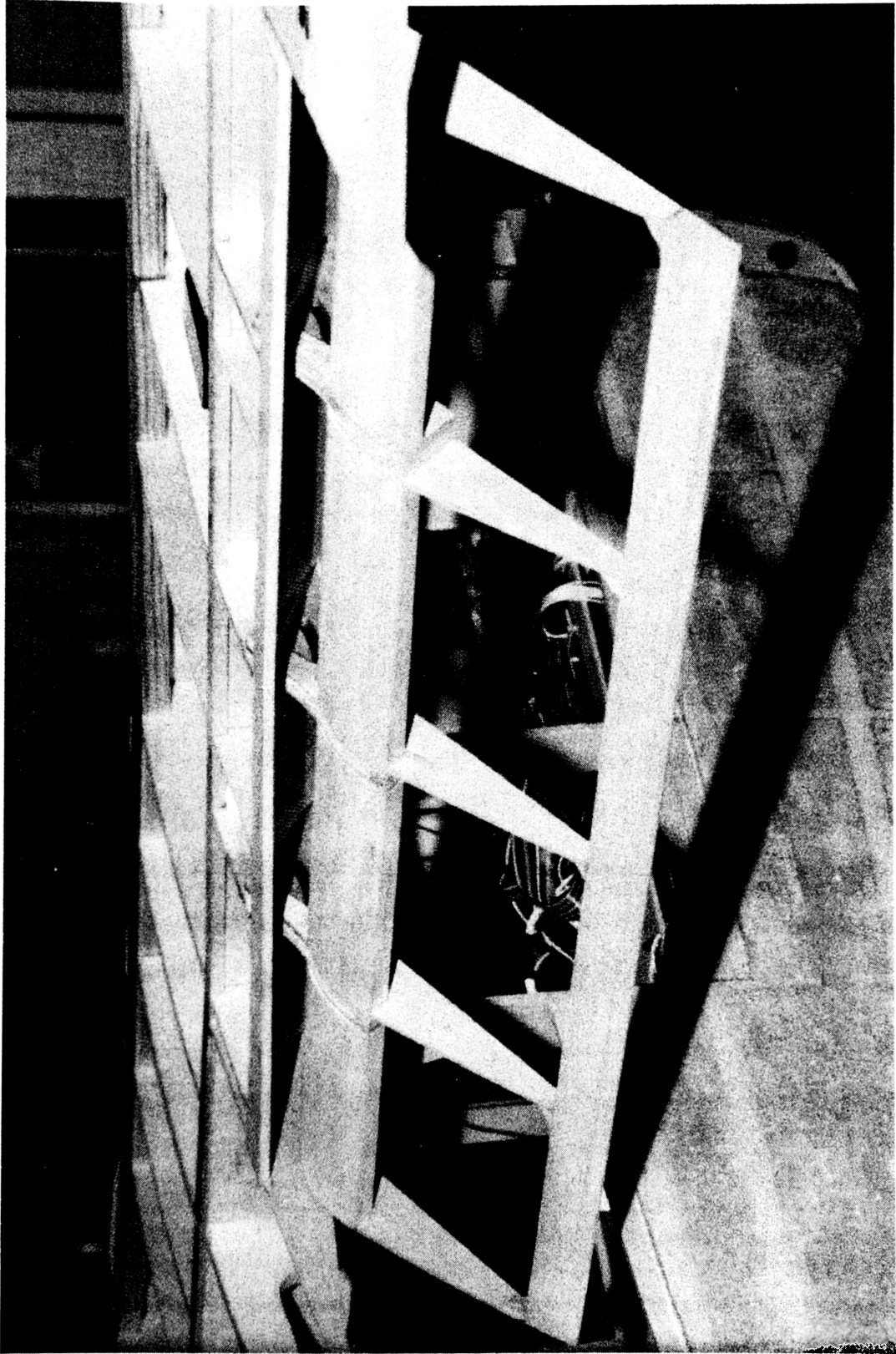
Figure B.22: Right-Hand Fowler Flap Detail
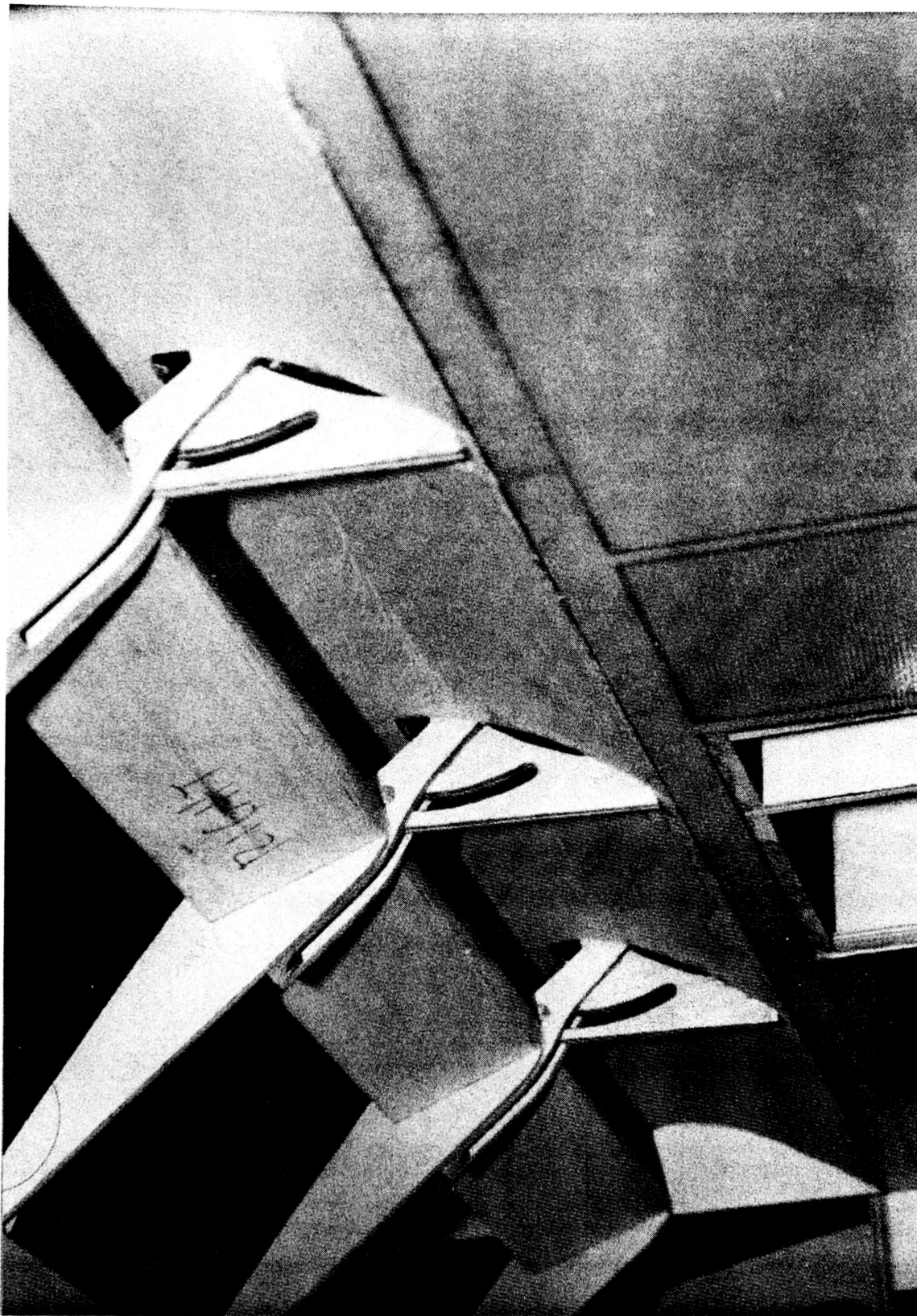
Figure B.23: Right-Hand Fowler Flap Track Detail
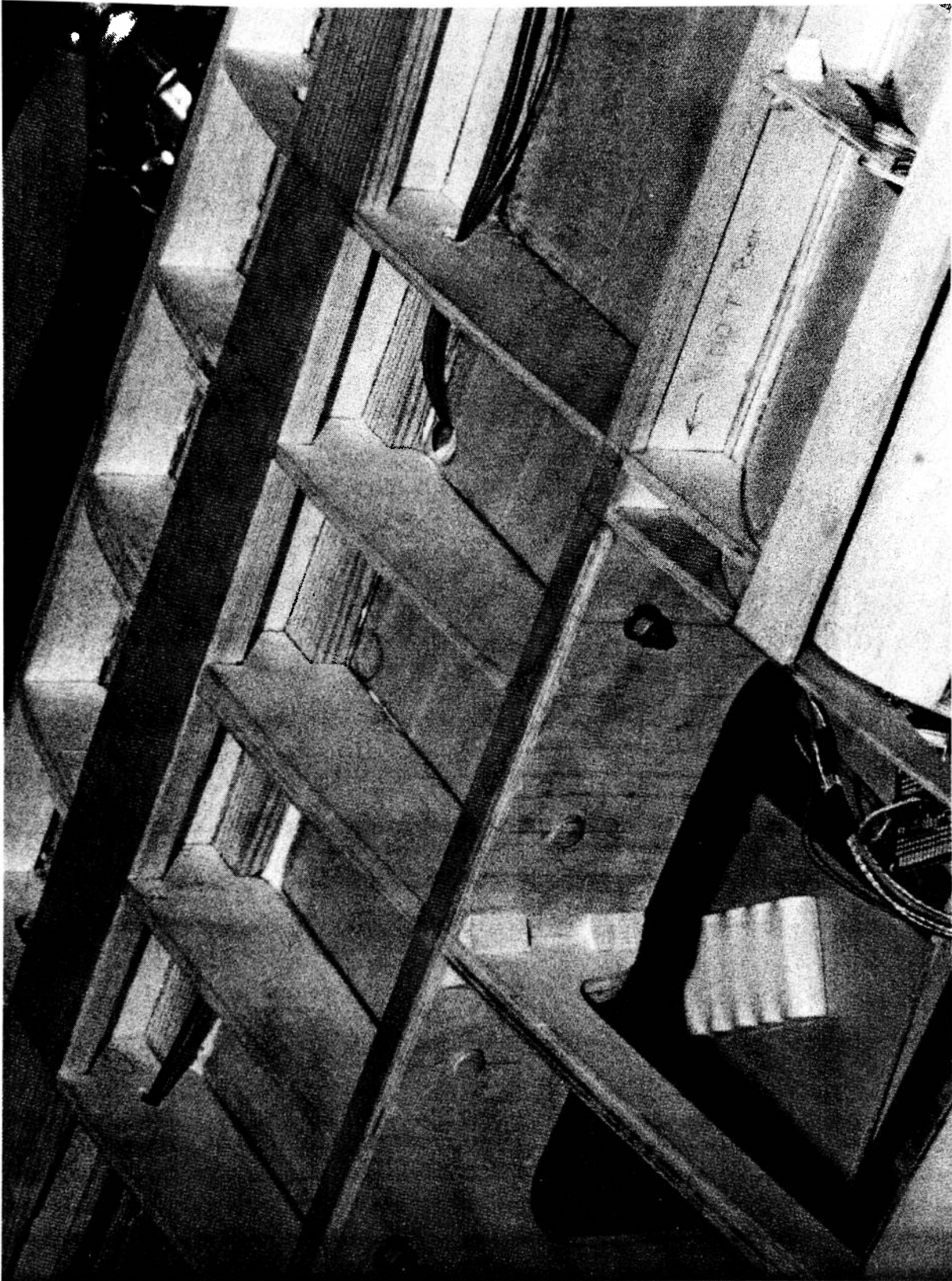
Figure B.24: Wing/Fuselage Mounting Detail

B.25
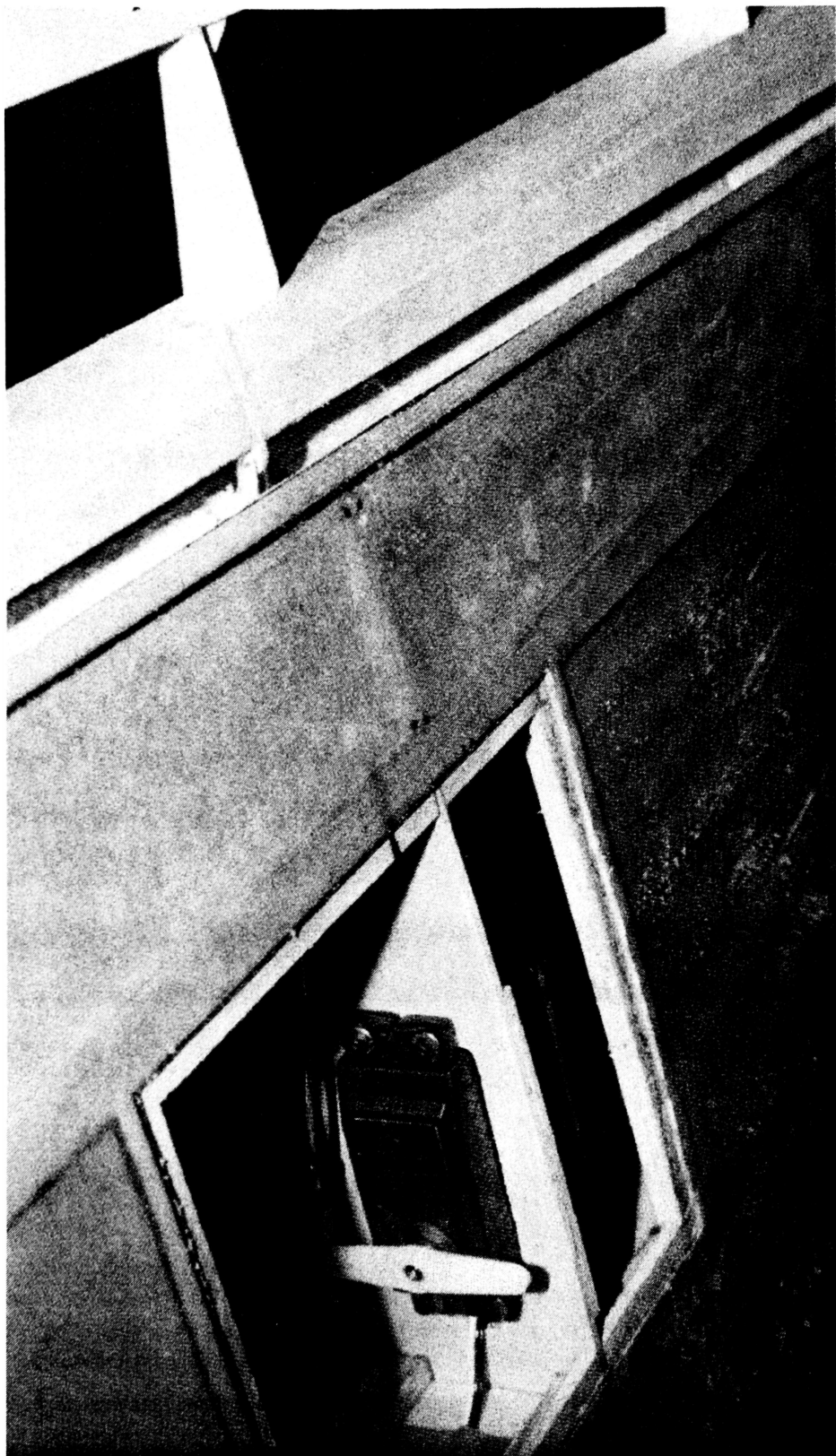
Figure B.25: Aileron Servo Mounting Detail
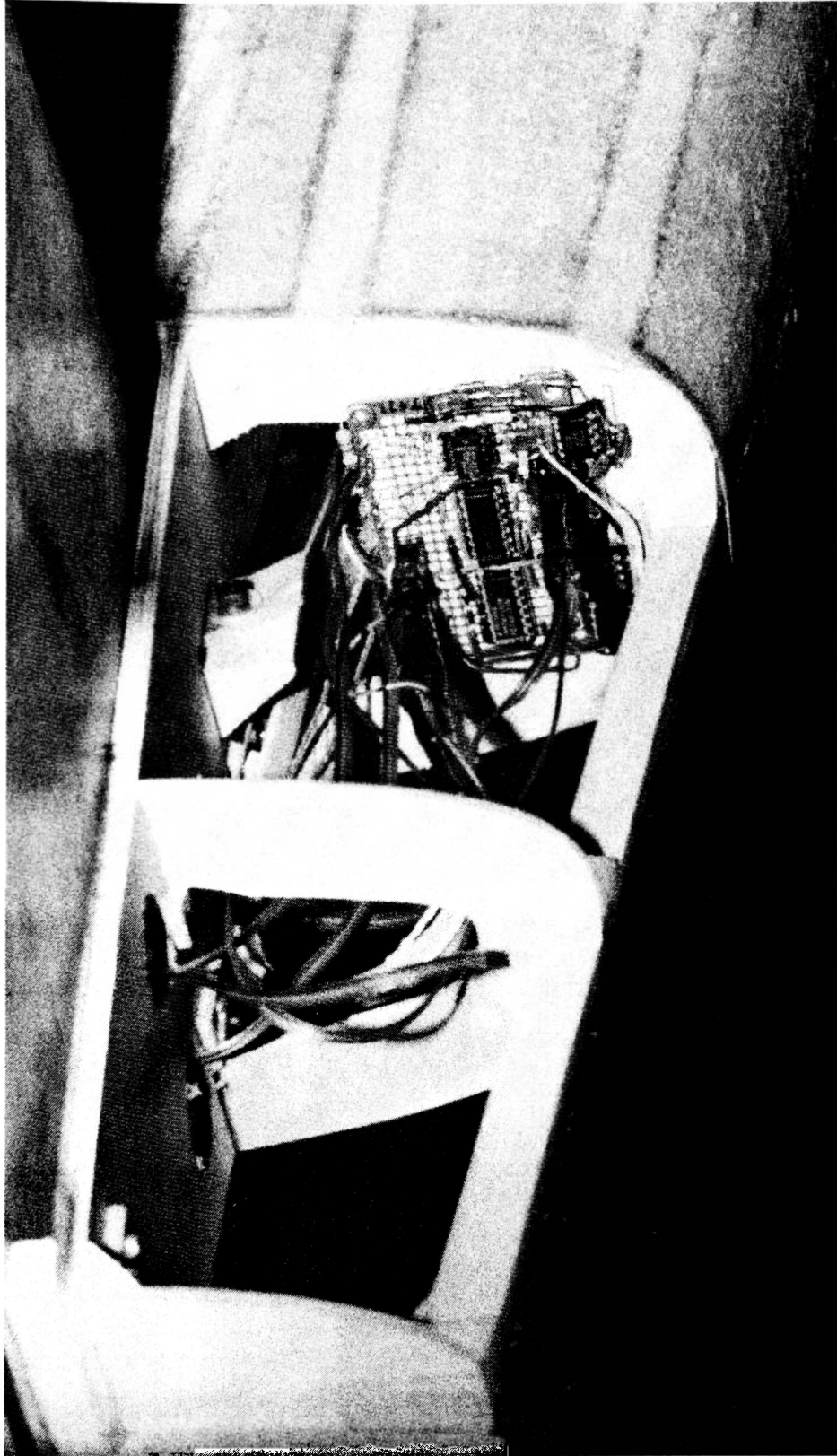
Figure B.26: Aft Fuselage Tailcone Data Collection Board Mounting Location
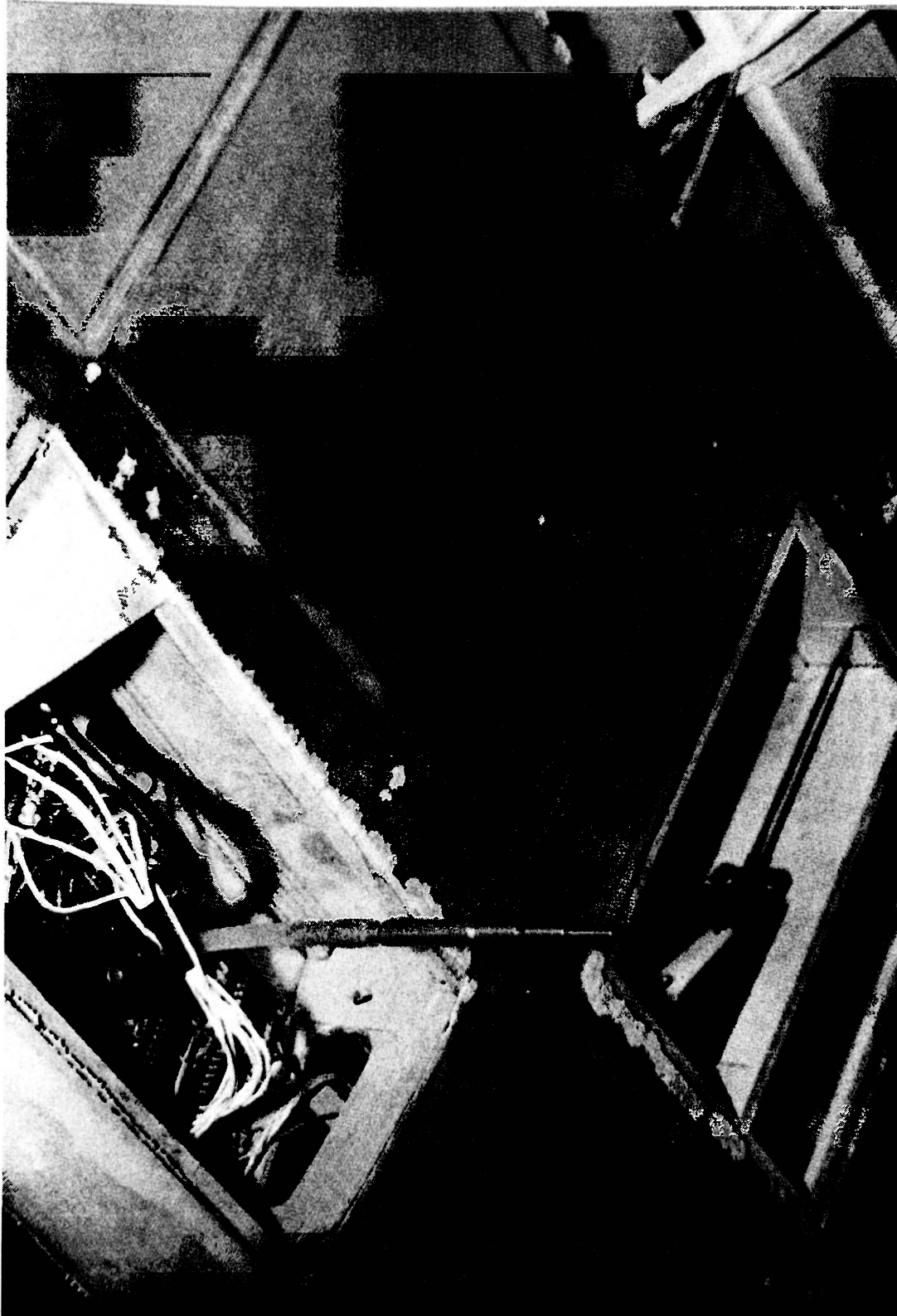
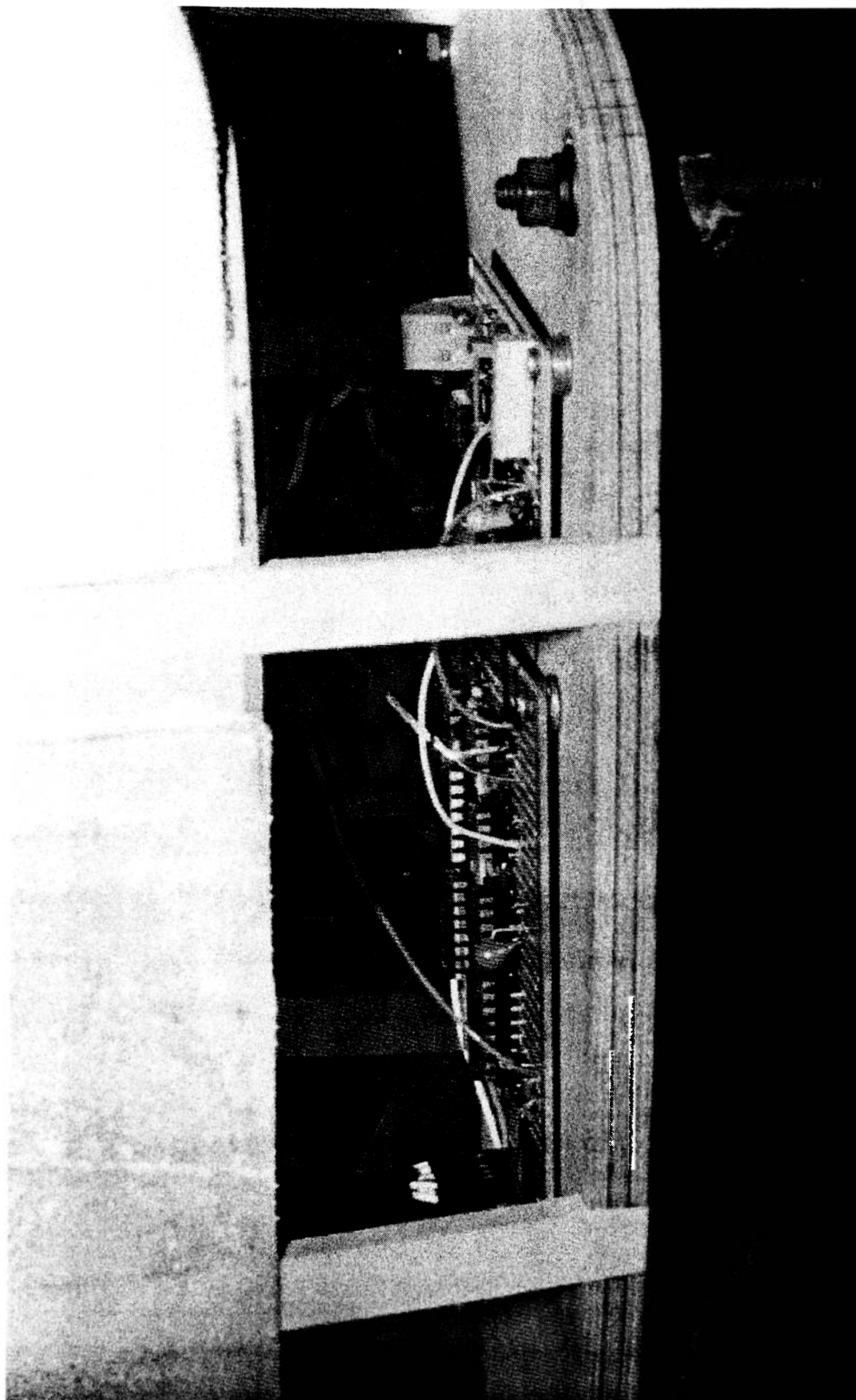**Figure B.27: Wing Data Collection Board Mounting Location**

Figure B.28: Firewall Data Collection Board Mounting Location

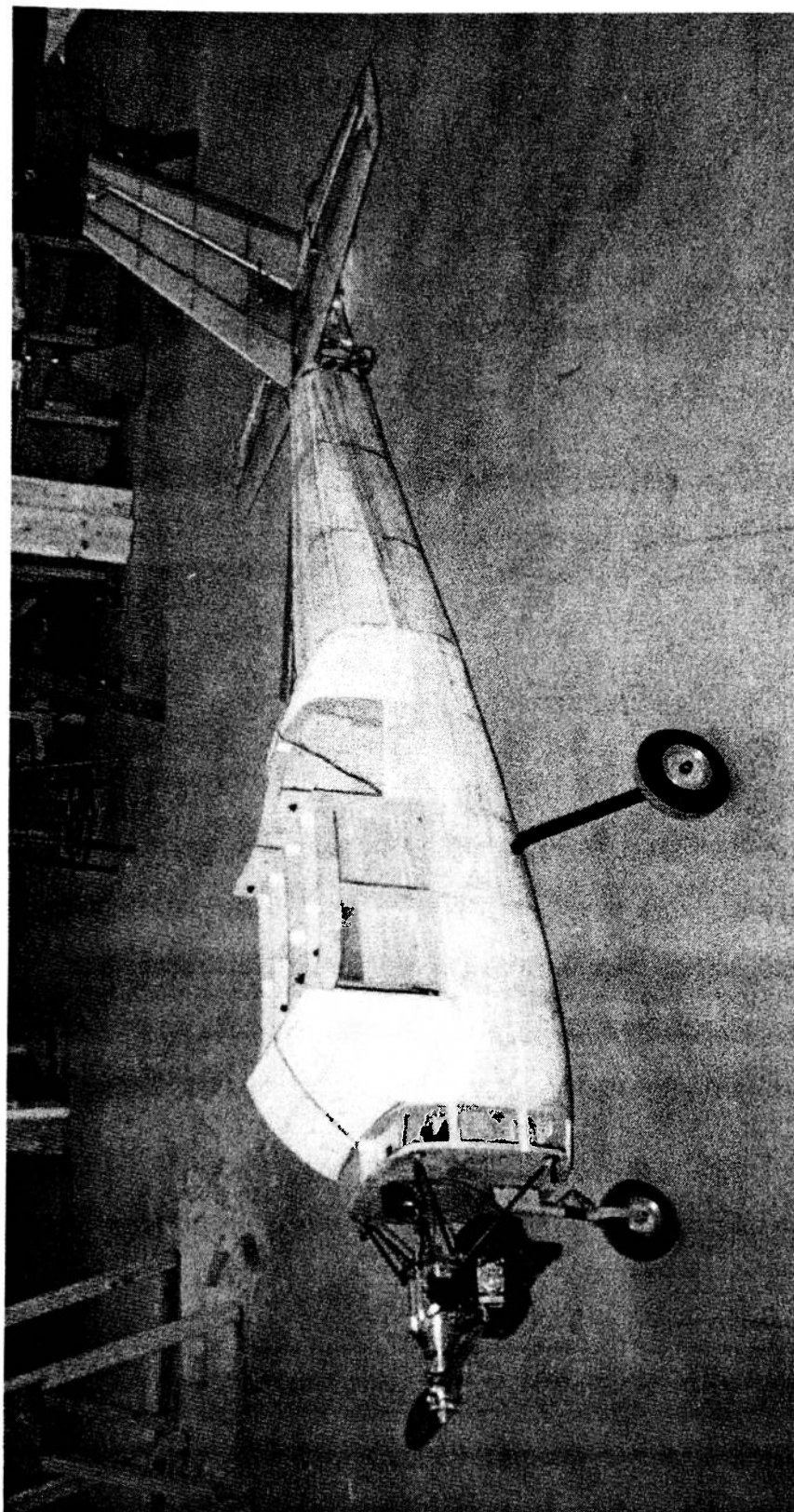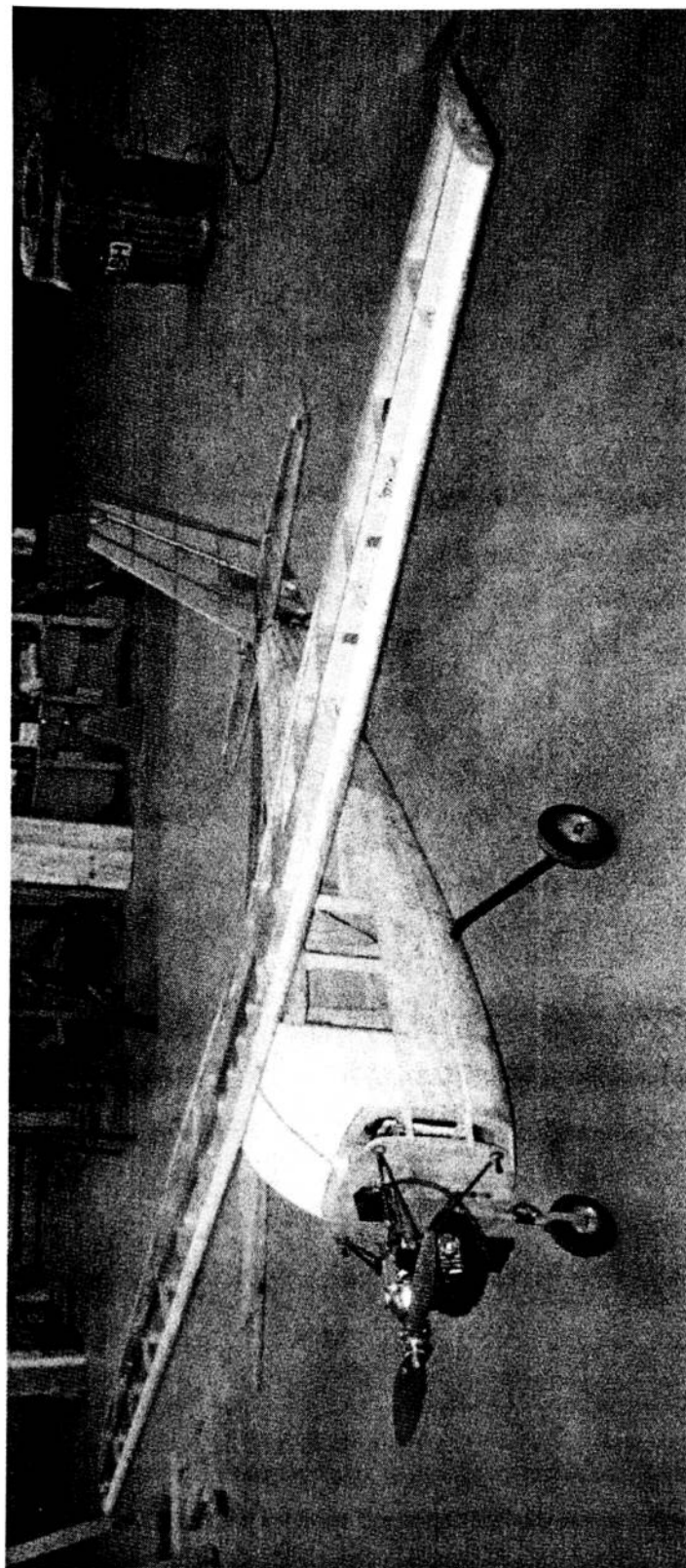**Figure B.29: Assembled 1/3-Scale C172P – Less Wing**

Figure B.30: Assembled 1/3-Scale C172P